A 3D Image-based Measurement Approach for Analysing Dynamic Foot Posture and Mobility

A dissertation submitted by

Duaa Alshadli

BSc, PGDipSci (Otago)

for the award of

Doctor of Philosophy

2015

Abstract

The original contribution achieved from this research was the development of a low-cost 3D high-accuracy photogrammetric technique for measuring dynamic changes in foot anthropometry during gait. In clinical settings, the approach of determining foot mobility is achieved through measuring changes in bone landmarks between the static unloaded foot and the static loaded foot. From previous reliability assessment tests, it was found that static clinical foot mobility assessments based on the dorsum bone as a point of landmark reference provides high levels of measurement reliability. However, the relationships between these static dorsum measurement techniques have not been assessed against dynamic dorsum measurements collected during foot mobility. In this thesis, two assessment techniques based on the dorsum as a point of reference; namely the Foot Mobility Magnitude (FMM) and Arch Height Index (AHI) were compared statically and dynamically. The purpose for this was to validate these static measurements against the actual foot mobility during dynamic activities.

An imaging platform was developed which consisted of 12 video cameras synchronised with force plate data to continuously capture the foot during gait while simultaneously obtaining ground reaction force information. The developed system achieved measurement accuracies within 0.3 mm with high levels of measurement precisions and insignificant random and systematic errors. From the research study, it was found that the correlation between the static and dynamic FMM measurements was insignificant, whereas significant correlations were found between the static and dynamic AHI measurements. Agreements between the static and dynamic AHI measurements were higher when the dorsum measurements were normalised to the truncated foot length (AHI 1) than normalising the dorsum measurements to the total foot length (AHI 2). Another major finding from the research was the higher measurement correlations achieved when the dynamic FMM and AHI were assessed between heel-strike and mid-stance compared to between heel-strike and active propulsion. This indicates that measuring the static FMM and AHI between 10% WB and 50% WB instead of between 10% WB and 90% WB might lend better insight in determining the behaviour of the foot dynamically.

The Foot Posture Index (FPI) was used to classify foot postures and the relationship between the FPI scores and the dynamic FMM and AHI were assessed. It was found that the FPI was significantly correlated to the AHI measures but no correlation was found between the FPI and the FMM. The highest correlation was found for AHI 1 at active propulsion where the FPI predicted 48.9% of the variation of the AHI 1. The only FPI classification criteria to have a significant influence on the AHI at heel-strike, mid-stance and active-propulsion was the congruence of the MLA with the highest prediction of 66.7% of the variation in the AHI 1 at heel-strike.

Statement of Authenticity

This is a statement headed 'Certification of Thesis ' to the effect that the work contained in the thesis is the bonafide work of the candidate, that the work has not been previously submitted for an award, and that, to the best of the candidate's knowledge and belief, the thesis contains no material previously published or written by another person except where due acknowledgement and reference is made in the thesis to that work. The signature and date is placed beneath the statement.

Duaa Alshadli

…….. Date: 7 November 2014

Candidates' signature

Endorsement

Dr. Albert Chong

……. Date: 7 November 2014

Principal supervisor's signature

Professor Peter Milburn

……. Date: 7 November 2014

External co-supervisor's signature

Acknowledgment

The production of this thesis would have not been possible without the support of numerous people.

First, I would like to thank my principal supervisor Dr. Albert Chong for his continuous support, guidance and encouragement for the duration of my Ph.D. Despite his many obligations, he always made the time for discussions. I also appreciate the support of Associate Professor Kevin McDougall at the early stages of my research.

Thanks to Professor Peter Milburn and Dr. Richard Newsham-West from Griffith University for their assistance with the clinical training prior to the data collection. Your feedback, support and knowledge made me feel confident in my research.

To all the support and technical staff at USQ particularly Ms. Juanita Ryan, Ms. Sandra Cochrane, Mr. Adrian Blockland, Mr. Terry Byrne and Mr. Chris Galligan – Thank you! Also, special thanks to Mr. Sha Pather for his assistance in the data collection.

I would like to thank my dearest friends, Raed, Nimra and Saba for being my family away from home. Thank you all for your unconditional support and amazing friendship! Thanks to all the wonderful people that I had the pleasure of working with including all the staff and students at USQ. I have gained invaluable experiences from you all.

Finally, I would like to thank my family and relatives for their encouragement. Special thanks to my little sister Nadeen who always manages to cheer me up with her incredible personality. I love you!

Table of Contents

List of Figures

List of Tables

List of Acronyms

ACL: Anterior Cruciate Ligament

AHI: Arch Height Index

AMTI: Advanced Mechanical Technology Inc.

BLS: Bilateral stance

CCD: Charge-coupled device

CI: Confidence Interval

CMOS: Complementary metal-oxide semiconductor

CPP: Central Perspective Projection

CSL: Coded structured light

DH: Dorsum height

FL: Foot length

FMM: Foot Mobility Magnitude

FPI: Foot Posture Index

FW: Foot width

ICC: Interclass Correlation Coefficient

MAD: Mean Absolute Difference

MLA: Medial Longitudinal Arch

NDT: Navicular Drop test

NH: Navicular height

PP: Projection Plane

RMS: Root Mean Square

SEM: Standard Error of Measurement

SSNDT: Sit-to-stand Navicular Drop Test

SLS: Single-limb stance

TEM: Technical Error of Measurement

TFL: Truncated foot length

ToF: Time-of-flight

WB: Weight bearing

Publications

Papers published from this thesis

Alshadli, D., Chong, A., Newsham-West, R., Milburn, P. 2014. Assessing the dynamic foot mobility magnitude using an image-based analysis System, *IEEE 7th International Conference on Biomedical Engineering and Informatics,* 14-16 October 2014, Dalian, China.

Alshadli, D., Chong, A., Newsham-West, R., Milburn, P. 2014. A video-based imaging technique for accurate foot measures during different weight bearing conditions, *IEEE 7th International Conference on Biomedical Engineering and Informatics,* 14-16 October 2014, Dalian, China.

Alshadli, D., Chong, A., Newsham-West, R., Milburn, P., McDougall, K. 2013. A comparison between static and dynamic foot mobility measures, *International Conference on Biomechanics and Sports*, 7- 11 July 2013, Taipei, Taiwan.

Alshadli, D., Chong, A., McDougall, K., Al-Baghdadi, J., Milburn, P., Newsham-West, R. 2013. Reliability of a high accuracy image-based system for 3D modelling of the medial longitudinal arch during gait. In: Abdul Rahman et al. (eds.) *Developments in Multidimensional Spatial Data Models.* Springer, Berlin, Heidelberg, pp. 85-101.

Alshadli, D., Chong, A., McDougall, K., Al-Baghdadi, J. 2011. *Skin texture enhancement for automated 3D point cloud generation in Charcot-Marie-Tooth disease application, IEEE 2011 10th International Conference on Electronic Measurement and Instruments,* 1, pp. 6-10.

Al-Baghdadi, J., Chong, A., Alshadli, D. (2013). Compensation of measurement errors caused by glass refraction for photogrammetric plantar surface mapping, *The Photogrammetric Record*, 28,143, pp 261-275.

Chong, A., Alshadli, D., Al-Baghdadi, J., Milburn, P., Newsham-West, R. 2013. A video-based system for plantar surface acquisition during gait, *International Conference on Biomechanics in Sports*, 7-11 July, Taipei, Taiwan.

Al-Baghdadi, J., Chong, A., Alshadli, D., Milburn, P., Newsham-West, R. 2013. Plantar surface contour using close range photogrammetry, *Proceedings of the eleventh footwear Biomechanics Symposium*, Natal, Brazil.

Al-Baghdadi, J., Chong, A., McDougall, K., Alshadli, D. 2011. A dense surface modelling technique for foot surface imaging, *Surveying and Spatial Sciences Conference: Innovation in Action: Working Smarter (SSSC 2011)*, 21-25 Nov, Wellington, New Zealand.

Chapter 1: Introduction

This chapter provides an outline of the background and research motivation by defining the research gaps, problem statements, research aim and objectives, scope of research and the contribution to the current literature. The chapter concludes with a framework outlining the contents of the remaining chapters of the thesis.

1.1 Background and research motivation

The foot is one of the most complex structures of the human body, comprising of multiple active and passive components which provide important support and functionality to the rest of the human body (Richie Jr, 2007). The interaction of the foot components with each other and with the ground reaction forces acting on the foot from the supporting surface provides important functions for the rest of the body. Some of the functions include the maintenance of body balance, support, body weight distribution and the creation of the forces required for locomotion (Scott et al., 2007). Any foot malfunctions will hence have a direct impact on the rest of the body (Khamis and Yizhar, 2007; Powers, 2003; Wrobel and Najafi, 2010).

It has been identified that during foot loading, the largest amount of foot mobility occurs around the Medial Longitudinal Arch (MLA) (Hunt et al., 2001; Leardini et al., 2007). The MLA is the largest arch of the foot and is regarded as the most important foot arch in clinical foot assessments due to its direct influence on foot function, stability, pain and predisposition of injury (McCrory et al., 1997; Nack and Phillips, 1990; Ogon et al., 1999; Shiang et al., 1998). Depending on the structure of the MLA, each foot can either be classified as supinated (high-arched), pronated (low-arched), or normally arched (Gilmour and Burns, 2001; Kanatli et al., 2001; Murphy et al., 2003; Razeghi and Batt, 2002). Each foot type classification displays different biomechanical foot functions; therefore quantifying foot posture is essential for predicting these functions (Menz, 1998). In addition, quantitative foot posture classification is linked to musculoskeletal overuse injuries and pain (Burns et al., 2005; Cain et al., 2007; Korpelainen et al., 2001). Hence, in order to lend insight into foot function and injury patterns, relating foot posture with dynamic foot mechanisms becomes an essential requirement (Villarroya et al., 2009).

In clinical settings, the approach of determining foot and mobility is achieved through static anthropometric measurements. Foot mobility measurements are often inferred from differences in the positions of bone landmarks between the static unloaded foot and the static loaded foot. There are currently a myriad of methods based on static measurements including the Navicular Drop test (Brody, 1982), Navicular Drift test (Menz, 1998), Foot Mobility Magnitude (FMM) (McPoil

et al., 2009), Arch Height Index (AHI) (Williams and McClay, 2000) and the Foot Posture Index (FPI) (Redmond et al., 2006a).

1.1.1 Navicular Drop and Navicular Drift tests

The most frequently used clinical assessment techniques of foot mobility identified in the literature are the Navicular Drop test and the Navicular Drift test. Both techniques provide quantitative measures of the change in the navicular bone when the subject's foot position is changed from a subtalar neutral position (loaded) to a relaxed weight-bearing state (minimally loaded) (Brody, 1982; Menz, 1998). The Navicular Drop and Navicular Drift tests measure the changes in the sagittal and the medial-lateral plane of the MLA respectively. Although the tests are commonly used in clinical foot evaluations, the reliability of both assessment methods investigated yielded variable results between studies ranging from poor reliability (Vinicombe et al., 2001) to excellent reliability (Allen and Glasoe, 2000). The conflicting results are mainly due to inconsistencies between testers in identifying the location of the navicular bone through palpation and the difficulty with positioning the foot in the subtalar neutral position (McPoil et al., 2008a). Another source of inconsistencies in the navicular bone assessments is due to the requirement for the subjects to maintain the weight-bearing percentage exerted on their feet for the duration of the measurements (Deng et al., 2010).

1.1.2 Foot Mobility Magnitude and Arch Height Index

The Arch Height Index (AHI) and the Foot Mobility Magnitude (FMM) were developed to overcome the problems identified for the above navicular bone tests. The AHI and FMM replaced measuring the changes in the navicular bone with measuring the changes in the dorsum of the foot between weight-bearing and non-weight bearing. The selection of the dorsum to replace the navicular bone as a point of reference was based on the results obtained by Williams and McClay (2000). The authors found that measuring the dorsum height provided significantly higher reliability than the navicular height measurements. In their study, Williams and McClay (2000) measured the reliability of the dorsum measurements based on two variations of the Arch Height Index (AHI); one normalised to foot length (FL) and the other to the truncated foot length (TFL). The dorsum measurements also provided higher validity than the navicular bone measurements when compared using radiographs (McPoil et al., 2008b).

Due to the high reliability and validity results of the Dorsum measurements obtained from the AHI test, McPoil et al.(2009) developed the FMM test which collectively measures the sagittal and medial-lateral changes in the Dorsum of the foot during weight-bearing and non-weight bearing. The FMM also provided high levels of measurement reliability when tested with a large cohort of subjects (McPoil et al., 2009).

1.1.3 The Foot Posture Index

In recent years, another foot classification method known as the Foot Posture Index (FPI) has gained popularity due to its high validity and reliability (Cornwall et al., 2008; Keenan et al., 2007; Redmond et al., 2006a). The main advantage of the FPI foot classification method is the ability to assess the foot posture based on six collective foot components. This in turn provides a more comprehensive indication of the dynamic foot behaviour (Nielsen et al., 2010).

1.2 Research gaps

Although the FMM, the AHI and the FPI have improved the reliability of static foot mobility assessments, to the knowledge of the author, the following research gaps were identified in the literature:

- The association between static FMM and AHI assessment techniques with the dynamic foot behaviour is not reported in any previous studies.
- The association between the FPI scores and the dynamic FMM and AHI are not reported in the literature.
- A detailed analysis of the effect of dynamic weight-bearing on the FMM and AHI is not reported in the literature.

1.3 Problem statement

As the current clinical assessment techniques rely on static measurements, the ability to predict dynamic foot function is therefore limited. In addition, there is a lack of a non-invasive 3D measurement technique which can be used to measure the foot dynamically during gait to a high level of accuracy and reliability.

1.4 Research aim

Hence the main aim of the research is to:

'Develop high accuracy dynamic 3-D measurement and analysis techniques to determine the extent of agreement between conventional static foot measurements based on the dorsum bone and the same measurements dynamically'.

Static conventional measurement and analysis techniques will be modified for dynamic foot measurement and analysis. To achieve this, an image-based analysis technique based on high measurement accuracy close-range photogrammetric concepts will be developed as part of the research for measuring 3D changes in foot anthropometry during gait. From the developed system, the Foot Mobility Magnitude (FMM) and Arch Height Index (AHI) will be determined

dynamically and compared to the same measurements collected using conventional static caliper measures. The developed photogrammetric measurement system will also be used to correlate Foot Posture Index (FPI) scores with the dynamic FMM and AHI measures.

1.5 Research objectives

The research aim and questions will be addressed through the following research objectives:

Objective 1: to develop a 3D image-based measurement system for accurate dynamic foot mobility and posture measurements (Chapter 3)

This objective will be achieved through the following:

- Designing the 3D image-based measurement system and developing a methodology for obtaining high accuracy anthropometric foot measurements during gait.

- Calibrating the components of the developed 3D image-based measurement system.

Objective 2: To determine whether conventional static foot measurement and analysis techniques can be applied to dynamic foot measurement and analysis (Chapter 4).

The objective will be achieved through the following:

- Assessing the accuracy, precision and reliability of the measurements acquired from the dynamic measurement system.

- Analysing the effect of increasing the static and dynamic weight-bearing applied on the foot on the measurement precision, accuracy and reliability.

Objective 3: to determine the extent of agreement between the static and dynamic Foot Mobility Magnitude (FMM) and Arch Height Index (AHI) (Chapter 5).

The objective will be addressed through the following:

- Conducting conventional static manual clinical anthropometric measurements of subjects' feet using calipers.

- Conducting non-invasive dynamic anthropometric measurements of subjects' feet using the developed high accuracy image-based measurement technique.

- Investigating agreements between the static and dynamic FMM and AHI measurements using statistical tests of significance, reliability and agreement.

Objective 4: to determine the influence of arch height determined from Foot Posture Index (FPI) scores on the dynamic FMM and AHI measurements (Chapter 6).

The objective will be addressed through the following:

- Conducting the clinical FPI assessments.
- Investigating the statistical levels of significance between the FPI scores and the FMM and AHI measurements.
- Identifying which of the six FPI components has the highest impact on the dynamic FMM and AHI measurements.

1.6 Significance of research

- Developing a technique which allows for high-accuracy 3D anthropometric measurements of the foot to be obtained during gait.
- Developing a methodology which allows for accurately synchronising dynamic foot measures with corresponding ground reaction forces and the different steps of the gait cycle.
- Determining the relationship between conventional static FMM measures and the dynamic foot behaviour during gait.
- Determining the relationship between the static and dynamic AHI measures.
- Determining whether the foot length or the truncated foot length provide a better prediction of the AHI during gait.
- Determining whether changes in weight-bearing between 10% and 50% or 10% and 90% for static measurements provide a better predictor of the dynamic behaviour of the foot during gait.
- Determining whether there is a level of correlation between FPI classification scores and the dynamic FMM and AHI.
- Identifying whether any of the individual components of the FPI provide a better prediction of the dynamic FMM and the AHI scores.

1.7 Research scope

This thesis focuses on applying accurate image-based close-range photogrammetric techniques for determining the behaviour of the foot dynamically. The dynamic foot measurements are then compared with conventional static foot measurements to identify the association between the two measurement techniques. The scope of the

study will be limited to two measurement techniques based on the dorsum as a point of reference during changing weight-bearing conditions acting on the foot. The two techniques; namely the AHI and FMM are selected based on their higher reliability and validity when compared to other clinical foot posture and mobility assessment techniques. After the relationships between the static and dynamic measurements are identified, the FPI will be used to analyse the relationship between foot posture and the dynamic FMM and AHI. The FPI will also be used to assess which segment of the foot is most closely related to dynamic AHI and FMM measures.

1.8 Thesis outline

The thesis outline is provided separately for each chapter as follows:

Chapter 2: Literature review.

The chapter provides a review of the existing literature on static clinical foot posture assessment methods and measurement techniques based on the structure of the MLA that are used to predict foot mobility. It then examines the current technologies used to create 3D shape information for deriving anthropometric measurements statically and dynamically.

Chapter 3: Design of an accurate 3D image-based system for dynamic foot measures.

This chapter details the design of the accurate image-based measurement technique used for dynamic foot anthropometric data collection during gait based on the concepts of close-range photogrammetry. Accuracy, precision and reliability assessments of the designed system will be investigated in this chapter.

Chapter 4: The effect of changing weight-bearing on foot measurement accuracy.

The between-tester measurement accuracy of conventional caliper measurements will be investigated in Chapter 4. The chapter focuses on the effect of changing foot weight-bearing on the measurement accuracy and comparing conventional caliper measurements with the developed image-based, dynamic data capture system measurements.

Chapter 5: Comparing static and dynamic Foot Mobility Magnitude (FMM) and Arch Height Index (AHI) measures.

This chapter addresses the application of the developed high accuracy dynamic data capture photogrammetric system for collecting the foot anthropometric measurements used in calculating the dynamic FMM and AHI. These dynamic measurements are then correlated with static conventional clinical FMM and AHI measures conducted by two testers. Statistical analysis of reliability, correlation and

significance will then be used to conclude whether current static clinical assessments of the FMM and AHI reflect the behaviour of the foot during dynamic gait.

Chapter 6: Relationship between Foot Posture Index (FPI) and dynamic FMM and AHI.

This chapter describes the relationship between foot postures obtained from clinical FPI assessments and the dynamic foot mobility based on the FMM and AHI measures. The six components of the FPI assessment will be individually compared with the dynamic FMM and AHI to determine whether any of the components provides higher levels of correlation to the dynamic foot measures.

Chapter 7: Conclusion, limitations and future recommendations.

The thesis concludes with a brief discussion of the research outcome along with limitations identified from the research. Finally, recommendations for future research will be presented.

Chapter 2: Literature review

2.1 Introduction

In the previous chapter, the fundamental research issues were outlined. This chapter aims to provide a detailed review of relevant literature to aid in the detailed understanding of the research issues, direct the reader to the research gap and provide an understanding of the research aim and objectives. The first part of the chapter focuses on the conventional foot assessment techniques used by clinicians to predict the dynamic behaviour of the foot. The second part details the current measurement methods and technologies specific to foot measurement applications and highlights their limitations.

2.2 Static clinical foot assessment techniques

In an attempt to identify the functionality of the human foot, a large number of studies have been dedicated to identifying the influence of foot morphology on foot function. Differences in foot morphology between individuals have been identified as a result of many factors including; ethnicity (Igbigbi and Msamati, 2002), type of foot wear (Pezzan et al., 2009), injury (Bandholm et al., 2008; Bennett et al., 2001) and gender (Nielsen et al., 2009). As the foot shape and its biomechanics differ between individuals, clinical assessments regard the Medial Longitudinal Arch (MLA) as the main source of foot variability (Razeghi and Batt, 2002). The MLA is the largest arch of the foot and is regarded as the most important foot arch in clinical assessments due to its influence on lower limb function (Murley et al., 2009; Nigg et al., 1993), postural stability (Cote et al., 2005) and foot pain (Burns et al., 2005; Statler and Tullis, 2005). Each foot is classified as either pronated (low-arched), supinated (high arched) or normally arched based on the structure of the MLA (Fan et al., 2011).

The foot is comprised of 26 bones (Figure. 2.1) and the MLA is collectively made up of the calcaneus, talus, navicular, cuneiform, and the medial metatarsal bones (Abboud, 2002). Being the largest arch of the foot, the MLA absorbs most of the body's impact during gait and provides the most significant support to the foot during weight-bearing activities.

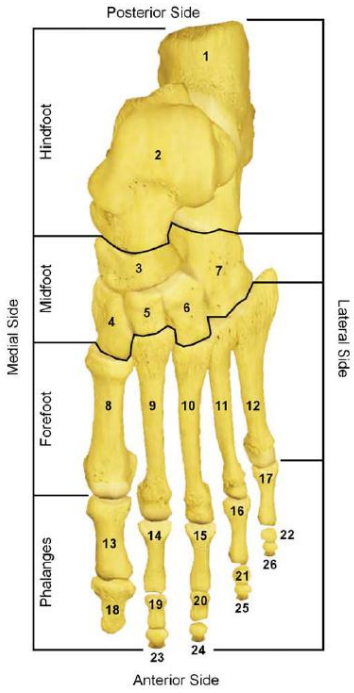

Figure 2.1: Structure of the foot (Abboud, 2002).

There are currently a number of techniques used to classify the foot in a static state based on measurements of the MLA. The most popular techniques use the navicular bone measurements as a point of reference for assessing the MLA. These static measurements are then used to predict the behaviour of the foot arch in a dynamic state.

2.3 Assessment techniques based on changes in the navicular bone

2.3.1 The Navicular Drop Test (NDT)

The Navicular Drop Test (NDT) was originally developed by Brody (1982) to quantify the sagittal plane mobility of the mid-foot. The NDT measures the change in height of the navicular bone when the foot position is changed from subtalar neutral (loaded) to a relaxed weight-bearing state (minimally loaded). The first applications of the NDT were to evaluate foot pronation in runners and to predict injuries amongst them (Brody, 1982; Sell et al., 1994). Three variations of the Navicular Drop Test were found in the literature; namely: 1) bilateral stance (BLS) Navicular Drop, 2) Single-limb stance (SLS) Navicular Drop and 3) Sit-to-Stand Navicular Drop (SSNDT).

2.3.1.1 Bilateral Stance (BLS) Navicular Drop Measurements

This technique was the original Navicular Drop test developed by Brody (1982) and it requires the subject to stand with double-limb support on a firm surface while the tester places the subtalar joint in a neutral position by palpation. Measurements of the navicular bone height are then collected from the supporting surface. The subject is then instructed to relax their foot and once again the navicular bone is measured from the supporting surface. The height of the navicular bone in the subtalar neutral position is then subtracted from the height of the navicular bone in the relaxed foot state and this gives the value of the ND as a result of the change in weight-bearing (Figure 2.2).

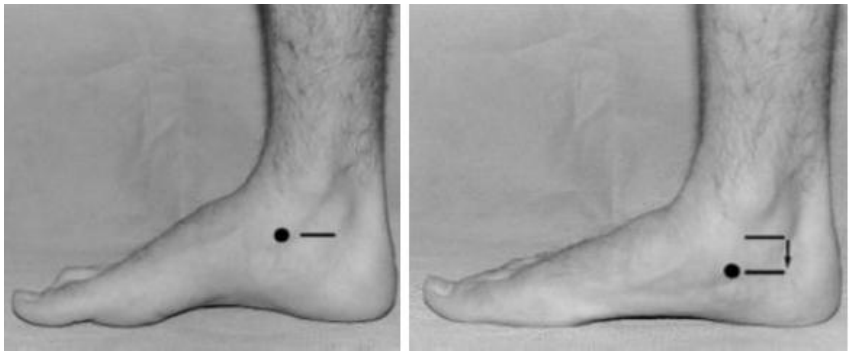

(a) (b)

Figure 2.2: (a) Navicular bone position at subtalar joint neutral and (b) navicular bone position when the foot is relaxed. The navicular Drop is the result of the change in weight-bearing (Menz, 1998).

Brody (1982) reported that a Navicular Drop value of approximately 10 mm is regarded as normal and anything greater than 15 mm is classified as abnormal. Since then, a number of studies have challenged these results due to conflicting BLS ND results evident between studies. Mueller et al. (1993) obtained averaged Navicular Drop values of 7.3 mm whereas Woodford-Rogers et al. (1994) noted values for Anterior Cruciate Ligament (ACL) injured football players of 8.4 mm and 5.9 mm for non-ACL injured players. In contrast, an average ND value of 8.1 mm was obtained by Allen and Glasoe (2000). In a study conducted by Moul (1998) differences in the bilateral Navicular Drop results were found between genders where ND values between 8.50 mm and 8.87 mm were reported for males and 7.31 mm to 7.37 mm for females. The between-gender results were also confirmed by Nielsen (2009) who found that the foot length also influences the ND measurements. It is hence recommended that the Navicular Drop must be tested for subjects with similar foot lengths and gender.

Reliability studies based on Intra-tester reliability (between-sets) and Inter-tester reliability (between-testers) have also been shown to be largely varied between studies. Intraclass Correlation Coefficients (ICCs) were found to be ranging between 0.33 which indicates poor reliability (Vinicombe et al., 2001) to 0.97 which signifies excellent reliability (Allen and Glasoe, 2000). The variations in the reliability studies are the result of inconsistencies between different testers in placing the subtalar joint in a neutral position and in palpating and identifying the location of the navicular bone (McPoil et al., 2008a). Another source of between-tester inconsistencies is the difficulty in determining and maintaining the required weight-bearing during measurements (Deng et al., 2010). Nielsen et al. (2010) quantified the amount of uncertainty in identifying the location of the navicular bone through between-day measurements and reported a variability of 4-5 mm.

To validate the Navicular Drop test as a measurement technique for predicting the behaviour of the foot with changing weight-bearing, Williams and McClay (2000) used lateral radiographs. The navicular height measures were taken at 10% and 90% weight-bearing (WB) stance conditions. It was assumed that at 10% WB, the foot plantar surface is in a minimally weighed position while the entire plantar surface is in contact with the ground. The 90% WB condition is the percentage sufficient to observe any changes in the foot under load and hence provide a good description of foot mobility. The results of the ICCs for comparison between the clinical and radiographic measures of NH were 0.874 and 0.918 for 10% WB and 90% WB respectively. Inter-tester reliability was 0.924 for 10% WB and 0.608 for 90% WB. The higher reliability results for the 10% WB were speculated to be due to the difficulty in identifying the position of the navicular bone during clinical measurements when the foot is in the 90% WB stance condition. This is the direct result of the stretching of the underlying tissue with increasing weight-bearing which inadvertently changes the location of the navicular bone.

2.3.1.2 Single-limb stance (SLS) Navicular Drop test

A few studies used a variation of the Double limb support NDT in which only single leg support was used for the duration of the navicular height measurements. These studies selected Single-Limb Stance (SLS) Navicular Drop based on the study conducted by McPoil and Cornwall (1996) who found that the SLS was a better predictor of the foot mobility and function during the mid-stance phase of gait. To conduct the SLS measurements, subjects stand with equal weight-bearing on each foot and the navicular height is measured. The subjects then shift their full weight on just one limb (Shrader et al., 2005) and the difference in the position of the navicular bone is used to determine the SLS ND. Vinicombe et al.(2001) used the SLS ND technique and achieved ICC values ranging from 0.44 to 0.91 for intra-tester reliability and between 0.56 and 0.78 for inter-tester reliability. The authors speculated that the poor reliability results compared to the Double-limb support NDT was likely due to measurement errors resulting from the participants changing their foot posture to maintain their balance during the SLS measurements.

Following on from these studies, Bennett et al. (2001) and Shrader et al. (2005) both used the SLS technique for subjects with foot problems. The study

conducted by Bennett et al. (2001) was for the purpose of identifying the relationship between foot pronation and the occurrence of Medial Tibial Stress Syndrome (MTSS). From the SLS Navicular drop results, a positive relationship was identified between the two. Similarly, the aim of the study conducted by Shrader et al. (2005) was to test the reliability of the NDT measurements for patients with Rheumatoid Arthritis. Both the traditional bipedal stance and SLS Navicular drop techniques were used and the results were compared. Their findings indicated that there was no increase in the Navicular Drop values when the two results were compared. ICC values for inter-tester reliability ranged between 0.85 and 0.96, whereas intra-tester reliability was consistent between three examiners and ranged between 0.90 and 0.98. The similarities in the reported results to the double-limb support Navicular Drop indicate no improvement in the measurement technique and hence the disadvantages were also found to be significant.

2.3.1.3 Sit-to-stand Navicular Drop test (SSNDT)

Another version of the Navicular Drop test was used by Deng et al. (2010) to determine the change in the navicular height between subjects exert 5% WB on their foot while sitting and when standing with 70% - 80% body weight applied on their foot. From their study, the authors found lower than expected intra-tester (ICC = 0.68 – 0.78) and inter-tester (0.72) reliabilities for the SSNDT technique compared to SLS ND measures. The authors speculated the reason to be due to the two Navicular height measurements used to calculate the SSNDT not being perfectly reliable. Although the SSNDT eliminated the need for the testers to place the foot in a Subtalar position and hence improving the intra-tester agreement, errors resulting from having to palpate and mark the navicular bone remained.

2.3.2 Navicular Drift test

Menz (1998) suggested that in order to correctly identify the foot posture, medial-lateral movement of the navicular bone during weight-bearing should also be assessed alongside the sagittal plane movements determined from the ND test. Cornwall and McPoil (1999) confirmed the suggestion made by Menz (1998) when they assessed the navicular bone during movement using an electromagnetic tracking system. This was the motivation behind the development of the Navicular Drift test.

The Navicular Drift test is conducted in a manner which is similar to the BLS Navicular Drop but the only difference is that the change in the navicular bone is measured in the traverse plane after changing the loading on the foot (Figure 2.3).

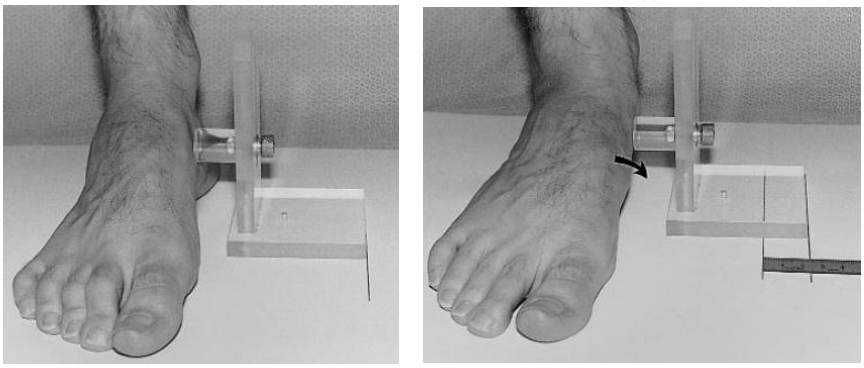

Figure 2.3: Navicular Drift as a result of change in weight-bearing (Menz, 1998).

Similar to the Navicular Drop, the reliability of the Navicular Drift measurements were found to be inconsistent between studies. Vinicombe et al. (2001) obtained intra-tester ICC values ranging from 0.44 to 0.77 with a Standard Error of Measurement (SEM) ranging between 1.75 mm and 2.24 mm. Inter-tester reliability was in the range of 0.32 to 0.53 with SEM ranging between 2.30 and 2.47 mm. These results signified poor results. The mean Navicular Drift measurement was 7 mm ± 3 mm. The authors concluded from these results that the clinicians must practice caution when making informed decisions regarding measurements obtained using the Navicular Drift method.

In another study, Billis et al. (2007) assessed the Navicular Drift on 26 subjects for the purpose of correlating two different foot posture assessment techniques. Each subject's foot was assessed both in single-leg and bipedal stance. One examiner conducted all the Navicular Drift measurements and the mean result was 14.1 mm ± 4.4 mm for single-limb stance and 10.1 mm ± 3.2 mm for bipedal stance. The intra-tester reliability of the Navicular Drift measurements were regarded as good with ICC values ranging between 0.95 and 0.99. However, because only one tester conducted the measurements, inter-tester reliability values were not reported.

2.4 Assessment techniques based on changes in the dorsum bone

2.4.1 Foot Mobility Magnitude (FMM)

The Foot Mobility Magnitude (FMM) was developed by McPoil et al. (2009) in an attempt to incorporate both the sagittal and medial-lateral mobility of the mid-foot in a single test while maintaining a high level of measurement reliability. The main aim of the test was to eliminate the problems identified with the Navicular Drop and Navicular Drift measurements. To achieve this, the FMM replaced measuring the navicular bone with collectively measuring the sagittal and medial-lateral changes in the dorsum of the foot at 50% of the total foot length (FL) during weight-bearing and non-weight bearing. To measure the FMM, the following equation is used:

$$FMM = \sqrt{(AH_{max} - AH_{min})^2 + (FW_{max} - FW_{min})^2} \quad (2.1)$$

Where, AH_{max} is the dorsum height at 50% FL during maximum weight bearing,

AH_{min} is the dorsum height at 50% FL during minimum weight bearing,

FW_{max} is the foot width at 50% FL during maximum weight bearing, and

FW_{min} is the foot width at 50% FL during minimum weight bearing

The selection of the dorsum as a reference point for the FMM measurements was based on the results from a study originally conducted by Williams and McClay (2000). In the study, the authors found that measuring the height of the dorsum under different weight-bearing conditions provided better results than using the navicular bone for the same weight-bearing measurements. It was found that the reliability dropped significantly (from ICC = 0.924 to ICC = 0.565) when the weight-bearing was changed from 10% to 90% when the navicular height was measured relative to the foot length. Measuring the dorsum height provided significantly higher reliability when the weight-bearing was changed from 10% to 90% (from ICC = 0.854 to ICC = 0.848). The dorsum measurements eliminated the need to palpate the navicular bone and hence reduced the inconsistencies between testers for conducting the ND test. This is particularly useful for the 90% weight-bearing condition when it becomes difficult to identify the locations of the bone landmarks as the underlying soft tissue becomes taut with increased weight-bearing acting on the foot. Another advantage of the dorsum measurements is the high validity achieved when compared to radiographs (McPoil et al., 2008b).

To test the reliability and normative values for the FMM, 345 subjects' FMM measurements were collected between 90% weight-bearing and 10% weight-bearing using calipers (McPoil et al., 2009). The results of the study showed that the measurements for the change in dorsum height, change in foot width and the collective FMM measurements demonstrated high intra-tester and inter-tester ICC values. Intra-tester reliability ranged between 0.83 and 0.86 with a Standard Error of Measurement (SEM) ranging from 0.07 mm to 0.13 mm. The inter-tester reliability of the measurements ranged from 0.82 to 0.93 for both the left and right feet of the participants; with SEM values ranging from 0.06 mm to 0.13 mm. Hence the results signified excellent reliability when compared to previous measurement techniques which assessed the changes in the navicular bone. Sheykhi-Dolagh et al. (2014) used the FMM for an application of assessing the influence of three different types of foot orthotics (soft, semi-rigid and rigid) on foot mobility. The study found that the semi-rigid orthotic provided the highest level of foot mobility.

2.4.2 Arch Height Index (AHI)

The Arch Height Index (AHI) is calculated as a ratio of the dorsum height of the foot (vertical height at 50% foot length) to the truncated foot length (distance between the

most posterior point of the calcaneus to the first metatarsophalangeal joint). Figure 2.4 shows the dorsum height as distance D-C and the truncated foot length as distance B-E.

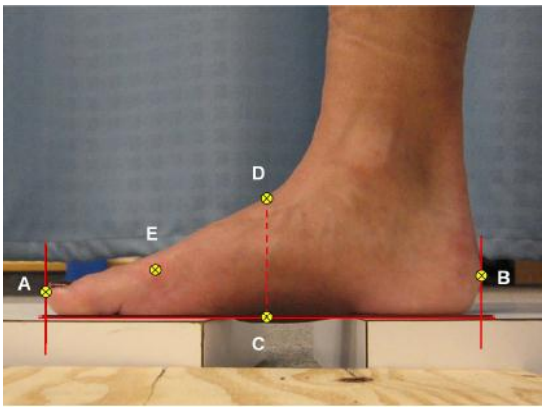

Figure 2.4: Measurements used to determine the AHI (Pohl and Farr, 2010).

The AHI was first used by Williams and McClay (2000) to determine whether normalising a number of bone landmarks on the total foot to the foot length would provide a better estimate of foot mobility. In their study, the navicular height and the dorsum height at 50% FL were normalised both to the total foot length as well as the truncated foot length for each subject during both 10% weight-bearing and 90% weight-bearing. The most reliable results were achieved from the ratio of the Dorsum height to the truncated foot length. Inter-tester reliability values reported were ICC = 0.811 for 10% weight-bearing and ICC = 0.848 for 90% weight-bearing. To obtain concurrent validity of the results, the authors also used lateral radiographs for participants in 10% weight-bearing and 90% weight-bearing stance conditions. ICC values for the agreement between the clinical and radiographic measurements of the AHI ranged from 0.844 to 0.851 for the 10% weight-bearing and 90% weight-bearing stance conditions respectively. Hence it was concluded that measuring the AHI with the dorsum as a reference for the MLA measurements provides better reliability and a better prediction of the behaviour of the MLA under loading than using the navicular bone.

Butler et al. (2008) also assessed the reliability of the AHI for 100 runners (50 males and 50 females) and obtained very high inter-tester (ICC = 0.98 - 0.99) and intra-tester (ICC = 0.96 - 0.99) reliability results. From their study, they concluded that the AHI results are not influenced by gender.

2.5 Assessment technique based on multiple foot components

2.5.1 Foot Posture Index (FPI)

The Foot Posture Index (FPI) was developed to be a multifunctional, visual foot posture assessment tool which was originally developed by Redmond et al. (2001). The first version of the FPI integrated eight variables (FPI-8) that were used collectively to describe the foot using a scoring system. However, the eight variables were eventually reduced to six variables (FPI-6) after revision and the FPI-6 has since been confirmed as a valid, reliable and popular tool for assessing foot posture (Redmond et al., 2008; Keenan et al., 2007; Cornwall et al., 2008).

The six-component foot posture classification criteria are collected with the patient standing in a relaxed stance position with double limb support. The six components are as follows: 1. talar head palpation, 2. supra and infra lateral malleolar curvature, 3. inversion/eversion of the calcaneus, 4. prominence in the region of the talonavicular joint, 5. height of the congruence of the MLA and 6. abduction/adduction of the forefoot on the rear foot. The six classification criteria are shown in Figure 2.5.

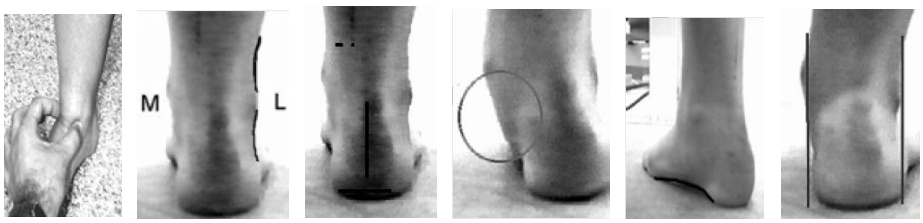

Figure 2.5: The FPI-6 Index components from left to right: talar head palpation, supra and infra lateral malleolar curvature, inversion/eversion of the calcaneus, prominance in the region of the talonavicular joint, height of the MLA congruence and abduction/adduction of the forefoot.

Each of the six observations are graded 0 for neutral arch, a maximum score of +2 for the maximum amount of pronation (low arch) and a minimum score of -2 for the maximum amount of supination (high arch). Therefore a collective score for all the six variables is expected anywhere between -12 and +12. A range from -12 to -1 indicates a supinated foot, 0 to +5 is classified as a normal foot and between +6 and +12 as pronated.

The intra-tester and inter-tester reliability of the FPI-6 was assessed by Cornwall et al. (2008). Although they obtained very high levels of intra-tester reliability for all the measurements (ICC > 0.90), their inter-tester reliability results were found to be only moderate (ICC ranging from 0.525 to 0.655). From the results, the authors indicated that the FPI foot posture assessment is influenced by the

tester's perspective of the measurements. Nielsen et al. (2010) conducted a study to investigate the relationship between the FPI scores and the ND during mid-foot movement. The authors found that the FPI scores were only 13.2% correlated with the dynamic ND results.

Table 2.1 provides a summary of the current foot clinical assessment techniques based on the navicular bone and the dorsum bone measurements. It is clearly identified from the literature review that the foot assessment techniques based on the dorsum measurements provide more advantages than the navicular measurements, particularly in terms of reliability and validity tests.

Table 2.1: Summary of foot assessment techniques for posture and mobility

Method	Equipment used	Authors	Reliability and accuracy	Advantages	Disadvantages
1. Bilateral Navicular Drop	Rulers and calipers	Allen and Glasoe (2000), Brody (1982), Mueller et al. (1993), Nielsen et al. (2010), Sell et al. (1994), Vinicombe et al. (2001), Woodford-Rogers et al. (1994), Williams & McClay (2000).	Inter-class correlations (ICC) for reliability range from 0.33 – 0.97. Validity range from ICC 0.874 – 0.918	Quick and simple to conduct. Does not require costly and complicated measuring equipment	Conflicting reliability, and validity between studies and requires normalising for foot length and gender. Multiple measurement error sources.
2. Single limb stance Navicular Drop	Rulers and calipers	Bennett et al. (2001), Vinicombe et al. (2001), Shrader et al. (2005).	Intra-tester ICC = 0.44 - 0.98 Inter-tester ICC = 0.56 – 0.96	Quick and simple. Does not require costly and complicated measuring equipment. Useful for linking foot problems to posture.	Conflicting reliability and validity between studies. Difficulty for subjects to maintain balance on one foot.
3. Sit-to-stand Navicular Drop	Rulers and calipers	Deng et al. (2010)	Intra-rater ICC = 0.68 -0.78 Inter-rater ICC = 0.72	Quick and simple to conduct.	Only moderate reliability was achieved. No correlation with dynamic gait.
4. Navicular Drift	Rulers and calipers	Andreasen et al. (2013), Billis et al. (2007), Cornwall and McPoil (1999), Jonely et al. (2011), Menz (1998).	Intra-rater ICC = 0.44 – 0.77 Inter-rater ICC = 0.95 -0.99	Allows for measuring medial-lateral mobility.	Inconsistent reliability between studies.
5. Foot Mobility Magnitude (FMM)	Calipers	Cornwall and McPoil (2011), McPoil et al. (2009), Sheykhi-Dolagh (2014).	Intra-rater ICC = 0.83 – 0.86 Inter-rater ICC = 0.82 – 0.93	Incorporates both sagittal and medial-lateral changes. Palpation of bony landmarks not required. High reliability and validity.	Time consuming and labour intensive.
6. Arch Height Index (AHI)	Rulers and calipers	Butler et al. (2008), Teyhen et al. (2009), Williams et al. (2001).	Intra-rater ICC = 0.96 – 0.99 Inter-rater ICC = 0.83 – 0.99	Palpation of bony landmarks not required. High reliability and validity.	Time consuming and labour intensive.

2.6 Conventional static foot measurement techniques

2.6.1 Calipers and rulers

Through the literature review, no single assessment equipment was used for all the studies including comparative studies between authors. This makes comparisons between measurement methods difficult. The current conventional foot measurement techniques use a combination of rulers and calipers to conduct the manual measurements (Figure 2.6). Details on the measurements can be found in De Mits et al. (2010), Cornwall and McPoil (2011) and Pohl and Farr (2010).

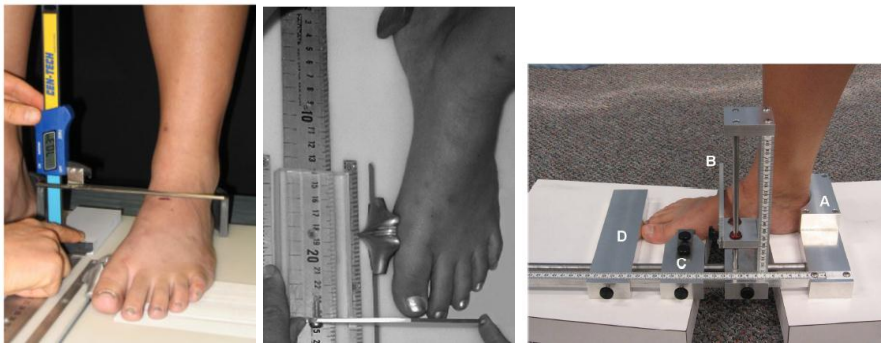

Figure 2.6: Calipers and rulers used to measure the foot. Left: Cornwall & McPoil (2011), middle: McPoil et al. (2008a), right: Pohl and Farr (2010).

2.6.2 Brannock device

The Brannock device (www.brannock.com) is the most common foot measurement technique for developing shoe lasts. It works by placing the foot on the left or right heel cup while a moveable arch length pointer and a moveable width bar are aligned to coincide with the ball joint of the foot (Figure 2.7).

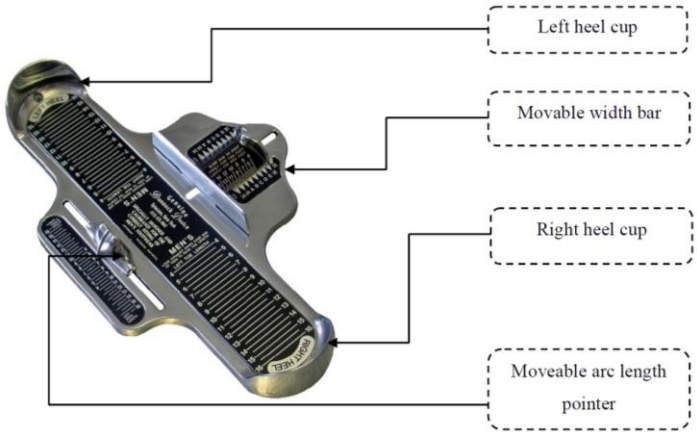

Figure 2.7: Brannock device (Viswanathan, 2013)

Although the device is suitable for most foot measurements, it is not suitable for measuring a person with foot deformity such as subjects with Hallux Valgus (Witana et al., 2006). Therefore, their use is limited to measuring normal subjects' feet, particularly for the manufacturing of shoe lasts or fitting shoes.

2.6.3 Footprint measurements

Footprint measurements involve taking an imprint of the sole of the foot and the contact area with the surface of the imprint is used for the foot classification. A number of indices have been developed to quantify the footprint measurements and these are summarised in Figure 2.8. The two most common indices are the Arch Index (AI) (Onodera et al., 2008) and Footprint Index (Razeghi and Batt, 2002; Reel et al., 2010). Footprint measurements are usually obtained with an ink mat, capacitive mat transducer (Chen et al., 2006) or a mirrored foot photo box (Mall et al., 2007). The disadvantages of the footprint measurements are numerous and include limited information regarding the bony landmarks on the foot, lack of normative values for the measurements and the high cost of capacitive mat transducers and mirrored photo boxes.

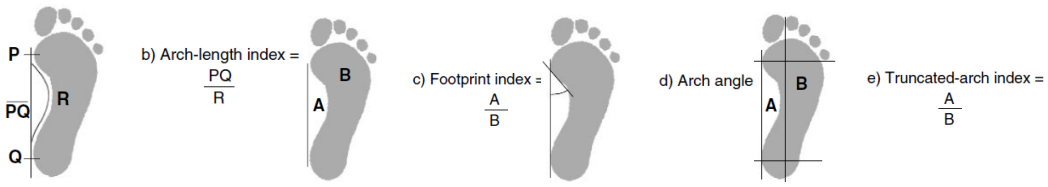

Figure 2.8: Common footprint measurements (Menz, 1998).

2.6.4 Radiographic measurements

Radiographic measurements of the foot are regarded as the 'gold standard' in clinical examination of foot posture prediction as it can directly measure the locations of bony landmarks while the subject is standing in a full weight-bearing position. The commonly derived measurements from radiographs which are used for comparisons with other static foot measurement techniques are shown in Figure 2.9.

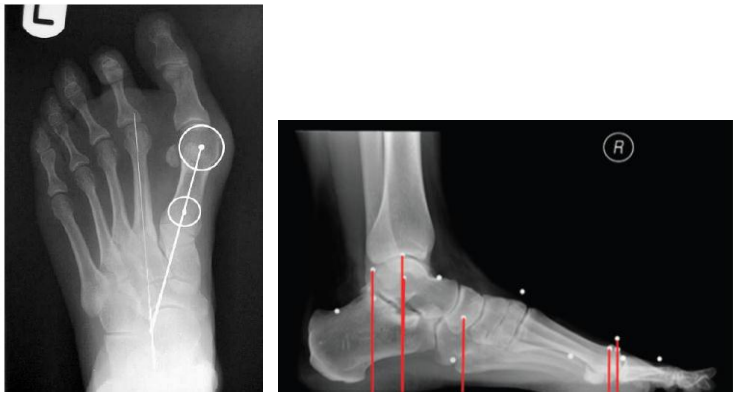

Figure 2.9: Radiographic measurements used to classify the foot arch. Left: (Taylor et al., 2012) and right: (De Mits et al., 2010)

Radiographs have become less feasible in recent years due to time consumption of data collection, expense and the negative effects on health from the radiographic exposure. Radiographs have been used to study the reliability of other foot posture measurement techniques and identify how the techniques correlate with each other (Menz and Munteanu, 2005).

2.6.5 Static 3D foot scanning techniques

In recent years, digital scans in the form of 3D reconstructions of the foot have become popular among foot clinicians and specialists for a number of applications. Some of the applications include footwear manufacturing, insole and orthotic design, surgical planning and intervention, and foot deformity studies (Yu et al., 2008; Kouchi and Mochimaru, 2001; Telfer et al., 2012; Mavroidis et al., 2011; De Mits et al., 2009). This section provides a review of the technologies used to create 3D foot scans with their strengths and limitations.

2.6.5.1 Time-of-flight (ToF) cameras

Time-of-flight (ToF) cameras are active range sensors which are composed of an infrared emitter and a CMOS/CCD sensor housed in a single unit. The emitter illuminates the object with the infrared light and the depth information of the object is determined based on the time-of-flight principle which measures the two-way travel time of the infrared light from the emitter to the sensor (Figure 2.10). Each

pixel in the sensor obtains the depth information and together a depth image is acquired (Castaneda et al.; Cui et al.).

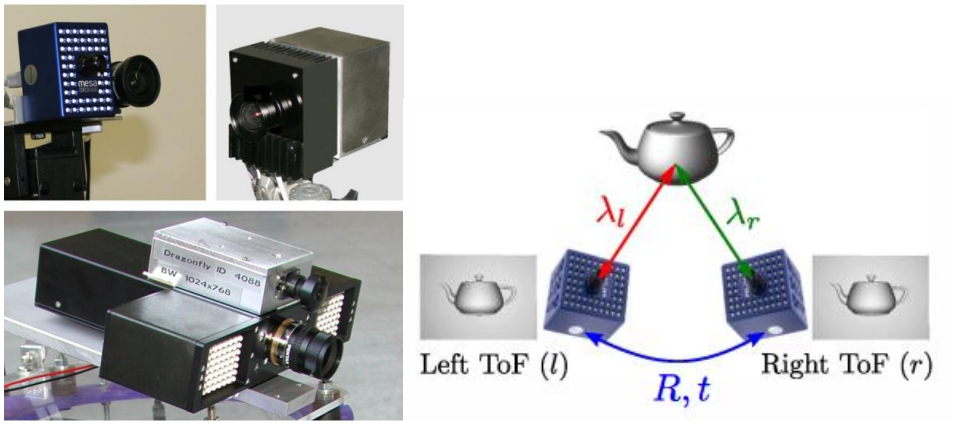

Figure 2.10: left: example of a time-of-flight camera setup (Lindner et al., 2010) and right: two-way travel time of the light travel (Castaneda et al.).

The advantages that time-of-light cameras include their compact size, relative low cost and the fast data acquisition frame rates. However, they have resolutions lower than 320 x 240 pixels (Bartczak and Koch, 2009; Schuon et al.) and different sources of measurement errors. Calibration of the sensors is often complex and time consuming as most of the calibration models developed for the technology can only cover one error source at a time (Lindner et al., 2010). Although the ToF technology has been used for human body scanning (Tong and Kong, 2013; Diraco et al.; Schwarz et al.), only one study was found for the application of foot scanning. In the study conducted by Liu et al. (2011), a housing system with three ToF cameras was used to measure the dorsum and the sole of the foot for foot deformation analysis. However, the study did not include any information regarding the reliability and the validity of the system for accurate 3D foot measurements.

2.6.5.2 Structured light scanning

This type of imaging technique is based on object surface illumination with spatially varying intensity generated by a projector or spatial light modulator. The digital signal which is projected represents the intensity of each pixel on the structured light pattern. The illuminated object is then captured using an imaging sensor and the distortion of the light pattern caused by the geometric shape of the imaged object is recorded (Figure 2.11).

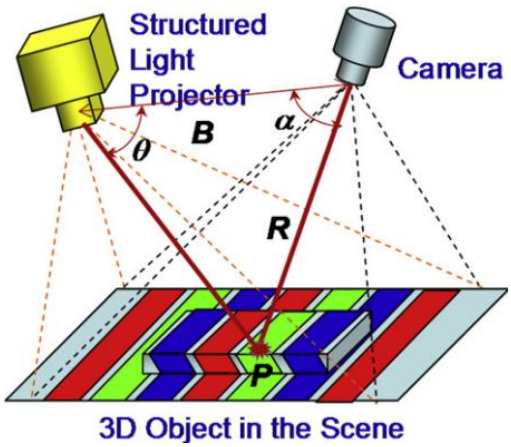

Figure 2.11: Structured light principle (Geng, 2011).

The 3D shape of the object along with accurate 3D profiles of the surface can then be determined by using different principles and algorithms (Ishii et al., 2007; Guan et al., 2003). The illuminated pattern can either be random or structured. Adding a structured light is often referred to as Coded Structured Light (CSL) and allows for a simpler and more efficient solution to 3D surface modelling. The CSL projected can be in the form of a coded sequence or a coloured pattern of stripes (Figure 2.12) which further aids in the object detection (Thabet et al., 2014). There are numerous structured light surface imaging techniques and more details regarding the different options are provided by Geng (2011), Salvi et al.(2010) and Chen et al. (2008).

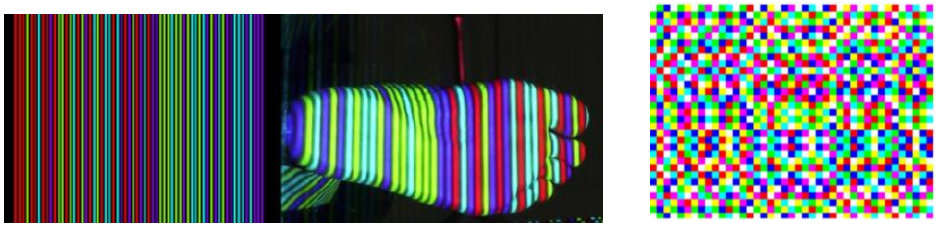

Figure 2.12: Projected Structured Light patters. Left: Coloured stripe pattern (Thabet et al., 2014) and right: random speckled pattern (Chen et al., 2008).

In 2009, Jezeršek and Možina developed high-speed multi camera-laser pairs based on structured lighting to create a 3D foot surface. The authors' motivation for the study was to develop the technique to eliminate the problem of mutual interference between multiple measurement sensors used in structure lighting as it limits the object shape reconstruction to a single-view configuration. The system proved to be an accurate and reliable method for constructing an entire static 3D foot shape. However, the only limitation with the system was its complexity as it requires the use of additional mirrors in order to create a complete 3D model of the entire foot surface.

In similar studies, Ke et al. (2009), Schmeltzpfenning et al.(2011) and Schmeltzpfenning et al. (2009) used the structured light technique to create 3D foot models for different applications. More recently, the accuracy and repeatability of the Coded Structured Light technique for measuring the 3D plantar shape of the foot was tested by Thabet et al. (2014). The accuracy obtained for a static plantar surface of the foot was less than 0.3 mm while the repeatability results had a mean error of 2.4 mm and a standard deviation of 2.1 mm. Although the accuracy of the technique was sufficient for a static plantar foot surface, a 3D model of the entire foot surface could not be achieved and the technique is hence unsuitable for foot anthropometry.

2.6.5.3 Laser scanning

Using range-based laser scanners to create 3D shapes of the foot is the most common technique found in the literature. Laser scanners are typically composed of a laser, an optical system and a sensor housed in a single unit. There are many different manufacturers of laser scanners designed for medical applications including K-Scan (Metris/ Nikon Metrology), Vectra 3D scanner (MedEIM) and FastSCAN (Polhemus). Some of the differences in the laser scanners depend on the measurement technique which can be based either on triangulation or time-of-flight. The difference between the two laser scanning technologies is illustrated in Figure 2.13.

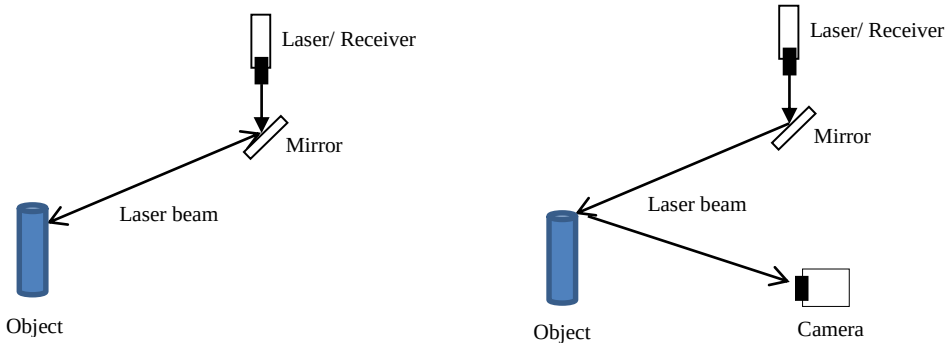

a) Time-of-flight b) Triangulation

Figure 2.13: Laser scanning technology based on a) Time-of-flight and b) Triangulation.

As the name suggests, the triangulation method is based on measuring the location of the laser on the object through triangulation. With the ToF method, the distance is determined by calculating the two-way travel time of the laser from the scanner to the object.

Kouchi and Mochimaru (2001) used an INFOOT scanner to determine the reproducibility of anthropometric foot measurements by comparing the INFOOT measurements to traditional measurement techniques. Although the maximum difference in the measurement was less than 1.5 mm, six out of the seven measurements showed significant differences from a paired t-test statistical analysis.

Luximon and Goonetilleke (2004) used a laser scanner to determine whether a parametric approach to foot shape prediction was suitable from a number of anthropometric measurements on the foot. The errors in the results obtained were 2.1 mm and 2.4 mm for the left and right foot models respectively when compared with measurements from a Brannock device. These errors were identified as a result of the foot movement during scanning as it was not possible to remove the effects of slight movements in the foot during the relatively long duration of the measurements which can take up to 30 seconds.

In a similar comparison analysis tests, Zhao and Goonetilleke used a YETI (Company: Vorum) foot scanner and nine foot dimensions were compared on the scanned foot with manual measurements. The highest measurement variation between the scanner and manual measurements were found in the foot length measurements. This is indicative of measurement sensitivity to changes in the subjects' foot posture for the duration of the scanning. The results obtained for the comparison with manual measurements from Witana et al. (2006) were also significant for eight out of ten measurements. The authors identified that differences were attributed to changes in the geometry of the laser system during scanning which could introduce measurements errors in the order of millimetres. Martedi et al.(2009) identified another problem when studying the 3D sole of the foot from laser scanning. The authors found that the intensity of the skin on the sole of the foot changes with different weight-bearings and hence creates more noise on the 3D data model.

Foot scanning has also been used in foot surface database records. Yu and Tu (2009) used a Gemini 3D foot scanner (Company: ITRI) to obtain a foot surface area database for 135 subjects (Figure 2.14). The resulting measurement errors were all less than 1.0 mm however a limitation was identified in the acquisition rate which takes approximately six seconds to complete a full scan which deteriorates the measurement accuracy.

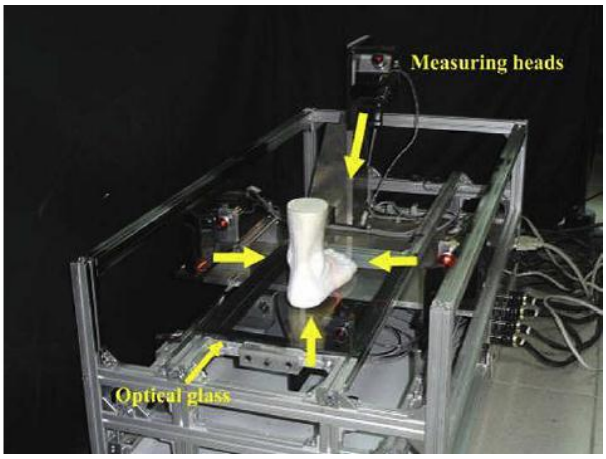

Figure 2.14: The Gemini 3D foot scanner used by Yu & Tu (2009).

2.6.5.4 Moiré technique

The first application of the Moiré technique for human body measurement was conducted by Takasaki (1970) to evaluate the back. Other authors including Madden and Karlan (1979), Xenofos and Jones (1979) and Creath (1988) followed up to study other parts of the human body. In these older studies, the Moiré technology relied on fringe counting for measurements which introduced measurement uncertainties and sign ambiguities. To deal with this issue, a great deal of information regarding the shape of the measured object was required.

More recently, Vecchio et al. (2012) used a variation of the Moiré technology where a phase shifted Moiré projection was applied on a plaster mould of the foot to determine the level of measurement uncertainty. The phase shifting technology used a Moiré pattern that was projected at an oblique angle on the foot mould and shifted digitally (Gomes et al., 2010) while a single CCD camera imaged the foot mould normal to the centre of the mould (Figure 2.15).

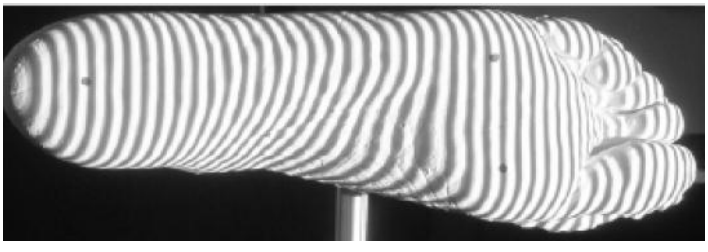

Figure 2.15: The Moiré technique applied on the foot plantar (Vecchio et al., 2012).

Although the current technology had the advantage of automation and fast processing, disadvantages were found for the measurement accuracy test. Measurement errors of 2.0 mm were reported around the MLA and high levels of uncertainties were found in the Z coordinate. This was due to uncertainties with the fringe order and geometric parameters apparent from the phase shifting method.

2.6.5.5 Image-based close-range photogrammetry

Close-range photogrammetry is often defined as the science of deriving the size, shape and location of an object from images sourced from film or electronic media when the imaging sensor is positioned at close range to the object (Atkinson, 1996; Luhmann et al., 2006). The basic principle of close-range photogrammetry relies on the Central Perspective Projection Model geometry. The perspective projection is determined through the transformation of data from a higher dimensional space to a lower dimensional space (Mikhail et al., 2001). A pinhole camera model is then used to model the perspective projection where light rays travel from the object through the 'pinhole' aperture onto the image plane (Figure 2.16 left).

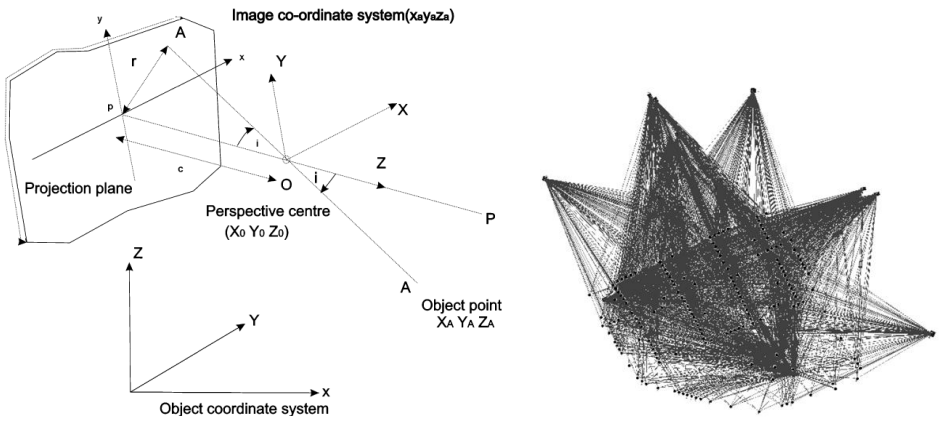

Figure 2.16: The central perspective projection (left) and the multi-camera 3D network configuration (right) of dense image rays (Luhmann, 2010).

The image of the object is then produced through the light intersection with the image plane and the coordinates of the objects are determined through the collinearity condition that exists between the imaged object point, the pinhole model and the image point.

In brief, 3D photogrammetry uses multiple images of an object from multiple views and angles to reconstruct a dense array of points in 3D space which is often referred to as a 'point cloud' (Wong et al., 2008). The 3D dense object points are interrelated by their positional information along an x, y and z coordinate system which allows for the 3D distances along these points to be determined. When a multiple set of images of an object are collected with an imaging sensor, the images are considered a multi-station bundle network. This network provides a high level of

redundancy and reliability for the object coordinates, camera position and camera calibration parameters (Figure 2.16 right).

In addition to the high precision and accuracy of the 3D multi-image photogrammetric technique (below 0.3 mm in recent studies such as Chong, 2012; De Menezes et al., 2010; Luhmann, 2010), several advantages are provided. These advantages include its low cost when compared to other 3D measurement technologies (Chong, 2011; Chong, 2007), non-invasiveness (Rieke-Zapp and Nearing, 2005; Ladeira et al., 2013), instantaneous data capture ability (Wong et al., 2008), ability for data post processing (Luhmann, 2010), and rapid data acquisition capability (Kau et al., 2011; Ladeira et al., 2013).

Although photogrammetry has been found to be a common method in the literature for human body mapping (Kau et al., 2007; Van Loon et al., 2010; Catherwood et al., 2011; Kau et al., 2010), specific applications for foot modelling using this technique are scarce. Kondo et al. used photogrammetry to generate low cost customised virtual 3D foot models by using a number of feature points between images taken from different angles and views using a single camera. The reported average error was 1.1 mm with a standard deviation of 0.23 mm. The error could have been significantly reduced if multiple synchronised cameras were used as it would have reduced the error sources resulting from the involuntary foot movement during imaging.

Luo et al. (2012) used eight cameras to obtain a multi-view of a static foot for constructing customized shoe lasts and reported an accuracy of 2.42 mm for the final barefoot model which was then used to create the shoe last. A trial of the customized shoe lasts indicated a higher level of comfort for volunteers during walking when compared to different generic shoe lasts (Luo and Gong, 2014).

2.6.6 Dynamic 3D foot measurement techniques

As discussed in the previous section, a number of technologies are suitable for static 3D foot scanning measurement applications. However, to be able to understand the complex dynamic foot behaviour, accurate dynamic 3D foot scanning and accurate measurement techniques are required (Ball and Afheldt, 2002a; Ball and Afheldt, 2002b). Most of the existing 3D foot measurement systems use laser scanning technologies which take several seconds to scan the foot which is not feasible for dynamic foot applications.

The earliest work found in the literature where a complete dynamic foot model was achieved was developed by Coudert et al. (2006). In the study, six cameras were setup in three stereo-pairs to image a foot from three different angles and views. A limitation of the study was that the cameras were low speed cameras and they were not synchronised during imaging which caused numerous data gaps in their model.

Kimura et al. (2005) were the first to develop a technique for capturing 3D cross sections of the foot while walking using triangulation between multiple images captured from cameras. As the study was preliminary, there were errors due to camera calibrations and image matching which contributed to low levels of measurement accuracy. The authors then scaled up the project and included more participants in Kouchi et al. (2009). The authors found the measurement error to be significantly higher (1.6 mm) for breadth measurements compared to a minimum error of 0.4 mm for height measurements. In Kimura et al. (2011), the study reduced some of the error sources addressed in Kimura et al. (2005) and validated the results of the developed system by comparing cross-sections on a foot plaster model obtained using a static 3D foot scanner. The average error reported was between 0.23 mm and 0.37 mm.

Yoshida et al. (2012) followed up the study above and provided a summary of the limitations of the technique. The limitations included low measurement frequencies and the inability of the technique to provide complete 3D foot models as only cross sectional information could be achieved. Blenkinsopp et al. (2012) used three stereo-pairs of high speed cameras (250 frame-per-second) to reconstruct a 3D model of the dorsum of the foot during high speed running. The method enabled foot morphology to be assessed but no accuracy information was provided in the study. The limitation of the study was that no complete coverage of the dorsum of the foot could be achieved and the use of additional high speed cameras would be costly in a clinical environment.

Jezeršek et al. (2011) used multiple-laser plane triangulation where three cameras and three laser projectors all synchronised on their own unique wavelengths were used to construct complete 3D scans of the foot. The given calibrated system accuracy was reported as ± 0.5 mm. The only limitation is that the system was not validated using statistical analysis or any cohort of participants. More recently, Novak et al. (2014) conducted a follow up to determine the accuracy of the system for measuring foot dimensions. The system achieved a precision within ± 1.12 mm for both the foot width and foot height and ± 1.73 mm for the girth measurements.

Similarly, Schmeltzpfenning et al. (2011) used structured light with three scanning units comprising of separate cameras and projectors to capture the plantar surface of the foot during five stance phases of gait. Significant differences were observed in five out of seven measurements on the foot. Although the study is promising, it only provided results for unloaded plantar differences and the loaded parts of the plantar surface could not be studied. The measurement frequency was limited to 50 Hz due to the multiple pattern projection technique used in structured lighting. In addition, the authors did not include information regarding the accuracy and repeatability of the system.

To compensate for the low measurement frequency in the study conducted by Schmeltzpfenning et al. (2011), Mochimaru and Kouchi (2011) studied the plantar deformation during walking and running at a measurement frequency of 200HZ. A single high-speed camera and a projector were utilised. As only one camera was used, a complete 3D shape of the foot was not obtained. In addition, the study did not provide any data regarding the accuracy of the technique. More

recently, Thabet et al. (2014) used the structured light technique to reconstruct the plantar surface of the foot over two trials for 27 subjects. The difference in the foot reconstruction from the two trials was found to be 2.8 mm ± 1.1 mm. The average error computed over five reconstruction sequences was reported as 3.0 mm with a range varying between 0.5 mm to 7.0 mm.

Liu et al. (2011) used three Time-of-flight (ToF) cameras to determine foot deformation from dynamic 3D models. The deformation was determined using the point set registration technique for consecutive image frames provided by Myronenko and Song (2010). Samson et al. (2014) also used the ToF technology with three cameras to investigate the behaviour of the foot during dynamic foot roll-over. The intra-class correlation (ICC) between trial reliability was greater than 0.88. Unfortunately no accuracy and validity assessments were provided for the study and the accuracy assessment is necessary if the technique is to be used for high accuracy measurement applications (Samson et al., 2012). A major drawback of the ToF method is reported as the time consumption required for the 3D reconstruction (Samson et al., 2014). A summary of the static and dynamic 3D measurement technologies with their accuracy capabilities, advantages and disadvantages is provided in Table 2.2.

Table 2.2: Summary of static and dynamic 3D foot measurement technologies

Technology	Authors	Accuracy	Advantages	Disadvantages
1. Time-of-flight (ToF) cameras	Liu et al. (2011), Myroneko and Song (2010), Samson et al. (2012), Samson et al. (2014).	Between-trial reliability ICC better than 0.88.	• Compact size. • Relatively lower cost than other scanning technologies. • Fast data acquisition rates. • High accuracy.	• Time consuming data processing. • High cost. • Low resolution. • Numerous sources of measurement errors • No validity and accuracy information for foot applications.
2. Structured light scanning	Jezeršek and Mozina (2009), Jezeršek et al. (2011), Ke et al. (2009), Novak et al. (2014), Schmeltzpfenning et al. (2009), Schmeltzpfenning et al. (2011), Thabet et al. (2014).	Static accuracy = 0.5 mm. Precision range = 1.12 mm – 1.73 mm for foot anthropometry. Repeatability = 2.8 mm ± 1.1 mm. Average error = 3.0 mm	• High accuracy for static foot scanning.	• Complex system. • Complete 3D foot shape reconstruction not possible. • High cost.
3. Laser Scanning	Kouchi & Mochimaru (2001), Luximon & Goonetilleke (2004), Zhao & Goonetilleke (2006), Witana et al.(2006), Martedi et al. (2009), Yu and Tu (2009).	Accuracy range = 1.5 mm – 2.4 mm for static foot. Std. dev. range = 4.7 mm – 13.1 mm.	• Quick. • Portable.	• High cost. • Relatively long measurement duration. • Not appropriate for dynamic applications. • Not suitable for changes in foot weight-bearing
4. Moire technique	Vecchio et al. (2012)	Errors greater than 2 mm.	• Automation. • Fast processing.	• Low measurement accuracy. • High levels of uncertainties in the z coordinate.
5. Image-based close range photogrammetry	Blenkinsopp et al. (2012), Coudert et al. (2006), Kimura et al. (2005), Kondo et al. (2007), Kouchi et al. (2009) Luo et al. (2012), Luo et al. (2014), Yoshida et al. (2012)	Accuracy range = 0.3 mm – 1.6 mm. Error range = 0.23 mm – 0.37 mm.	• High precision and accuracy. • Low cost. • Non-invasiveness. • Instantaneous data capture ability. • Post processing capability. • Rapid data acquisition.	• Requires camera synchronisation for dynamic applications.

2.7 Identified research gap and conclusion

A review of the conventional clinical foot posture and mobility assessment techniques was provided in this chapter. Although these conventional clinical techniques were found to be simple to conduct, their main limitation is their inability provide an accurate representation of the mobility and deformation of the foot during dynamic activities such as gait. Hence a gap was identified in the literature where accurate correlations between static and dynamic measures of foot deformations and mobility have not been established.

This thesis aims to bridge this gap by comparing measurements from conventional static clinical measurements based on the dorsum as a point of reference with the same measurements during gait by using a novel high accuracy 3D measurement system. The dorsum was selected as the point of reference for the measurements due to its higher reliability and validity when compared to the navicular bone measurements (Butler et al., 2008; McPoil et al., 2008b; McPoil et al., 2009; Williams and McClay, 2000).

A number of techniques can be used to obtain accurate 3D measurements of the human foot. These techniques are: 1) time-of-flight (ToF) cameras, 2) structured light scanning, 3) laser scanning, 4) Moiré technique and 5) image-based close range photogrammetry. As a result of the outlined advantages of the close-range photogrammetric technique provided in this chapter which outweigh the disadvantages, this technique is developed for the application of the dynamic assessment of the foot during gait. Details of the design and development of the close-range photogrammetric technique for the foot gait analysis are provided in the next chapter.

Chapter 3: Design of an accurate 3D image-based system for dynamic foot measures

3.1 Introduction

This chapter provides details of the design and development of the close-range photogrammetric technique which will be used for accurate 3D dynamic foot anthropometry to achieve the aim and objectives outlined in Chapter 1. The chapter begins with a theoretical background of the concepts used for constructing 3D models from 2D images. The concepts include the perspective projection, imaging sensor geometries, least squares estimation, and sensor calibrations. The different components of the designed dynamic photogrammetric system are illustrated and an initial testing of the capability of the developed system is investigated. The final part of the chapter includes a discussion of the capability of the developed system and the expected research contribution that can be achieved from its use.

3.2 Theoretical background

Photogrammetry is a technique used to derive accurate 3D sizes, shapes and locations of objects from 2D images sourced from film, digital sensors or video sensors (Luhmann, 2010). The application of video sensors allow for accurate modelling of dynamic complex objects (Cai, 2013; Brilakis et al., 2011; Paulsen et al., 2011). When multiple video sensors are used to record a dynamic scene, it becomes essential to synchronise the sensors to record the exact position on the object and minimise errors associated with motion artefacts (Hobbs et al., 2007; Leifer et al., 2011; Johnson et al., 2009).

3.2.1 The collinearity condition

A functional model known as the Central Perspective Projection (CPP) is used in close-range photogrammetry to determine the relationship between the coordinates of points on the object space (X,Y,Z) and the projection of the same points on the image space (x,y,z) (Mikhail et al., 2001). The Central Perspective Projection model consists of a projection plane (PP) which is the reference frame of the camera and a perspective centre (O) which is used to project the 3D object space points to the projection plane and the object space. An idealised ‘pinhole’ camera is used to describe the principles of the CPP model (Figure 3.1). Light rays travelling in a straight line connect the object point (X_B,Y_B,Z_B) to the projection plane by passing through the small aperture of the pinhole camera (O). Another line which is

orthogonal to the principle point (P) on the projection plane is used to define the principal distance (c).

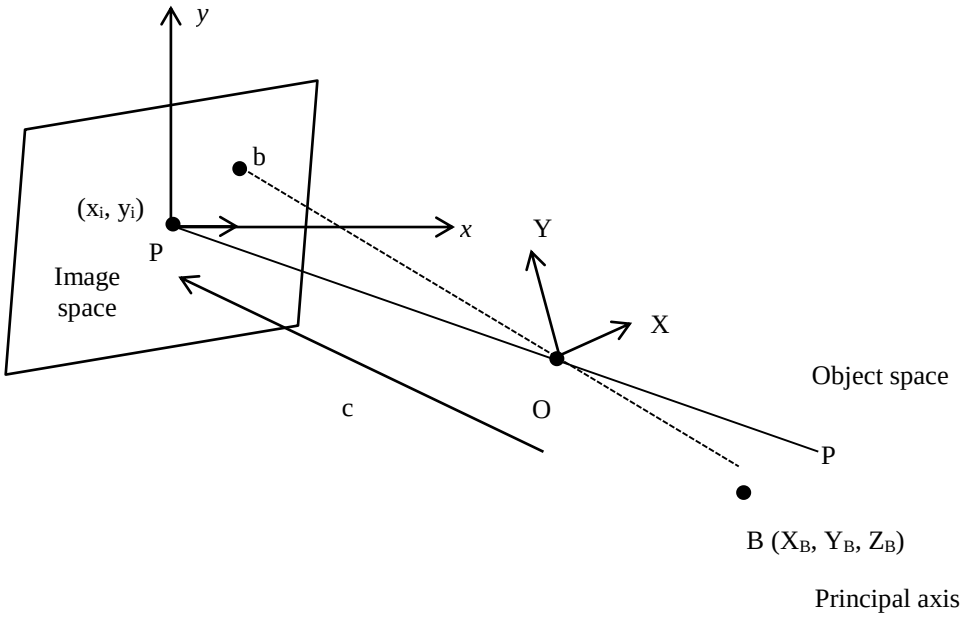

Figure 3.1: The Central Perspective Projection model.

The camera parameters used to reconstruct the bundle of rays relative to the object space from the image points are known as the interior orientation parameters. These parameters consist of: a) the perspective centre position, b) the principal distance, c) the principal point position (x'_i, y'_i) relative to the image plane's reference system and d) the lens distortion parameters (Δx and Δy). Any distortion in the lens alters the ideal central projection and hence need to be determined and accounted for. There are two types of lens distortion namely; radial lens distortion (δr) and tangential lens distortion (Δx and Δy).

Radial lens distortion is a result of the radial displacement of an imaged object from the principal point (Vass and Perlaki, 2003). The magnitude of radial distortion varies with the radial distance and is dependent on changes in the focus of the camera lens. A Gaussian radial distortion graph is used to depict the relationship between the radial distortion and the radial distance (Figure 3.2).

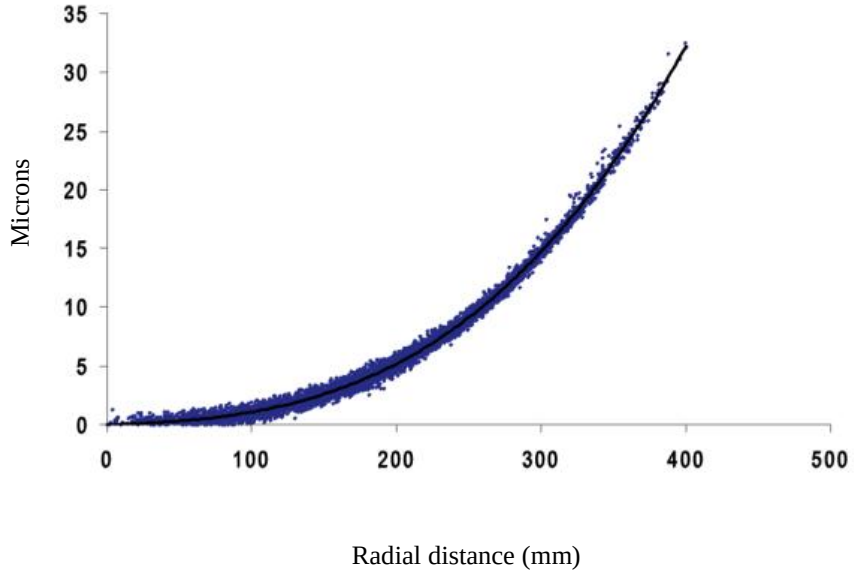

Figure 3.2: Typical radial lens distortion curve (Hartley and Kang, 2007).

The radial distortion (δr) which is measured in millimetres is modelled by using the following polynomial relationship:

$$\delta r = K_1 r^3 + K_2 r^5 + K_3 r^7 + \ldots \quad (3.1)$$

Where, K_1, K_2, K_3 are the radial distortion coefficients corresponding to infinity focus and,

r is the radial distance in millimetres which is calculated in Equation 3.2 as:

$$r = [(x_o - x_i)^2 + (y_o - y_i)^2]^{1/2} \quad (3.2)$$

The tangential lens distortion is a result of any vertical or rotational displacement of the lens elements within the objective. Brown (1971) developed a function to compensate for the tangential lens distortion (Δx, Δy) on an image point that is represented by x, y:

$$\Delta x = P_1 (r^2 + 2(x_o - x_i)^2 + 2P_2 (x_o - x_i) (y_o - y_i) \quad (3.3)$$

$$\Delta y = P_2 (r^2 + 2(y_o - y_i)^2 + 2P_1 (x_o - x_i) (y_o - y_i) \quad (3.4)$$

Where, P_1 and P_2 are the coefficients of the decentring distortion at infinity focus, and

r is the radial distance.

In order to solve the transformation of the object coordinates (X, Y, Z) into corresponding image coordinates (x, y, z), it is essential to determine the exterior orientation parameters for object transformations. This consists of six parameters which define the orientation and position of the camera coordinate system with reference to the object coordinate system (Luhmann et al., 2006). These parameters comprise of three projection centre coordinates (X_0, Y_0, Z_0) and three parameters around the three axes (ω, φ, κ). A set of equations; known as the collinearity equations (Equations 3.5 and 3.6) are then used to link the interior orientation and the exterior orientation parameters.

$$x_a = x_p - c\frac{[r11\,(XO-XA)+r12\,(YO-YA)+r13\,(ZO-ZA)]}{[r13\,(XO-XA)+r32\,(YO-YA)+r33\,(ZO-ZA)} + \Delta x \quad (3.5)$$

$$y_a = y_p - c\frac{[r21\,(XO-XA)+r22\,(Y0-YA)+r23\,(ZO-ZA)]}{[r31\,(XO-XA)+r32\,(YO-YA)+r33\,(ZO-ZA)} + \Delta y \quad (3.6)$$

Where, x_p and y_p represent the position of the offset principal point, and

Δx and Δy represent the lens distortion parameters.

3.2.2 Bundle adjustment

The main principle used to produce 3D coordinates in photogrammetry is triangulation. When multiple cameras are used to image an object from different convergent views, a multi-image triangulation is achieved. This produces line convergences in the image space which can be used to solve for the point in the object space. A bundle adjustment is a method used to simultaneously determine the 3D object coordinates, the camera calibration parameters, orientation of the images, and accuracy and reliability information through the process of triangulation in a single 'bundle' (Triggs et al., 2000; Luhmann et al., 2006).

The bundle adjustment computations are determined through a least squares estimate (Brown, 1976; Granshaw, 1980) which is used to determine the best possible agreements between the measurements and their residuals with the definite model (Cooper and Robson, 2001). The bundle adjustment technique is the most accurate, powerful and flexible technique used in photogrammetry due to the large number of degrees of freedom resulting from the large number of elements that are combined in the same calculation (Luhmann et al., 2006).

3.2.3 Photogrammetric system design considerations

When designing a photogrammetric system for a specific application, a formal framework must be followed to meet the specifications of the task. The type, location and accuracy requirement of the data are the minimum information necessary to initiate the photogrammetric design process. The type of data might be the determining factor for the type of imaging sensor selected. For instance, the requirement to measure a dynamic object would require utilising video-based imaging sensors. The project accuracy requirement, object size, and coverage may

then further influence the type of imaging sensors required. The number of cameras, camera geometry, image resolution, lens stability, and the type of imaging lens collectively impact the final project accuracy.

3.3 Design requirements for dynamic foot measurements

The main requirements for the practical work in this thesis include the design of an accurate image-based measurement tool to study the 3D dynamic changes in the foot during gait. The next sections will detail the design, assembly and calibration of the close-range photogrammetric system. The practical requirements for the designed measurement system for this project are as follows:

1. Ability to measure dynamic 3D anthropometric measurements of the foot.
2. Ability to achieve a high level of dynamic object measurement accuracy.
3. Ability to capture the foot from the medial, lateral, dorsal, anterior and posterior positions using multiple stereo and convergent images.
4. Ability to incorporate and synchronise ground reaction force data during imaging.
5. Be easy to setup.
6. Be a low cost solution.

3.3.1 Network design optimisation

To achieve high measurement accuracies from a photogrammetric system, planning and optimising the network design is a crucial requirement. Some of the most important design requirements that need to be addressed include the selection of number and type of imaging sensors, geometry and location of imaging sensors and density, target size and distribution of project control.

3.3.1.1 Choice of imaging sensors

As the main design requirement is to develop a photogrammetric system that can be used to measure a dynamic scene to a high level of accuracy, instantaneous records from multiple video-based sensors are required. For this purpose, High Definition (HD) JVC Everio GZ-HD500 video camcorders were selected. These camcorders provided the most cost-effective solution for high quality video recording and large internal memory storage capability. The camcorder specifications are listed in Table 3.1.

Table 3.1: JVC Everio GZ-HD500 camcorder specifications

Imaging sensor	1/5.8” 1.37 Megapixel CMOS
Pixel size	1.1 µm
Focal length	3.0 mm
Format size	1920 x 1080 pixels (5.17 x 2.91 mm)
Internal memory	80 GB

3.3.1.2 Gait imaging platform

An elevated imaging platform was designed and constructed to allow subjects to walk at a natural pace while the camcorders are setup around the platform to image the foot from the medial, lateral, dorsal, anterior and posterior sides simultaneously. The platform is elevated one metre from the ground and has a length of 4000 mm and a width of 1500 mm. Access to the platform is provided through a staircase with railings installed around the staircase and the platform to provide support and safety during the gait trials.

To continuously record the ground reaction forces acting under the foot during gait, an AMTI (Advanced Mechanical Technology Inc.) force plate was installed in the centre of platform. The force plate data were recorded on an office computer using the proprietory software NetForce AMTI (A-Tech Instruments Ltd.) A schematic diagram with the plan view of the imaging system is provided in Figure 3.3.

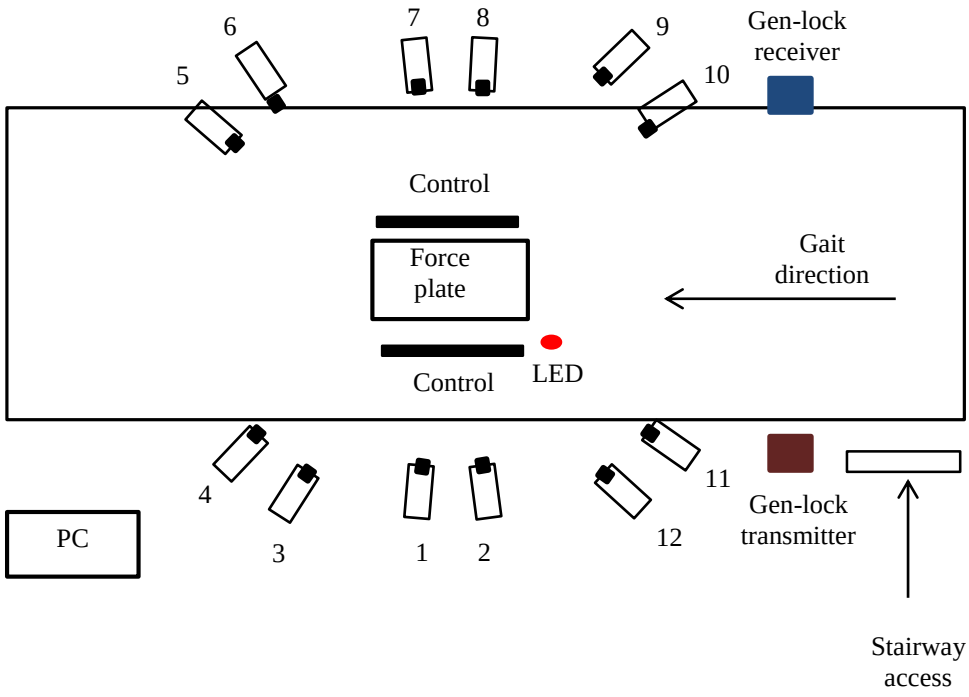

Figure 3.3: Schematic of gait platform.

3.3.1.3 Camcorder numbers and positions

The choice of the number of imaging sensors used in any photogrammetric project is dependent on the object coverage which requires sufficient overlapping correspondences between the images (Barazzetti et al., 2010). The optimal overlap strength between images is usually 55% - 60%. To simplify the network configuration design and to provide a first approximation of an optimal sensor configuration, a 'generic' network is generally used (Fraser, 1996). According to Mason (1995), a four-station network with a strong level of convergence is a suitable initial approximation and was used in this project. As it was a requirement for the foot to be imaged from the medial, lateral, dorsal, anterior and posterior positions, 12 camcorders were necessary to obtain the four-station network from each view point. The locations of the 12 JVC Everio GZ-HD500 camcorders were selected as shown in Figure 3.3.

The camera to object distance was determined through a number of factors which were reported by Saadatseresht et al. (2005). These factors include the image scale, image resolution, field of view, number of control points, and number of image points. The maximum allowable camera to object distance (d_{max}) was determined through Equation 3.7:

$$d_{max} = \frac{\bar{\sigma} c \sqrt{k}}{q \sigma} \tag{3.7}$$

Where, $\bar{\sigma}$ is the object point's coordinate standard errors,

σ is the image point coordinate standard errors,

c is the camera principal distance,

k is the average number of exposures at each camera station, and

q is the factor of the camera station configuration strength.

From Equation 3.7 the maximum allowable distance determined for this project was 850 mm. The values for q and k were representative of a strong network geometry and were selected as q = 0.7 and k = 1 (Fraser, 1996). A minimum camera to object distance of 750 mm was selected to provide sufficient coverage of the force plate, the foot anthropometric targets and the control targets placed around the force plate. The convergence angle between cameras was selected as 45 degrees with distances between camera pairs specified at 200 mm to achieve the appropriate overlap percentage between images.

To achieve the camcorder configurations, custom-built camera mounts were attached to the sides of the imaging platform in the positions shown in Figure 3.3. The custom-built mounts consist of an aluminium bar with predefined base distances where the distance between the centres of the camera lenses can be adjusted according to the project requirements (Figure 3.4).

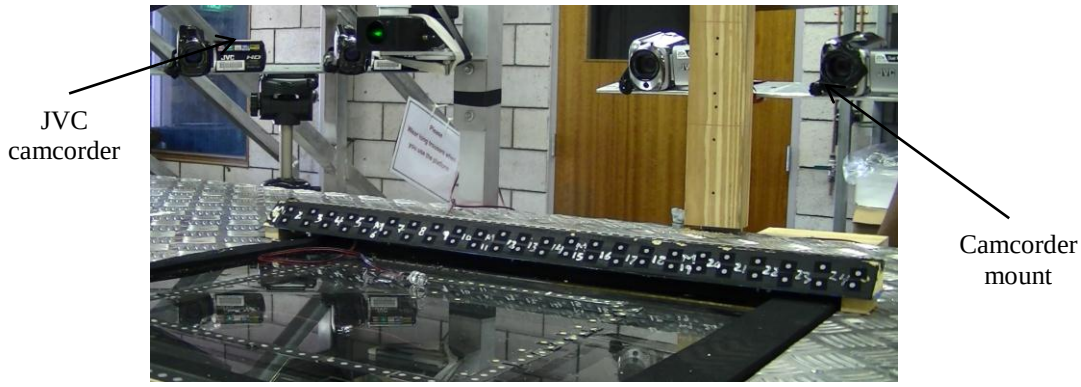

Figure 3.4: Position of the camcorders on the custom-built camcorder mount.

The camcorders were labelled JVC 1 to JVC 12 and were setup in the same position each time the gait trials were conducted. A schematic diagram of the convergent camera pair setups achieved through the camcorder configurations used to image the foot is shown in Figure 3.5.

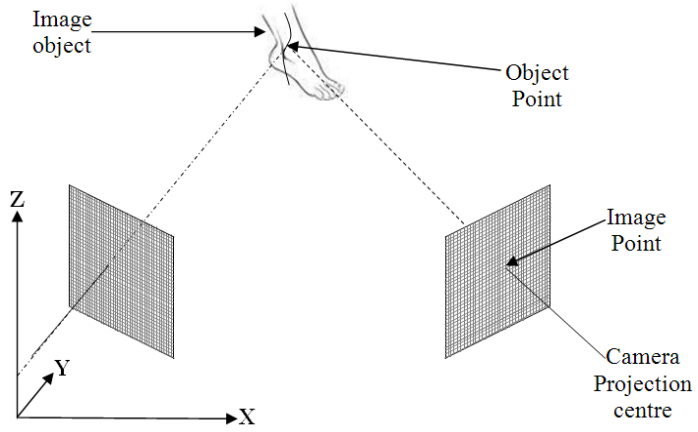

Figure 3.5: Convergent overlapping-pair photogrammetric configuration.

3.3.1.4 Control target design

A wooden wedge was positioned on each side of the force plate and 52 control targets with five millimetre diameters were added on each wooden wedge in two rows of 26 retro-reflective targets (3M Scotchlite Minnesota, USA) as shown in Figure 3.6.

Figure 3.6: Control targets around the force plate.

Additional control targets were also added on the surface of the force plate to strengthen the network geometry for improved accuracy of the 3D measurements. The wooden wedges were painted matte black to provide the best level of contrast for the retro-reflective targets. The selection of circular 5 mm targets for the control points was to meet the requirement of the automated point digitisation process in the software Australis (Photometrix Pty. Ltd., Victoria, Australia) which was used for all the 3D object measurements and camcorder calibrations. A maximum of 40 pixels can be specified in the centroid window of the software Australis when completing the automated digitisation process.

3.3.1.5 Camcorder synchronisation

To synchronise the camcorder images and the force plate data, a generator-locking (gen-lock) device was custom-built to trigger an LED light as soon as the subject's foot landed on the force plate. The gen-lock system consisted of a transmitter and a receiver which were setup opposite to each other on the platform (Figure 3.7).

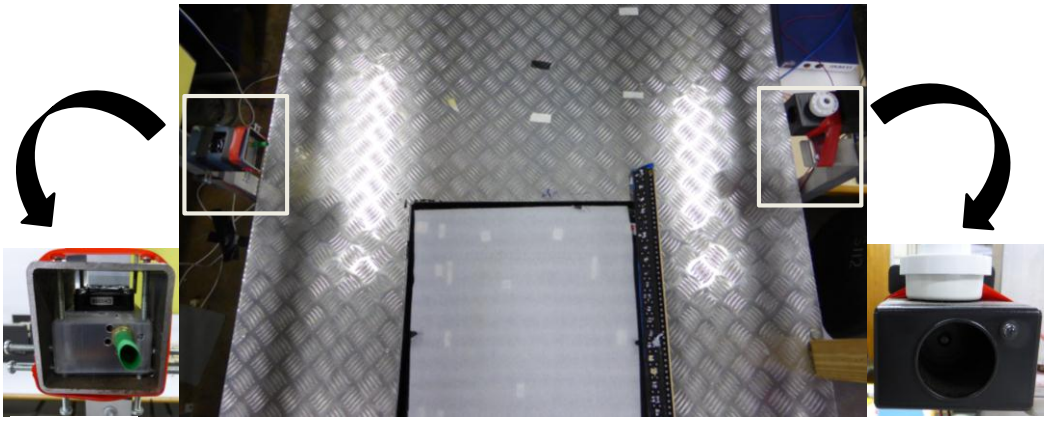

Figure 3.7: Gen-lock system set-up.

A laser is constantly emitted from the transmitter to the receiver and once the laser signal is intercepted when the subject crosses the path of the laser (during heel strike), the LED light is activated (Figure 3.8).

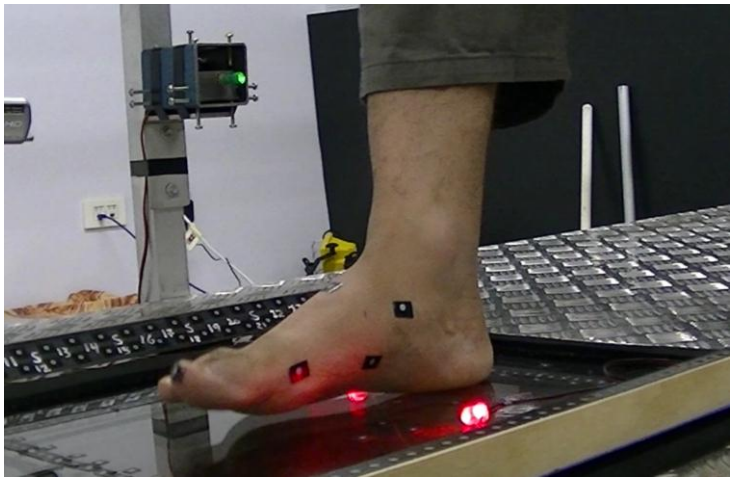

Figure 3.8: Gen-lock LED light activated at heel-strike.

The AMTI Netforce software settings were altered to automatically identify the external trigger source of the gen-lock device and start recording the force information as soon as the gen-lock was triggered.

3.4 Methods

Prior to using the designed system for data collection, all the necessary calibrations had to be completed. The system calibration process involved individual calibrations of the 12 HD JVC Everio HD500 camcorders and the calculation of the 3D coordinates of the control targets on the wooden wedges. The calibration methods will be discussed in the following sections.

3.4.1 Calibration of the designed system

3.4.1.1 Camcorder calibration

The test-field used to calibrate the camcorders consisted of a grid of 10 rows and 10 columns of steel pins (100 pins in total) which were attached to a polycarbonate board with 12 mm thickness. The pins had different elevations ranging from 10 mm to 60 mm above the surface of the board and retro-reflective targets with 5 mm diameters were attached on each pin. The RMS tolerance specified for the target coordinates were 0.05 mm across the X, Y and Z axes for each of the camcorders (Fraser, 1996).

Each individual camcorder was mounted on a tripod at a distance of 750 mm and at a convergent angle of 60 degrees from the test field. To maintain the camcorder distance to the test field throughout the calibration, the position of the tripod was maintained while the calibration test field was setup on a custom-built bar with a pivot point in the centre. The test-field could then be attached to the pivot point through a hole in the centre of the test-field and rotated freely around its axis. To provide accurate scaling dimensions during the camera calibration, an invar scale-bar with ±11 μm at 15°C factory calibration accuracy was positioned in the centre of the test field as shown in Figure 3.9.

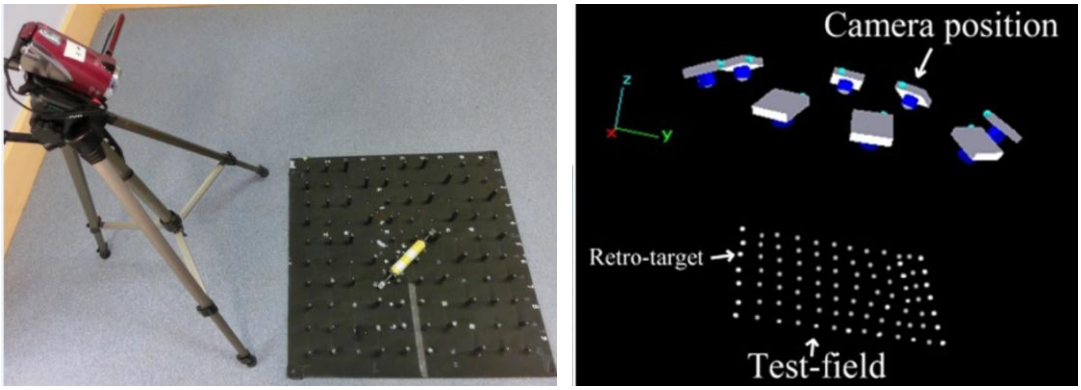

Figure 3.9: the camera calibration device setup.

The test-field was rotated multiple times to allow for 12 convergent, one-second video sequences (ten upright, one rotated 90° to the left and one rotated 90° to the right) to be recorded from different views. A total of four sets were recorded for each camera to improve the reliability of the measurements. The video sequences were then frame-grabbed using Tipard HD (Tipard Studio) video converter software (version 6.1.12) and converted to still images using the software Virtual Dub (version 1.6.15).

3.4.1.2 Calibration of the project control

To calculate the coordinates of the designed imaging system control targets, four sets of 16 convergent images were collected using a high resolution Sony Cybershot F828 still camera with the specifications listed in Table 3.2. The camera to object distance was maintained at 750 mm.

Table 3.2: Sony Cybershot F828 camera specifications

Imaging sensor	2/3” 8.0 Megapixel CCD
CCD pixel size	2.7 μm
Focal length	7.1 mm
Format size	3264 x 2448 pixels (8.8 x 6.6 mm)

An invar scale bar and an orientation device were setup in the centre of the control targets around the force plate (Figure 3.10).

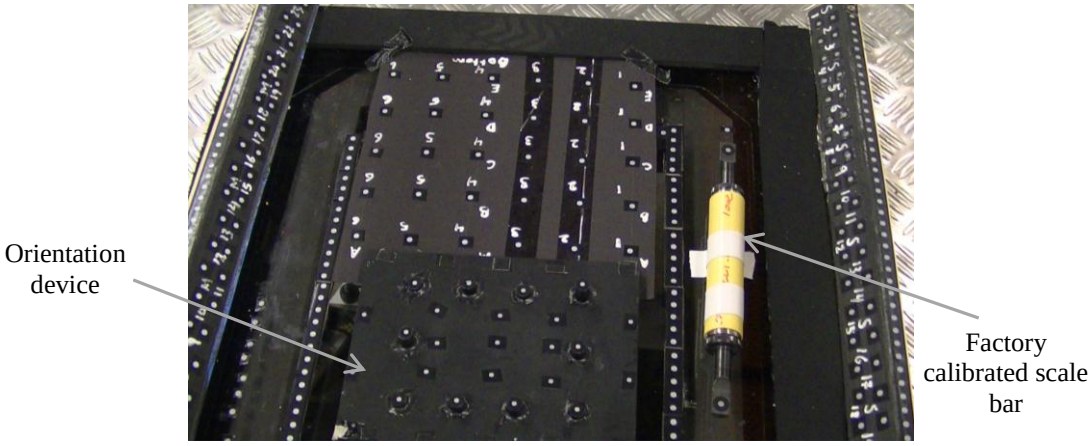

Figure 3.10: Setup for the project control calibration.

For each set of images, the control targets were digitised on each image using Australis and the bundle adjustment algorithms were used to determine the 3D coordinates of the new control targets.

3.4.2 Designed system accuracy testing

To validate the accuracy of the measurements obtained using the developed dynamic foot measurement system, a mannequin was used. As the mannequin is stationary, errors associated with human subject movement are eliminated. Seven retro-reflective targets were attached on the mannequin foot as shown in Figure 3.11.

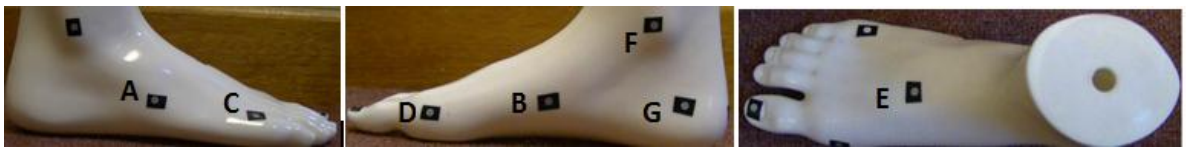

Figure 3.11: The location of the seven retro-reflective targets of the mannequin foot.

Two 5 mm targets were positioned on the lateral side of the mannequin foot (A and C); four were positioned on the medial side (B, D, F and G) and target E was placed on a location simulating to the dorsum of the foot. The locations of the seven anthropometric marks were selected as they represent similar locations of the landmarks that will be placed on the subjects' feet during the human gait trials.

3.4.2.1 High accuracy mannequin convergent data capture

A pre-calibrated orientation device was used to determine the coordinates of the seven mannequin targets based on the bundle adjustment technique. A scale bar (±11 μm at 15°C factory calibration accuracy) and additional control targets were used to provide additional control for the measured dimensions to strengthen the bundle adjustment calculation (Figure 3.12).

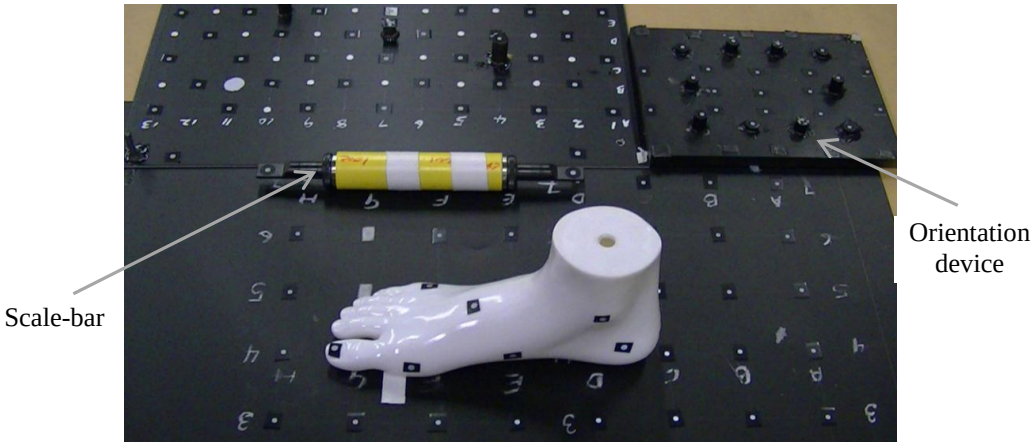

Figure 3.12: The setup used for coordinating the marks on the mannequin foot.

The mannequin foot was placed within the control targets and the calibrated, non-retractable lens Sony Cybershot F828 camera was used to capture 16 highly convergent images of the orientation device, the additional control targets, the scale bar and the mannequin foot from different angles and views. The camera to mannequin distance was maintained at 750 mm for all the images. The bundle adjustment technique was then used to determine the seven unknown coordinates and consequently seven distances on the foot mannequin. Four convergent imaging sets were collected and the results averaged.

3.4.2.2 Investigating the developed dynamic system accuracy

The mannequin foot was positioned on the elevated imaging platform as shown in Figure 3.13. The 12 JVC camcorders were setup in four three-camera configurations and were used to simultaneously record video sequences of the static mannequin foot. Four video imaging sets were recorded and the camcorders were switched off between sets. The seven distances on the mannequin foot were determined using a bundle adjustment calculation.

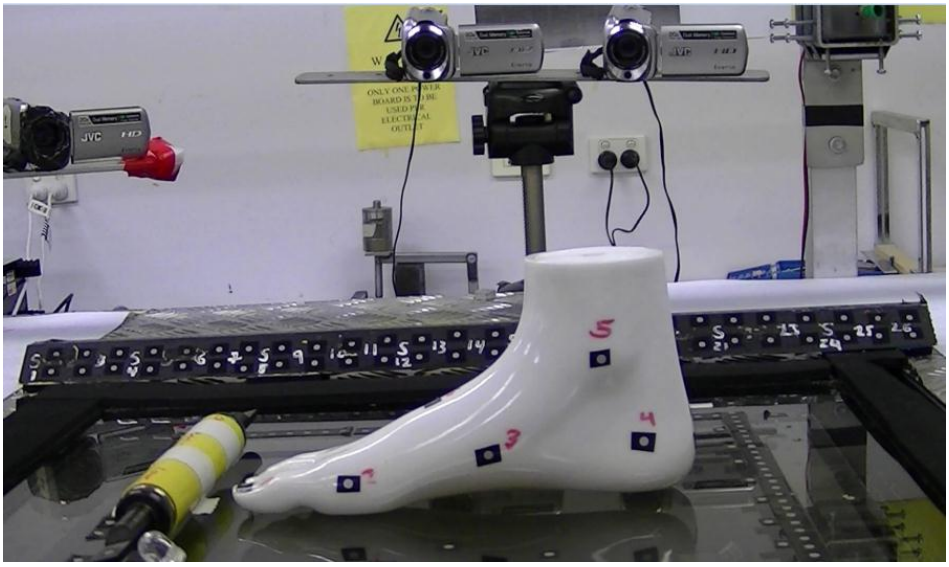

Figure 3.13: The mannequin foot position on the imaging platform.

3.5 Statistical analysis

The designed photogrammetric system precision was determined through Mean Absolute Differences (MAD) which were calculated across each data set. The MAD is the mean of the absolute differences between the values of two sets of measurements (Wong et al., 2008; de Menezes et al., 2010) and is determined using:

$$MAD = \frac{\Sigma\,|xi - \bar{x}|}{n} \tag{3.8}$$

Where x_i is the data value for the observation, $i = 1,2,3,\ldots n$.

$\bar{x}$ is the mean, and

n is the number of data values.

The random errors which are resultant from measurement variability when the same conditions are maintained during the measurement sessions were determined through the Technical Error of Measurements (TEM) and calculated using:

$$\text{TEM} = \sqrt{\left[\frac{(\Sigma D^2)}{2n}\right]} \tag{3.9}$$

Where, ΣD^2 is the summation of deviations between each couple of replicate measurements, and

n is the number of data pairs (de Menezes et al., 2010).

Paired Student's *t* tests were used to compare the systematic error between the replicate measurements and $p < 0.05$ was used to assess statistical significance. The systematic errors are a result of the effect of bias from the environment of data collection or measuring instruments and methods (Cooper and Cross, 1988).

3.6 Results

3.6.1. Initial camcorder calibration evaluation

An initial camcorder calibration evaluation was conducted for three of the JVC camcorders and the residual mean square (RMS) of the target coordinates across the three axes were calculated and listed in Table 3.3. The effect of increasing the number of images used in the camera calibration on the RMS results was also reported.

Table 3.3: The effect of increasing the number of images from the JVC Everio camcorders on the RMS across the X, Y and Z axes

Number of images	**JVC 1**			**JVC 2**			**JVC 3**		
	X (mm)	**Y (mm)**	**Z (mm)**	**X (mm)**	**Y (mm)**	**Z (mm)**	**X (mm)**	**Y (mm)**	**Z (mm)**
6	0.019	0.019	0.040	0.022	0.021	0.041	0.029	0.027	0.063
7	0.020	0.019	0.040	0.023	0.021	0.041	0.027	0.027	0.064
8	0.018	0.016	0.034	0.021	0.019	0.037	0.023	0.021	0.050
9	0.015	0.015	0.030	0.021	0.018	0.035	0.019	0.018	0.041
10	0.014	0.015	0.028	0.018	0.016	0.030	0.017	0.017	0.037
11	0.013	0.013	0.025	0.016	0.015	0.028	0.013	0.015	0.030
12	0.012	0.013	0.024	0.015	0.013	0.025	0.013	0.015	0.028

The range of the number of convergent images used for the camcorder calibrations was between 6 and 12. The results indicate that increasing the number of images increases redundancy of point measurements and hence improves the level of measurement accuracy. The RMS across the three axes was significantly lowered for all three camcorders when 12 images were used compared to six images. The RMS results across all three axes were significantly higher for JVC 3 compared to JVC 1 and JVC 2 when fewer than 9 images were used for the calibration. With the increase in the number of convergent images, the discrepancies in the RMS results between the three camcorders were minimised. To determine whether the RMS tolerance of 0.05 mm was achieved, the 3D distance RMS results were calculated for each of the camcorders (Table 3.4).

Table 3.4: The effect of increasing the number of images from the JVC Everio camcorders on the 3D distance RMS

	3D distance RMS (mm)		
Number of images	**JVC 1**	**JVC 2**	**JVC 3**
6	0.048	0.050	0.054
7	0.048	0.047	0.054
8	0.042	0.047	0.050
9	0.037	0.045	0.048
10	0.035	0.039	0.044
11	0.031	0.036	0.036
12	0.030	0.032	0.034

The effect of increasing the number of images on the 3D distance RMS results is illustrated in Figure 3.14. A minimum of eight convergent images were required for all the three camcorders to achieve the 0.05 mm RMS tolerance specified during the project design. Twelve images were necessary to stabilise the RMS values across all three camcorders which is evident with the very small discrepancies between the 3D RMS results across the three camcorders. From these results, 12 convergent images were selected to be used for calibrating all the camcorders used in the project.

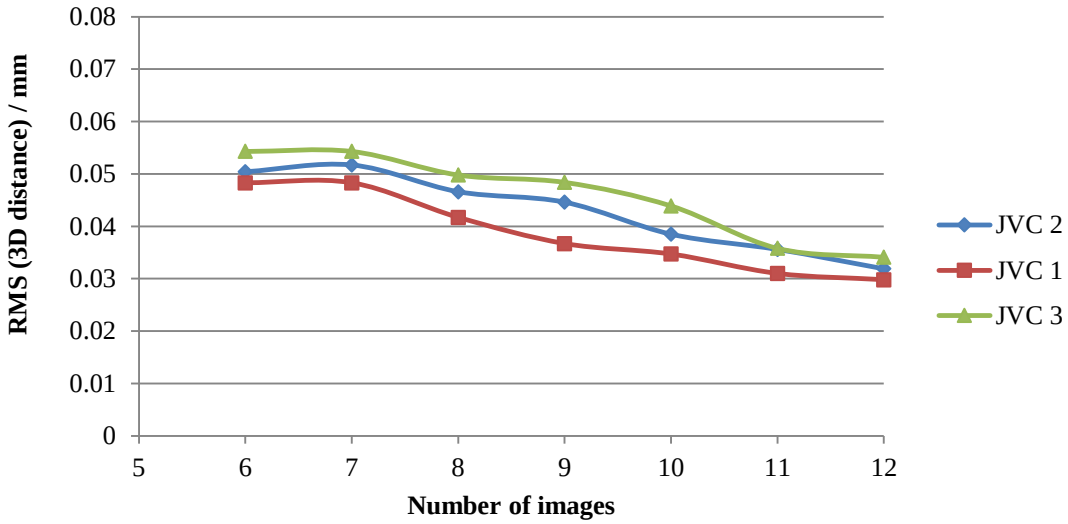

Figure 3.14: The effect of increasing the number of images used in the JVC Everio camcorder calibration on the 3D distance RMS results.

The effect of increasing the number of images on the measurement accuracy was investigated and the RMS of the target coordinates across all three axes is listed in Table 3.5. The RMS tolerance specified for the control targets was 0.03 mm across all three axes when the Sony Cybershot F828 camera was used for the project control calibration (Fraser, 1996).

Table 3.5: The effect of increasing the number of the Sony Cybershot F828 camera images on the RMS of the control targets across the axes

Number of images	X (mm)	Y (mm)	Z (mm)	3D RMS distance (mm)
8	0.018	0.019	0.022	0.034
9	0.016	0.017	0.021	0.031
10	0.016	0.015	0.019	0.029
11	0.015	0.013	0.017	0.026
12	0.015	0.011	0.017	0.025
13	0.014	0.011	0.016	0.024
14	0.013	0.010	0.015	0.022
15	0.011	0.010	0.015	0.021
16	0.010	0.009	0.014	0.019

The results indicate that there is minimal improvement in the target coordinate accuracy when more than 14 convergent images are included in the bundle calculation to determine the control target coordinates. A minimum of 10 convergent images were sufficient to meet the specified tolerance of 0.03 mm however, as the use of 16 images reduced the 3D RMS distance below 0.02 mm, 16 convergent images were used for coordinating the control targets. The effect of increasing the image number on the 3D distance RMS is illustrated in Figure 3.15.

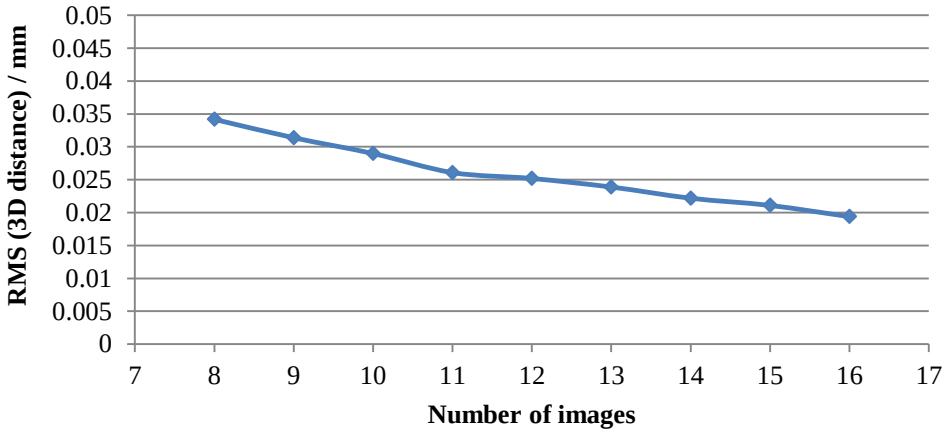

Figure 3.15: The effect of increasing the number of images used in the project control calibration using a Sony Cybershot F828 camera.

3.6.2 Developed data capture system accuracy

The seven mannequin distances obtained from the dynamic data capture system were compared to the same distances obtained using the high accuracy convergent photogrammetric technique and the results are listed in Table 3.6.

Table 3.6: Mean mannequin differences between the convergent measurements and the dynamic data capture system measurements.

	Convergent		Dynamic				
Distances	**Mean (mm)**	**SD (mm)**	**Mean (mm)**	**SD (mm)**	**Mean difference (mm)**	***t*-value**	***p*-value**
A-B	56.867	0.08	56.683	0.36	0.185	0.88	0.43
C-D	51.358	0.08	51.305	0.13	0.053	0.21	0.85
A-E	62.101	0.08	62.312	0.11	0.211	1.55	0.19
B-E	55.765	0.11	54.872	0.26	0.107	0.64	0.56
C-E	48.468	0.02	48.759	0.29	0.291	1.73	0.16
D-E	44.647	0.09	44.545	0.19	0.103	0.84	0.45
F-G	52.701	0.03	52.686	0.15	0.015	0.17	0.88

The largest mean differences were measured between distances C-E (0.291 mm) and A-E (0.211 mm) and the smallest mean difference was measured between F-G (0.015 mm). To determine whether the differences between the means were statistically significant, paired samples *t* tests were conducted and the level of significance was defined at 0.05. The results indicate that although the highest difference between the measurements was almost 0.30 mm, there were no significant differences between the two measurement techniques indicating the accuracy of the designed imaging system.

3.6.3 Camera lens stability analysis

A test was conducted to determine the effect of the slight variations in the JVC camcorders' lens parameters on the measurement accuracies. Two camera calibration sessions were completed on two separate days, a month apart for all the 12 JVC camcorders. The first calibration session was carried out on the 27th of December 2012 (session 1) and the calibration session was repeated one month later on the 24th of January 2013 (session 2). The parameters averaged from four sets for the 12 camcorders (labelled JVC 1 – JVC 12) were calculated through bundle adjustment algorithms and listed in Table 3.7. These parameters include the camera focal length (c), the coordinates of the principle point of auto-collimation (x_p and y_p) and the radial lens distortion parameters (K_1, K_2 and K_3). The affinity and shear parameters (P_1 P_2, B_1, and B_2) were excluded from the results as they are beyond the accuracy requirement for this research.

The results in Table 3.7 indicated the stability of the lenses for all 12 camcorders. A detailed investigation of the camcorder calibration parameters on the measurement quality will be discussed in Section 3.6.4.

Table 3.7: Mean JVC Everio GZ-HD500 camcorder calibration results four weeks apart

Camera	c	X_p	Y_p	K_1	K_2	K_3
JVC 1						
Session 1	3.442	-0.036	-0.023	1.62E-02	-6.29E-04	-2.30E-05
Session 2	3.427	-0.018	-0.060	2.36E-02	-5.93E-04	-2.97E-05
JVC 2						
Session 1	3.165	-0.034	-0.014	1.95E-02	-4.74E-04	-1.80E-05
Session 2	3.171	-0.039	-0.006	2.76E-02	-4.76E-04	-1.92E-05
JVC 3						
Session 1	3.172	-0.027	-0.007	1.860E-02	-7.12E-04	-2.81E-05
Session 2	3.168	-0.049	-0.014	2.721E-02	-5.80E-04	-5.21E-05
JVC 4						
Session 1	3.254	-0.039	-0.016	1.750E-02	-4.24E-04	-3.95E-05
Session 2	3.162	-0.049	-0.025	2.758E-02	-4.50E-04	-4.81E-05
JVC 5						
Session 1	3.169	-0.007	-0.025	2.833E-02	-5.37E-03	-3.19E-05
Session 2	3.168	-0.016	-0.010	2.715E-02	-7.74E04	-3.97E-05
JVC 6						
Session 1	3.109	-0.019	-0.011	2.357E-02	-8.29E-04	-3.61E-05
Session 2	3.164	-0.017	-0.007	1.835E-02	-5.36E-03	2.86E-05
JVC 7						
Session 1	3.042	-0.071	-0.034	3.080E-02	-4.07E-04	-4.04E-05
Session 2	2.971	-0.075	-0.034	3.217E-02	-5.87E-04	-3.74E-05
JVC 8						
Session 1	3.085	-0.021	-0.010	2.853E-02	5.65E-04	-3.05E-05
Session 2	3.028	-0.017	-0.024	2.948E-02	-4.67E-04	-3.29E-05
JVC 9						
Session 1	2.906	-0.010	-0.047	3.400E-02	-6.31E-03	-5.79E-05
Session 2	2.889	-0.004	0.016	3.215E-02	-5.37E-04	-1.82E-05
JVC 10						
Session 1	2.905	-0.022	-0.028	3.690E-02	-4.73E-04	-6.45E-05
Session 2	2.897	-0.031	-0.018	3.399E-02	3.99E-04	-7.31E-05
JVC 11						
Session 1	3.144	-0.012	0.019	3.123E-02	-2.49E-04	-3.48E-05
Session 2	2.982	-0.018	0.018	3.050E-02	-5.01E-04	-3.27E-05
JVC 12						
Session 1	2.943	-0.019	0.028	3.147E-02	7.20E-04	-2.61E-05
Session 2	2.865	-0.018	0.021	3.11E-02	-5.92E-04	-5.54E-05

3.6.4 Effect of camcorder calibration parameters on the measurement quality

To determine whether the effects of the small variations in the camera calibration parameters cause significant differences in measurement quality, the seven mean mannequin distances were determined after each calibration session and compared in Table 3.8.

Table 3.8: Measurement differences between calibration sessions

	Calibration 1		Calibration 2					
Distances	**Mean (mm)**	**SD (mm)**	**Mean (mm)**	**SD (mm)**	**Mean difference (mm)**	**MAD (mm)**	**TEM (mm)**	***p*-value**
A-B	56.576	0.04	56.641	0.07	0.065	0.05	0.10	0.16
C-D	51.945	0.03	51.977	0.03	0.032	0.02	0.07	0.21
A-E	62.641	0.08	62.627	0.01	0.014	0.02	0.05	0.55
B-E	55.449	0.05	55.468	0.02	0.019	0.02	0.04	0.78
C-E	48.342	0.02	48.322	0.02	0.020	0.02	0.01	0.56
D-E	44.411	0.03	44.457	0.03	0.046	0.03	0.07	0.34
F-G	52.789	0.05	52.781	0.01	0.008	0.03	0.02	0.82

From the results listed in Table 3.8, no systematic errors were found between the repeated measurements from the two calibration sessions as the *p* values from the paired student *t* test were all greater than 0.05 at the 95% confidence interval level. The mean measurement differences were all lower than 0.065 mm (A-B) with the highest Mean Absolute Difference (MAD) of 0.05 mm for the measurement A-B indicating a high level of measurement precision. The random errors ranged between 0.01 mm for distance C-E and 0.10 mm for distance A-B.

3.7 Discussion

In recent years, new technologies have emerged aiming to expand the use of 3D technologies for foot scanning. Although promising results were found through the use of 3D technologies for foot anthropometry, most of these technologies continue to have limitations. For example, time-of-flight cameras, structured light scanning, Moire techniques and laser scanning are all expensive technologies and are not suitable for motion artefacts (Yu and Tu, 2009; Thabet et al., 2014; Samson et al., 2014; Vecchio et al., 2012). To understand foot function, it is necessary to measure the foot in a dynamic state and hence the abovementioned technologies are unsuitable.

One technology was identified which eliminates all of the above mentioned limitations and is based on the concept of image-based close range photogrammetry. The numerous advantages provided through this technology include its high level of measurement accuracy and precision (Chong, 2012; de Menezes et al., 2010), its low cost (Chong, 2011), non-invasiveness (Ladeira et al., 2013), rapid rate of data acquisition (Kau et al., 2011) and post processing ability (Luhmann, 2010). In addition, the system can be developed to allow for instantaneous data capture from different imaging sensors making it ideal for measuring moving objects (Wong et al., 2008).

A 3D close-range photogrammetric system was hence designed and presented in this chapter to allow for accurate dynamic foot measurements to be obtained. Network design optimisation was conducted to select the most appropriate locations, geometries and type of imaging sensors to image the foot during gait. A custom-built gait imaging platform was necessary for optimising the network design. The platform allowed for incorporating ground reaction force information and

project control during gait while 12 low-cost HD JVC Everio GZ-HD500 camcorders are setup around the platform to image the foot during gait. A gen-lock device was custom-built to allow for synchronising all 12 camcorders with each other and with the ground reaction force information obtained from the force plate.

Initial calibration tests were carried out for three of the camcorders to determine the effect of increasing the number of convergent images on the RMS of target coordinates during camcorder calibrations. For the JVC Everio GZ-HD500 camcorders selected for this project, a minimum of eight convergent images were necessary to meet the 0.05 mm RMS tolerance specified during the project design. However, 12 images were required to stabilise the RMS values by minimising the discrepancies between the three camcorders tested. Similarly, the effect of increasing the number of convergent images on the RMS target coordinates was investigated for the project control calibration. A single Sony Cybershot F828 still camera was used to meet the 0.03 mm RMS tolerance specified during the project design stage. Although ten images were sufficient to meet the tolerance, the use of 16 images reduced the 3D RMS distance below 0.02 mm and was hence selected for coordinating new control targets.

The measurement accuracy capability of the developed dynamic data capture system was investigated using 3D measurements on a mannequin foot. As the mannequin foot is stationary, errors associated with movement are eliminated. Seven distances were determined on the mannequin foot using high accuracy bundle adjustment calculations from 16 convergent images using a high resolution Sony Cybershot F828 camera. This ‘gold standard’ measurement technique is based on the principle of convergent photogrammetry which is known to yield highly accurate measurements (Fraštia, 2005; Wackrow and Chandler, 2008; Wackrow and Chandler, 2011; Fraser and Al-Ajlouni, 2006; Gruen and Beyer, 2001; Remondino and Fraser, 2006). The same distances were determined using the designed system utilising all 12 JVC Everio GZ-HD500 camcorders and compared with the convergent imaging measurements. The highest mean difference between the two measurement techniques was less than 0.30 mm as shown in Table 3.6. To determine whether the difference between the two techniques was statistically significant, paired sample *t* tests were conducted and the results indicated no significant differences in any of the seven distances between the two measurement techniques ($p > 0.05$).

Calibrating non-metric sensors used in deriving spatial 3D measurements to account for any discrepancies in the lens significantly reduces some of the errors and in turn, directly influences the accuracy of the measurements (Cooper and Cross, 1988). In the current study, the geometric parameters of the 12 JVC Everio camcorders were assessed on separate days, one month apart. From the results, it was evident that the camera calibration parameter results had slight variations between the cameras. This indicates that although the cameras have the same manufacturer, slight variations are found in the camera lens as a result of manufacturing discrepancies. Another source of variation in the camera parameters is speculated to be the result of the slight changes in the environment of data capture during the two calibration days. Although care was taken to ensure that the environmental conditions did not change during the collection of the data sets the calibration images

for all the four sets were recorded during different times of the day and may have been exposed to slightly different room temperatures.

To determine whether the effects of the small variations in the camera calibration parameters resulted in significant differences in measurement accuracies, the seven foot mannequin distances were compared after each calibration session using the designed dynamic data capture system. The largest mean difference between the two calibration sessions was 0.065 mm with the precision of the repeated measures determined from the MAD ranging between 0.02 mm to 0.05 mm. Small random errors were found from the TEM results with a range between 0.01 mm and 0.10 mm indicating a good level of agreement of the repeatable measures. A high level of measurement stability was obtained from the two calibration sessions as indicated from the paired samples *t* tests ($p > 0.05$). It is therefore concluded that the slight changes in the camcorder calibration values collected one month apart do not have a significant influence on the measurement accuracy obtained from the image-based dynamic measurement system due to the stability of the imaging sensors used.

3.8 Conclusion

A low-cost 3D close-range photogrammetric measurement system for measuring the dynamic foot during gait was presented in this chapter. The system was developed as a cost-effective solution for obtaining high accuracy 3D dynamic foot measurements. The novelty of the designed low-cost system is in its ability to synchronise ground reaction force information with foot measurements during gait to a high level of 3D measurement accuracy (< 0.30 mm). This allows the end-user to determine the relationships between changes in foot anthropometry during dynamic activities and the forces acting on the foot during gait. The ability to synchronise the force information to the dynamic foot anthropometric changes will hence provide important insight into the appropriateness of current conventional static foot measurement techniques in the prediction of dynamic foot mobility. Detailed comparative accuracy, precision and reliability analysis tests between conventional static measurements and the developed image based system will be assessed in Chapter 4.

Chapter 4: Effect of changing weight-bearing on the foot measurement accuracy

4.1 Introduction

Current foot clinical assessments are limited to the use of conventional measurement instruments such as calipers and sliding rulers which are only suitable for static measurements (Andreasen et al., 2013; Cornwall and McPoil, 2011; Deng et al., 2010). A low cost close-range photogrammetric system was developed for the purpose of measuring 3D dynamic foot deformation and mobility during gait and was presented in the previous chapter. When measuring changes in foot anthropometry during movement, it is essential that the quantification system used is capable of achieving measurements with a high level of accuracy and reliability (Weinberg et al., 2004).

For anthropometric measurement accuracy, the ISO 20385 standard was developed to ensure that the measurements obtained from 3D measurement technologies are comparable with measurements from conventional equipment. For the specific application of foot anthropometry, the ISO 20385 lists the maximum mean allowable difference as 2 mm (Telfer and Woodburn, 2010). Maintaining mean differences of less than 2 mm have proved to be difficult in dynamic human body measurements (Nielsen et al., 2010; Vecchio et al., 2012).

The agreements between two testers in conducting foot anthropometric measurements are investigated through accuracy assessments and are reported in this chapter. Foot mannequin measurements obtained using a 'gold standard' high accuracy convergent image-based bundle adjustment technique is used to validate the measurements collected by both testers. A comparative test is then reported for the correlation between the developed imaging system measurements and the conventional measurements conducted by the testers. Finally the effect of the changes in weight-bearing during dynamic loading on the measurement accuracy is investigated through human subject trials. The chapter concludes with a discussion of the reported accuracy and agreement between the conventional foot measurements and the measurements collected using the developed 3D measurement system. The effect of changing weight-bearing on foot anthropometric measurement accuracy is also reported.

4.2 Methods

4.2.1 Mannequin measurements using caliper

Two testers conducted four sets of manual caliper measurements using a Kincrome digital caliper (0.1 mm resolution) of the same seven mannequin distances that were measured using the convergent measurement technique described in Section 3.4.2.1. The four sets were collected ten minutes apart for each tester.

4.2.2 Weight-bearing accuracy testing

To assess the effect of changing weight-bearing on the measurement accuracy during the conventional static foot measurements, three weight-bearing conditions were selected. 10% weight-bearing was chosen as it gives an indication of the minimally weighed foot position while the entire foot plantar is in contact with the supporting surface. Similarly, the 50% and 90% weight-bearing conditions represent the percentages sufficient to observe any changes in the foot under maximum load and double limb support respectively. The weight-bearing percentages were determined using calibrated digital scales.

4.2.2.1 Subjects

For the comparison of the weight-bearing measurements obtained using the conventional caliper measurement techniques and the developed photogrammetric imaging system, four male participants volunteered to be included in the study. The participants were required to read a participant information sheet and sign a written consent form prior to data collection as part of the ethical clearance process at the University of Southern Queensland. The participant information sheet and consent documentation are provided in Appendix A. The criteria for participant inclusion in the study were a minimum age of 18 years and no previous history of lower limb injury, disease or deformity. The mean age of the participants was 34.2 ± 4.6 years and the mean weight was 79.7 ± 11.6 kilograms. Only the right foot of all the participants was measured.

4.2.2.2 Subject foot markings

Each subject was instructed to stand with relaxed double limb support for the palpation, identification and marking of the foot anthropometric locations. Seven retro-reflective anthropometric marks were labelled on each subject's right foot in the following positions: 1) the most anterior location on the largest toe, 2) the most posterior side of the calcaneus, 3) the dorsum at 50% foot length, 4) the head of the first metatarsal bone, 5) the navicular bone, 6) the medial side of the foot at 50% foot length and 7) the lateral side of the foot at 50% foot length. The anthropometric marks allowed for the following measurements to be obtained: 1) the Foot Length (FL), 2) the Foot Width (FW), 3) the Dorsal Height (DH), 4) Navicular Height (NH), and 5) Truncated Foot Length (TFL) which are defined in Table 4.1.

Table 4.1: The subject distance measurements on each subject's foot

FL	Distance between the most posterior point of the heel to the tip of the toe.
FW	Distance between the medial side of the foot at 50% foot length and the lateral side of the foot at 50% foot length.
DH	Distance from the surface to the dorsum of the foot at 50% foot length.
NH	Distance from the ground surface to the navicular bone.
TFL	Distance from the most posterior part of the heel to the first metatarsal head.

The foot markings and distances are illustrated in Figure 4.1. The foot length is represented by distance C-D, the foot width is shown as B-E, the dorsum height is represented by the distance A to the ground surface, the navicular height is determined from distance G to the ground surface and the truncated foot length is represented as distance F-D.

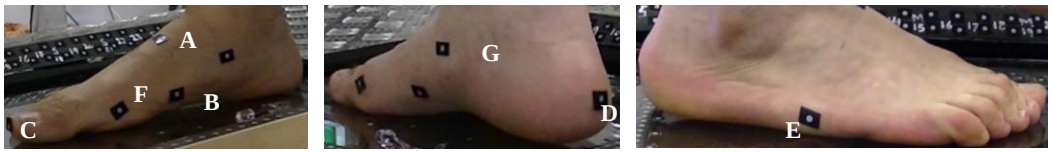

Figure 4.1: Foot anthropometric markings used to measure the foot length (C-D), foot width (B-E), dorsum height (A to surface), navicular height (G to surface) and truncated foot length (F-D).

4.2.2.3 Determining weight-bearing from subjects

The weight of each subject was obtained from digital scales and the 10%, 50% and 90% weight-bearings were determined for each subject. For the conventional manual caliper measurements, the subjects were instructed to place their right foot on a scale and exert weight until 50% of their weight was achieved. Four sets of manual caliper distance measurements for the FL, FW, DH, NH and TFL were then collected by the two testers while the subjects maintained their weight-bearing for the duration of the measurements. The measurements were repeated for each subject for the 10% weight-bearing and 90% weight-bearing conditions.

The same seven static measurements were then recorded non-invasively using the developed dynamic data capture system for the same weight-bearing conditions. The scale was placed on the force plate and the subjects were instructed to place weight on the scales while all 12 camcorders continuously captured the digital display on the scale. The video frames were then frame-grabbed using Tripard HD video converter software and Virtual Dub software at the instant that the 10%, 50% and 90% weight-bearing were observed on the video clips (Figure 4.2). Four sets of measurements were repeated at each weight-bearing condition and the camcorders were switched off between sets.

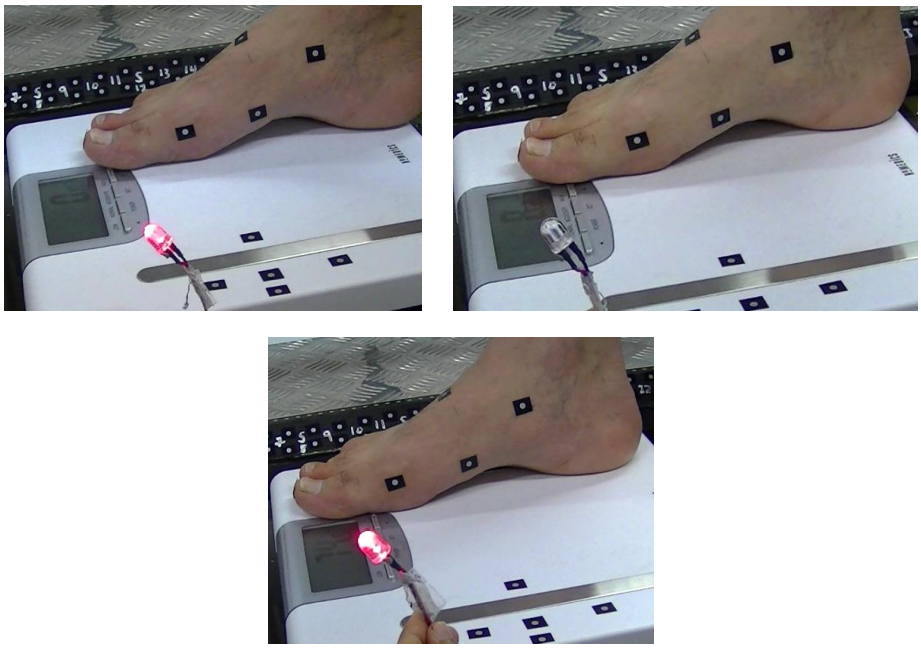

Figure 4.2: Weight-bearing recorded from video: a) at 10% WB, b) 50% WB and c) at 90% WB.

4.3 Statistical Analysis

To assess the differences in measurements between testers using the conventional foot measurements; means, standard deviations and paired Student t tests were used with $p < 0.05$ selected to determine the level of statistical significance.

Pearson's correlation coefficients for paired data (X_i, Y_i) with the level of significance $p < 0.01$ were used to assess the linear correlation between the conventional measurements from the two testers and the photogrammetric measurement techniques. The Pearson's correlation coefficient, r is calculated using:

$$r = \frac{1}{n-1} \sum_{i=1}^{n} \left(\frac{Xi-\bar{X}}{Sx}\right)\left(\frac{Yi-\bar{Y}}{Sy}\right) \quad (4.1)$$

Where, the standard score is represented by:

$$\frac{(Xi-\bar{X})}{Sx}$$

The sample mean is represented by:

$\bar{X} = \frac{1}{n} \sum_{i=1}^{n} Xi$, and

$\bar{Y} = \frac{1}{n} \sum_{i=1}^{n} Yi$,

S*x* is the standard deviation and is represented by:

$Sx = \sqrt{\frac{1}{n-1} \sum_{i=1}^{n} (Xi - \bar{X})^2}$, and

$Sy = \sqrt{\frac{1}{n-1} \sum_{i=1}^{n} (Yi - \bar{Y})^2}$

The strength of the measurement association increases as the Pearson correlation coefficient (r) approaches +1 or -1 signifying a perfect positive linear correlation or negative linear correlation respectively. The closer the Pearson's correlation value is to 0, the greater the variation from the linear model. All statistical analyses were computed using SPSS version 21.

4.4 Results

4.4.1 Effect of testers on measurement accuracy

The between-tester comparisons for the seven mannequin measurements are summarised in Table 4.2. The highest discrepancy between the testers was found in the distance A-B as indicated by the mean difference of 0.88 mm and the smallest discrepancy was 0.19 mm for distance C-D. From the Student's t-test, none of the measurement discrepancies were statistically significant as the *p*-values were all greater than 0.05 for the seven mannequin distance measurements.

Table 4.2: Mean mannequin differences between Tester 1 and Tester 2

	Tester 1		**Tester 2**				
Distances	**Mean (mm)**	**SD (mm)**	**Mean (mm)**	**SD (mm)**	**Mean difference (mm)**	***t*-value**	***p*-value**
A-B	56.31	0.55	55.43	0.66	0.88	2.06	0.09
C-D	51.52	0.87	50.10	0.73	0.19	0.33	0.76
A-E	62.66	0.70	62.97	0.79	0.31	0.44	0.64
B-E	55.52	0.76	55.10	0.41	0.42	0.67	0.45
C-E	48.91	0.64	48.58	0.47	0.33	0.46	0.61
D-E	44.24	0.51	43.46	0.56	0.78	2.09	0.08
F-G	52.26	0.88	52.03	0.64	0.24	0.43	0.69

4.4.2 Level of agreement between the conventional measurements and convergent system measurements

To determine the level of agreement between the caliper measurements obtained from each tester and the convergent imaging measurements for the mannequin distances, Pearson's correlation coefficients (*r*) were calculated (Table 4.3). The Pearson's correlation results indicated a strong measurement association ($p < 0.001$) between the convergent photogrammetric measurements and the measurements obtained by both testers for all the distances.

The statistically significant correlation coefficients ($p < 0.001$) ranged from 0.78 (B-E) for Tester 2 to 0.99 (D-E) for Tester 1. The highest discrepancies in the measurements between the two testers were found for the distances A-B and B-E. For the measurement A-B, the measurements collected by Tester 1 indicated a lower level of association with the convergent 'gold standard' measurements ($r = 0.85$) than the measurements collected by Tester 2 ($r = 0.96$). In contrast, for the distance B-E, the measurements conducted by Tester 2 had a weaker correlation ($r = 0.78$) than Tester 1 ($r = 0.94$) when compared to the convergent photogrammetric measurements.

Table 4.3: Pearson's correlations (*r*) between the testers' measurements and the 'gold standard' convergent imaging measurements

Correlations	**Tester 1**		**Tester 2**	
	r	***p*-value**	***r***	***p*-value**
A-B	0.85**	<0.001	0.96**	<0.001
C-D	0.85**	<0.001	0.88**	<0.001
A-E	0.93**	<0.001	0.92**	<0.001
B-E	0.94**	<0.001	0.78**	<0.001
C-E	0.93**	<0.001	0.97**	<0.001
D-E	0.99**	<0.001	0.97**	<0.001
F-G	0.91**	<0.001	0.89**	<0.001

** Significant at the 0.01 level.

The mean difference between the testers' caliper measurements and the dynamic data capture system measurements are provided in Appendix B. The largest measurement difference was 1.25 mm and hence the measurements are within the 2 mm agreement threshold listed for foot anthropometry in the ISO 20385.

To determine the level of association between the testers' mannequin distance measurements and the mannequin measurements collected using the developed dynamic data capture system measurements in Section 3.4.2.2, Pearson's correlation tests were used and the results are listed in Table 4.4.

Table 4.4: Pearson's correlations (r) between the testers' measurements and the developed dynamic data capture measurement system measurements

Correlations	Tester 1		Tester 2	
	r	***p*-value**	***r***	***p*-value**
A-B	0.98**	<0.001	0.99**	<0.001
C-D	0.96**	<0.001	0.93**	<0.001
A-E	0.91**	<0.001	0.97**	<0.001
B-E	0.92**	<0.001	0.99**	<0.001
C-E	0.96**	<0.001	0.94**	<0.001
D-E	0.98**	<0.001	0.99**	<0.001
F-G	0.93**	<0.001	0.81**	<0.001

** Significant at the 0.01 level.

The results show highly significant agreements ($p < 0.001$) between the dynamic data capture measurement system measurements and the conventional measurements. Overall, stronger levels of correlation were found for the comparisons between the testers' measurements and the developed dynamic data capture system measurements than the convergent imaging 'gold standard' measurements. Pearson's correlations (r) ranged between 0.81 (F-G) for Tester 2 and 0.99 for distances A-B, B-E and D-E (Tester 2). The highest measurement discrepancy between the two testers was found for the measurements F-G. For the measurement F-G, the measurements collected by Tester 2 depicted a weaker level of association with the developed data capture system measurements ($r = 0.81$) than the measurements collected by Tester 1 ($r = 0.93$).

4.4.3 Effect of weight-bearing changes on conventional measurement accuracy

The comparisons of the measurements collected by the two testers for the four subjects are summarised in Tables 4.5, 4.6 and 4.7 for the 10% WB, 50% WB and 90% WB conditions respectively.

Table 4.5: Mean subjects' measurement differences between Tester 1 and Tester 2 at 10% WB

	Tester 1		Tester 2				
Distances	**Mean (mm)**	**SEM (mm)**	**Mean (mm)**	**SEM (mm)**	**Mean difference (mm)**	***t*-value**	***p*-value**
FL	257.63	0.78	257.51	0.87	0.11	0.02	0.99
TFL	190.08	0.57	191.62	0.18	1.54	0.26	0.79
DH	66.61	0.85	66.93	1.02	0.32	0.25	0.81
NH	56.42	0.66	55.54	1.22	0.88	0.64	0.53
FW	85.06	0.83	86.48	0.81	1.42	1.22	0.23

Table 4.6: Mean subjects' measurement differences between Tester 1 and Tester 2 at 50% WB

	Tester 1		Tester 2				
Distances	**Mean (mm)**	**SEM (mm)**	**Mean (mm)**	**SEM (mm)**	**Mean difference (mm)**	***t*-value**	***p*-value**
FL	260.27	1.61	260.66	1.44	0.39	0.06	0.95
TFL	190.67	1.02	191.61	0.78	0.94	1.31	0.18
DH	61.84	0.93	62.17	0.64	0.33	0.24	0.81
NH	51.13	1.12	50.29	0.84	0.85	0.61	0.55
FW	87.25	0.92	88.05	0.52	0.80	0.76	0.45

Table 4.7: Mean subjects' measurement differences between Tester 1 and Tester 2 at 90% WB

	Tester 1		Tester 2				
Distances	**Mean (mm)**	**SEM (mm)**	**Mean (mm)**	**SEM (mm)**	**Mean difference (mm)**	***t*-value**	***p*-value**
FL	260.02	0.51	259.65	0.58	0.37	0.06	0.96
TFL	191.71	0.76	191.33	1.32	0.38	0.07	0.95
DH	62.70	0.92	64.35	0.44	1.65	1.62	0.12
NH	53.77	0.77	52.00	0.92	1.77	1.48	0.15
FW	87.95	0.76	87.96	0.57	0.07	0.08	0.99

The results for the measurement comparisons between the testers' conventional caliper measurements indicate that the FL measurements had a consistent and low mean difference for all the three weight-bearing conditions. Only four measurements across the three weight-bearing conditions had mean differences larger than 1 mm. These measurements were the TFL and FW at 10% WB and the NH and the DH at 90% WB. None of the measurements at 50% WB exceeded 1 mm. From the Student's t-test, the measurement discrepancies between testers at the three weight-bearing conditions were found not to be statistically significant as the *p*-values were all greater than 0.05 for the five distance measurements.

4.4.4 Level of agreement between the conventional caliper measurements and the developed data capture measures for different weight-bearing conditions

To determine the level of agreement between the conventional measurements and the developed data capture system measures at different weight-bearing conditions, Pearson's correlation coefficients (*r*) were calculated. The Pearson's correlations results between each tester's caliper measurements and the developed data capture

system measurements are listed in Tables 4.8, 4.9 and 4.10 for the 10%, 50% and 90% weight-bearing stance conditions respectively.

Table 4.8: Pearson's correlations between the testers' measurements and the developed data capture system measurements at 10% WB

Correlations	Tester 1 and dynamic system		Tester 2 and dynamic system	
	r	***p*-value**	***r***	***p*-value**
FL	0.95**	<0.001	0.98**	<0.001
TFL	0.88**	<0.001	0.98**	<0.001
DH	0.73**	0.007	0.72**	0.008
NH	0.58	0.05	0.50	0.07
FW	0.77**	0.003	0.90**	<0.001

** Significant at the 0.01 level.

Table 4.9: Pearson's correlations between the testers' measurements and the developed data capture system measurements at 50% WB

Correlations	Tester 1 and dynamic system		Tester 2 and dynamic system	
	r	***p*-value**	***r***	***p*-value**
FL	0.99**	<0.001	0.99**	<0.001
TFL	0.96**	<0.001	0.99**	<0.001
DH	0.77**	<0.01	0.74**	<0.01
NH	0.59	0.05	0.64	0.03
FW	0.76**	<0.01	0.73**	<0.01

** Significant at the 0.01 level.

Table 4.10: Pearson's correlation between the testers' measurements and the developed data capture system measurements at 90% WB

Correlations	Tester 1 and dynamic system		Tester 2 and dynamic system	
	r	***p*-value**	***r***	***p*-value**
FL	0.99**	<0.001	0.99**	<0.001
TFL	0.94**	<0.001	0.97**	<0.001
DH	0.91**	<0.001	0.79**	<0.001
NH	0.61	0.04	0.64	0.03
FW	0.74**	<0.01	0.71**	<0.01

** Significant at the 0.01 level.

All the measurements provided significant correlations across all the weight-bearing conditions between the caliper and the developed imaging system measurements ($p < 0.01$) except for the Navicular height (NH). No significant correlation was evident for the NH at any of the weight-bearing conditions with the lowest level of correlation apparent at 10% WB. The highest level of association between the two measurement techniques was found for the FL measurements for both testers and across all the weight-bearing conditions. The Pearson's correlation

(*r*) results were generally similar for both testers with the exception of the DH measurements at 90% WB, and the TFL and FW measurements at 10% WB.

4.5 Discussion

Non-metric, consumer-grade digital cameras have become commonplace for applications of deriving accurate spatial 3D measurements. Some of the applications include industrial (Jones and Lunsford; Ozbek et al., 2010), construction (Riveiro et al., 2011; Ordóñez et al., 2008) environmental, (Peter Heng et al., 2010; Telem and Filin, 2010) and medical (Chong et al., 2009; King, 2012). The quality of the spatial 3D measurements is dependent on numerous factors which could contribute to errors in the measurement system. These errors can be defined through accuracy, precision and reliability assessments.

In the previous chapter, an accuracy assessment of the developed dynamic data capture measurement system was conducted through comparative measurements of a mannequin foot obtained from 'gold standard' high accuracy convergent photogrammetric measurements. In this chapter, the accuracy of conventional caliper measurements conducted by two testers was validated through comparative analyses tests. Mannequin measurements collected by each tester were compared with the same measurements obtained from the high accuracy 'gold standard' convergent photogrammetric measurement method described in Section 3.4.2.1.

Four sets of seven distances were measured on the mannequin foot by each tester and compared with the same seven distance measurements collected from the 'gold standard' convergent photogrammetric technique. The between-tester mean measurement discrepancies were smaller than 0.88 mm for all seven measurements. To identify whether the measurement differences were significant, a Student t-test analysis was conducted. The results of the Student's t-test indicated that none of the measurement discrepancies were statistically significant as the *p*-values were all greater than 0.05 for all the measurements.

The agreements in the conventional caliper measurements with the 'gold standard' convergent photogrammetric measurement for the mannequin distances were assessed through Pearson's correlation coefficient tests. The Pearson's correlation results indicated a strong linear measurement correlation ($p < 0.001$) between the convergent photogrammetric measurements and the measurements obtained by both testers for all the mannequin distance measurements. The highest discrepancies in the measurements between the two testers were found for the distances A-B and B-E. Overall, the discrepancies between the testers were not statistically significant. Direct caliper measurements are the conventional techniques used for quantifying foot anthropometry clinically (Pohl and Farr, 2010; Cornwall and McPoil, 2011). The high levels of agreements between the caliper measurements and the 'gold standard' measurements indicated from this study, proves the soundness of the caliper measurement method as a static foot clinical measurement tool.

The level of linear correlations between the testers' measurements and the developed dynamic data capture system measurements were further investigated through Pearson's correlations. The seven mannequin measurements were all found to be significantly correlated between the two measurement techniques. The discrepancies between the testers evident from the Pearson's correlations were lower when the measurements were compared to the developed imaging system measurements than the 'gold standard' measurements.

Current clinical foot classification measurements are determined by tracking the positional changes of landmarks between maximum weight-bearing and minimum weight-bearing exerted on the foot (McPoil et al., 2013; Williams and McClay, 2000; Pohl and Farr, 2010). The difference in the bone landmark positions between the two weight-bearing conditions is then used to assess foot mobility. In the current study, the effect of increasing weight-bearing on the conventional measurement accuracy was investigated. The level of agreement between the conventional tester measurements and the developed dynamic data capture system measurements were also assessed.

Four sets of five foot measurements were collected by the two testers for four subjects. The five measurements were: 1) the foot length (FL), 2) truncated foot length (TFL), 3) dorsal height (DH), 4) navicular height (NH) and the 5) foot width (FW). The results for the measurement comparisons between the testers when conducting the conventional caliper measurements indicated that only four measurements across the three weight bearing conditions had mean differences between 1 mm and 2 mm. These measurements were the TFL and FW at 10% WB, and the NH and the DH at 90% WB. None of the measurements at 50% WB exceeded 1 mm indicating that higher accuracy measurements were yielded at the 50% WB condition. This is expected to be the result of the ease of the subjects in maintaining their weight-bearing for the duration of the measurements at 50% WB due to standing on double limb support. In contrast, at 10% WB and 90% WB, the subjects were required to balance and maintain the required weight on one foot for the measurement duration (McPoil et al., 2008a). From the Student's t-test, the measurement discrepancies between testers at the three weight-bearing conditions were not found to be statistically significant as the *p*-values were all greater than 0.05 for the five distance measurements.

The levels of agreement for the subjects' foot measurements for both testers at the different weight-bearing conditions were compared with the same measurements derived from the developed dynamic data capture system. Significant Pearson's correlations ($p < 0.01$) were found between all the measurements except for the navicular height across all the three weight-bearing conditions. The lowest level of correlation for the NH between the conventional measurements for both testers and the developed system was apparent at 10% WB. This confirms the results of previous studies which found the navicular bone measurements to be less consistent than the DH measurement were inconsistent due to difficulty in palpating the navicular bone (McPoil et al., 2008a) and their sensitivity to changing weight-bearing (Deng et al., 2010). Nielsen et al. (2010) reported errors between 4 - 5 mm for the navicular bone measurements as a result of the difficulty between testers in locating and marking the Navicular bone.

The highest level of association between the two measurement techniques was found for foot length measurements for both testers and across all the weight-bearing conditions indicating the ease of measuring the foot length compared to the other foot measurements. The Pearson's correlation (*r*) results were generally similar for both testers with the exception of the DH measurements at 90% WB, and TFL and FW measurements at 10% WB. These differences between testers are likely to be attributed to small discrepancies in the subjects' foot morphology during different measurement sets (Wearing et al., 2004; Billis et al., 2007). By and large, these discrepancies were not found to be significant.

4.6 Conclusion

The purpose of the study conducted in this chapter was to assess the accuracy of conventional measurements conducted by two testers and to investigate the effect of changing weight-bearing on measurement accuracy. Mannequin measurements collected using a high-accuracy 'gold standard' convergent imaging technique was used to validate caliper mannequin measurements collected by both testers. The levels of measurement correlations were excellent between the caliper and 'gold standard' mannequin measurements.

Similarly, high levels of linear measurement correlations were found when the conventional mannequin measurements were compared to measurements collected using the developed dynamic data capture system. The effect of changing static weight-bearing under the foot on foot length, truncated foot length, dorsum height, navicular height and the foot width measurement accuracies was investigated. Significant correlations were found between the static caliper and dynamic system measurements for all the measurements except for the Navicular height. This confirms the lack of reliability for the navicular bone measurements found in previous studies.

The validation of the conventional measurements was essential as calipers are the current equipment used to determine the changes in foot bone landmarks at different weight-bearing conditions which are used to assess foot mobility. The results of the study conducted in this chapter indicate that the caliper measurements are suitable for comparing foot anthropometry using conventional static measurements and dynamic foot measurements collected using the developed dynamic data capture system. Hence in the following chapter, the static conventional Foot Mobility Magnitude (FMM) and Arch Height Index (AHI) measures will be correlated with the dynamic FMM and AHI measures. This will determine whether the conventional static FMM and AHI measurements can accurately predict foot mobility.

Chapter 5: Comparing static and dynamic FMM and AHI measures

5.1 Introduction

The aim of the study presented in this chapter is to utilise the developed dynamic 3D data capture measurement technique to measure changes in the dorsum of the foot during changing dynamic loading and relate foot structural information with foot function. The Foot Mobility Magnitude (FMM) (McPoil et al., 2009) and the Arch Height Index (AHI) (McPoil et al., 2008b) are the two measurement techniques based on the dorsum which will be investigated. These two measurement techniques were selected as they are found to yield high reliability and validity results compared to other foot assessment techniques (McPoil et al., 2009; Butler et al., 2008). Measurements collected from the developed dynamic data capture system will be correlated with the conventional clinical measurement techniques using calipers to identify the level of association between dynamic and static clinical measures of FMM and AHI.

5.2 Methods

5.2.1 Subjects

For the comparison of conventional static measurements and dynamic foot mobility measurements based on the Dorsum as the reference point, 17 male participants volunteered for the study after providing a written informed consent (Appendix B). The criteria for participant inclusion in the study were a minimum age of 18 years and no previous history of lower limb injury, disease or deformity. The mean age of the participants was 32.1 ± 6.7 years and the mean weight was 86.8 ± 9.9 kilograms. Only the right foot of all the participants was measured.

5.2.2 Anthropometric retro-target placements

Each subject's anthropometric measurements were conducted by two testers; one who had 24 months experience with conducting the foot dimension measurements (Tester 1) and the other who had six months experience (Tester 2). The variation in the clinical assessment experience was to determine whether the level of experience has an effect on the measurement variations. The purpose of conducting the manual measurements was to provide a benchmark for measurement comparisons between conventional static measures of foot mobility and the actual behaviour of the foot during the changes in the weight-bearing during gait.

To determine the foot length (FL) of each subject, a retro-reflective target was placed at the most posterior part of the foot indicating the location of the heel and another target was placed at the tip of the large toe. The subjects were then instructed to stand in a relaxed double-limb support position where their weight is divided across both feet. A Kincrome digital caliper with a resolution of 0.1 mm was used to measure the distance between the two targets and infer the 50% distance of the total right foot length. The 50% foot length measurement was then used to place three retro-reflective targets in the following locations: 1) the dorsum of the foot at 50% FL, 2) the medial side of the foot at 50% FL and 3) the lateral side of the foot at 50% FL.

As the dorsum height was required to be measured to the ground during gait, a reference line was required on the foot. The distance from the reference line to the ground surface could then be added to the distance from the dorsum to the reference line to determine the dorsum height during processing. To create the baseline, two anthropometric marks were added in the following medial locations on the foot: 1) two centimetres anterior to the most posterior part of the foot and two centimetres from the ground, and 2) on the first metatarsal head. The location of the first metatarsal head was identified and marked through palpation by the same tester who had 24 months clinical experience with locating and marking the anthropometric marks. The locations of the marks are shown in Figure 5.1.

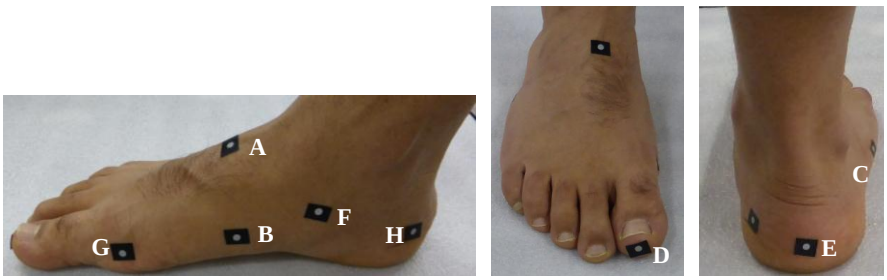

Figure 5.1: The location of the anthropometric targets.

From Figure 5.1, the dorsum is depicted as point A, the medial side of the foot at 50% foot length is represented by point B, the lateral side of the foot at 50% foot length is represented as point C, the most posterior point of the foot is shown as point E and the most anterior point on the foot is shown as point D. The baseline is represented as the line G-H where G is positioned on the first metatarsal head and H is the point two centimetres anterior to the most posterior part of the foot.

5.2.3 Manual static anthropometric measurements

Each participant's weight was collected using a digital scale and 10%, 50% and 90% weight bearings (WB) were calculated from the weight of each subject. The participants were then instructed to place their right foot on the digital scale and exert weight until 10% of their total weight was displayed on the scale. When the required 10% WB was achieved, the subjects were instructed to maintain their foot position and weight-bearing while manual caliper measurements were collected by the two testers. Each subject was then required to repeat the same process with

changing the weight-bearing until the digital scales displayed 50% of their total weight and again at 90% body weight and the same measurements were repeated by the two testers. A total of four measurement sets were collected for each weight-bearing condition by each tester and the subjects were required to relax their foot between sets. The dorsum was measured from the surface of the digital scale while the remaining distances were measured between the retro-reflective targets.

5.2.4 Dynamic anthropometric measurements

After the static measurements were collected, each participant practiced walking on the elevated imaging platform for 10 minutes before data collection until they felt comfortable walking at a natural, self-selected pace. The 12 camcorder configuration was then setup around the platform and the video sequences were recorded as described in Section 3.4.2.2. The gen-lock system was triggered and the LED light was activated at the instant the subject's foot landed on the force plate (at heel-strike) as shown in Figure 5.2.

Figure 5.2: Gen-lock activation at heel-strike.

The three dynamic foot positions that were used to study the relationship between the static weight-bearing measurements were: 1) heel-strike, 2) mid-stance and 3) active propulsion as demonstrated in Figure 5.3.

Figure 5.3: Foot gait positions at: a) heel-strike, b) mid-stance and c) active propulsion.

These foot gait positions were chosen as it was previously identified that these positions are the closest to full weight-bearing, minimal weight-bearing and mid-stance which will be correlated to the 10% WB, 50% WB and 90% WB caliper measurements respectively (Kappel et al., 2012; Jensen and Juhl, 2009).

The flashing LED was time-stamped with the camcorders and the force plate data to determine the exact photo frames for the three foot positions (Figure 5.4). Four sets were repeated for each subject's walk and the Netforce AMTI software was used to record the force plate data during walking and to correlate the time of the gen-lock system with the force plate measurements. The video sequences were then converted to still images using the software packages Tripard HD virtual converter (version 6.1.12) and Virtual Dub (version 1.6.15). The required distances for the foot width and Dorsum height were determined using the bundle adjustment algorithms in the software Australis. Figure 5.4 displays the synchronised Ground Reaction Force (GRF) graph with the images frame-grabbed at heel-strike, mid-stance and active propulsion.

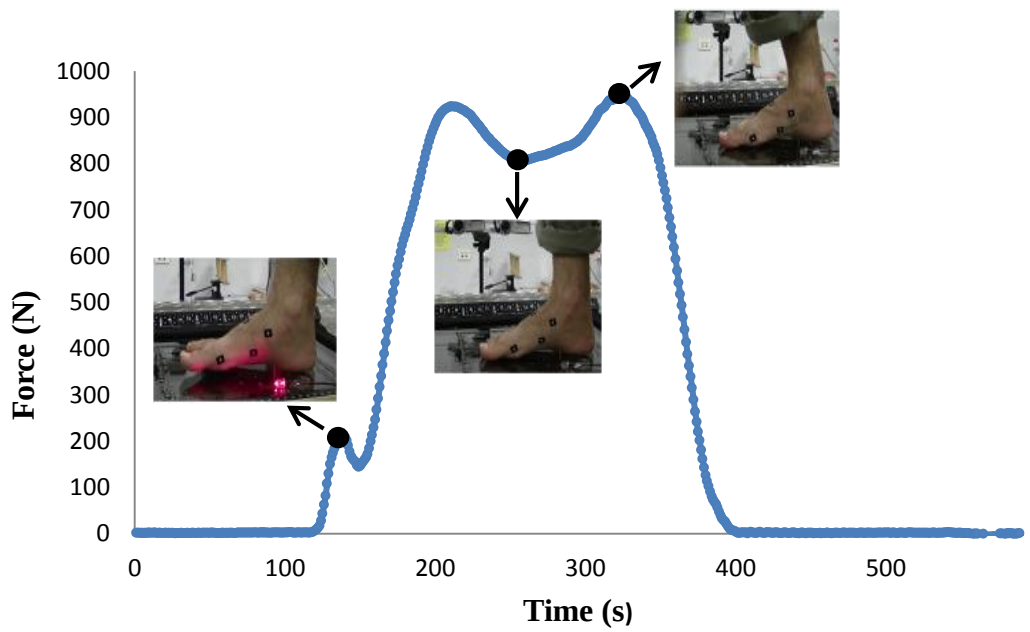

Figure 5.4: The location of heel-strike, mid-stance and active propulsion of the GRF graph.

5.2.5 Foot Mobility Magnitude (FMM) calculations

The Foot Mobility Magnitude (FMM) developed by McPoil et al. (2009) for each subject was calculated using Equation 2.1:

$$FMM = \sqrt{(AH_{max} - AH_{min})^2 + (FW_{max} - FW_{min})^2}$$

Where, AH_{max} is the dorsum height at 50% FL when the foot weight bearing is 90% for static measurements and when it is at active propulsion for dynamic measurements,

AH_{min} is the dorsum height at 50% FL when the foot weight bearing is 10% for static measurements and when it is at heel-strike for dynamic measurements,

FW_{max} is the foot width at 50% FL when the foot weight bearing is 90% for static measurements and when it is at active propulsion for dynamic measurements and,

FW_{min} is the foot width at 50% FL when the foot weight bearing is 10% for static measurements and when it is at hee-strike for dynamic measurements.

Originally, McPoil et al. (2009) used the equation to calculate the FMM for static measurements between 10% and 90% weight-bearing. However in this study, the equation was also used to determine the changes in weight-bearing between 10% and 50% to gain insight on whether one weight-bearing condition is a better indicator of dynamic foot mobility than the other. For the dynamic measurements, the difference between 10% WB and 50% WB will be compared to measurement differences between heel strike- and mid-stance.

5.2.6 Arch Height Index (AHI) calculations

Two versions of the Arch Height Index were found in the literature (Williams and McClay, 2000) and both were used in this study. For the purpose of simplicity, the two variations of the AHI will be referred to as AHI 1 and AHI 2.

AHI 1 measures the change in the Dorsum height relative to the total foot length for all the weight-bearing conditions and is expressed as the following ratio:

$$AHI\ 1 = DH / FL \quad (5.1)$$

Where, *DH* is the Dorsum height at 50% foot length, and

FL is the total foot length which is measured from the most posterior part of the foot to the most anterior part of the foot (the tip of the largest toe).

AHI 2 measures the change in the Dorsum height relative to the truncated foot length for all the weight-bearing conditions and is expressed as the following ratio:

$$AHI\ 2 = DH / TFL \quad (5.2)$$

Where, *DH* is the Dorsal height at 50% foot length and,

TFL is the Truncated Foot Length and is measured from the first metatarsal head to the most posterior part of the foot.

The static AHI 1 and AHI 2 will be calculated at 10% WB, 50% WB and 90% WB. The dynamic AHI 1 and AHI 2 will be calculated at heel-strike, mid-stance and active-propulsion.

5.3 Statistical analysis

Intraclass correlation coefficients (ICC), which are measurements of reliability, were used to determine the level of consistency in measurement repetitions, as well as the level of agreement of the same measurements between the caliper measurements and the 3D dynamic measurements (Shrout and Fleiss, 1979). Intra-rater reliability (ICC [2,4]) was used to determine the agreement of each tester in performing four repetitions of the measurements and to determine the consistency of the dynamic gait measurement repetitions. Inter-rater reliability (ICC [2,4]) was used to determine the agreement in the DH and FW measurements between the two testers. The classifications of the ICC values were selected based on the study conducted by Landis and Koch (1977) and are listed in Table 5.1. The strength of the inter-class and intra-class correlations increases as the ICC approaches 1.

Table 5.1: Strength of ICC agreements and their classifications (Landis and Koch, 1977)

ICC statistic range	Agreement strength
< 0.00	poor
0.00-0.20	Slight
0.21-0.40	Fair
0.41-0.60	Moderate
0.61-0.80	Substantial
0.81-1.00	Almost perfect

To assess the linear correlation between the caliper and the dynamic data capture system measurements, Pearson's correlation coefficients were used. All statistical analyses were computed in SPSS version 21.

5.4 Results

5.4.1 Comparing static and dynamic FMM measurements

The descriptive data for the Dorsal height (DH) and foot width (FW) at 10%, 50% and 90% WB for Tester 1, Tester 2 and the dynamic measurements collected using the dynamic data capture system are summarised in Table 5.2.

The mean DH and FW values for the 10% WB and 50% WB conditions were consistent across both testers and dynamic data capture system. The mean FW values for both testers increased at 50% WB and 90% WB, whereas the FW decreased during the dynamic measurements when the weight-bearing was increased. The results also revealed that the standard deviations and SEM were higher for the FW measurements across all weight-bearing conditions indicating that the measurements of the width of the foot are more variable than the dorsum height measurements.

Table 5.2: Descriptive data for static and dynamic measurements of the DH and FW at 10%, 50% and 90% WB

% WB		**Tester $1_{caliper}$**			**Tester $2_{caliper}$**			**Dynamic measures**		
		Mean (mm)	**SD (mm)**	**SEM (mm)**	**Mean (mm)**	**SD (mm)**	**SEM (mm)**	**Mean (mm)**	**SD (mm)**	**SEM (mm)**
10%	**DH**	69.02	4.39	0.66	68.98	5.25	0.65	69.994	4.76	0.71
	FW	90.11	5.64	0.84	90.15	4.71	0.70	89.742	5.22	0.78
50%	**DH**	64.51	4.36	0.65	65.77	4.29	0.64	65.817	3.90	0.58
	FW	92.17	5.71	0.85	91.95	5.11	0.76	89.514	5.70	0.85
90%	**DH**	63.85	4.94	0.74	65.07	4.51	0.67	67.341	4.41	0.66
	FW	93.52	5.20	0.78	92.96	5.30	0.79	87.173	6.81	1.01

The reliability of the DH and FW measurements were assessed using Intraclass Correlation Coefficients (ICC) and the results are summarised in Tables 5.3 and 5.4 for the intra-rater and inter-rater reliability respectively. Intra-rater reliability values between the four repeated sets (Table 5.3) were rated *almost perfect* for all the measurements and across all the weight-bearing conditions, ranging from 0.901 (Tester 2) to 0.992 (dynamic measurements). Overall, the dynamic data capture system provided higher ICC values across all the measurements and weight-bearing conditions. The only exceptions were for the FW measurements at the 10% WB and the 90% WB conditions where both testers obtained higher ICC values. For the dynamic measurements, the highest reliability was observed at 50% WB whereas for the manual tester measurements the highest reliability was achieved for the 90% WB measurements.

Table 5.3: Intraclass correlation coefficients (ICC) for intra-rater reliability (between sets) for DH and FW measurements

		Tester $1_{caliper}$		Tester $2_{caliper}$		Dynamic measurements	
% WB		**ICC**	**95% C.I**	**ICC**	**95% C.I**	**ICC**	**95% C.I**
10%	**DH**	0.929	0.843-0.972	0.921	0.823-0.969	0.983	0.961-0.994
	FW	0.980	0.955-0.992	0.988	0.974-0.995	0.951	0.884-0.982
50%	**DH**	0.924	0.828-0.970	0.901	0.780-0.961	0.988	0.971-0.995
	FW	0.980	0.955-0.992	0.990	0.981-0.997	0.992	0.982-0.997
90%	**DH**	0.940	0.867-0.976	0.934	0.848-0.974	0.971	0.933-0.990
	FW	0.990	0.978-0.996	0.991	0.979-0.996	0.989	0.975-0.996

The inter-tester reliability results for the agreement between the testers' measurements and the agreement between each tester's measurements and the dynamic measurements are listed in Table 5.4. The inter-tester results again yielded *almost perfect* agreement between the two testers in conducting the same manual measurements. The lowest ICC value (0.824) was achieved between Tester 1 and Tester 2 for the DH measurements at 50% WB and the highest (0.953) was obtained for the FW measurements at 50% WB. The DH provided less reliability across all the weight-bearing conditions compared to the FW when the two testers' measurements were compared.

It is clearly evident from the results that the measurement agreements between the two testers' caliper measures were better than the agreements between the dynamic measures and each of the testers' measures. The ICC results between Tester 1 and Tester 2 for the FW across all weight-bearing conditions were *almost perfect* (0.932-0.953). The correlations between the dynamic measurements and the testers' caliper measurements provided mainly *substantial* ICC results (0.693-0.859). The agreements between the dynamic image-based measurements and the testers' caliper measurements improved for the DH and FW measurements at the 50% WB condition.

Table 5.4: Intraclass correlation coefficients (ICC) for inter-rater reliability for DH and FW measurements between the static and dynamic measures

		Tester 1 and Tester 2		Tester 2 and dynamic measures		Tester 1 and dynamic measures	
% WB		**ICC**	**95% C.I**	**ICC**	**95% C.I**	**ICC**	**95% C.I**
10%	**DH**	0.862	0.765-0.919	0.750	0.548-0.862	0.784	0.608-0.881
	FW	0.932	0.881-0.961	0.833	0.511-0.927	0.719	0.579-0.915
50%	**DH**	0.824	0.665-0.904	0.836	0.670-0.914	0.900	0.818-0.945
	FW	0.953	0.920-0.972	0.859	0.743-0.992	0.780	0.505-0.892
90%	**DH**	0.828	0.682-0.904	0.727	0.400-0.894	0.815	0.434-0.921
	FW	0.936	0.871-0.966	0.696	0.204-0.907	0.693	0.192-0.896

To determine whether 50% WB might be a better indicator of the dynamic behaviour of the foot, ICC results were calculated for the Foot Mobility Magnitude (FMM) between 10% WB and 50% WB and also between 10% WB and 90% WB (Table 5.5).

Table 5.5: Intraclass correlation coefficients (ICC) for the intra-rater reliability of the FMM at different weight-bearing conditions (between sets)

FMM	**Tester 1**		**Tester 2**		**Dynamic system**	
	ICC	**95% C.I**	**ICC**	**95% C.I**	**ICC**	**95% C.I**
10%-50% WB	0.827	0.607-0.933	0.718	0.385-0.888	0.960	0.905-0.985
10%-90%WB	0.556	0.03-0.828	0.559	0.117-0.841	0.912	0.790-0.968

From Table 5.5, *almost perfect* ICC values were calculated for the dynamic FMM measurements, particularly when the weight-bearing was changed from 10% to 50% (ICC = 0.960). The lowest ICC values were for Tester 1 between 10% and 90% WB (ICC = 0.556) and for Tester 2 between 10% and 90% WB (ICC = 0.599) which were both classified as only *moderately reliable*. Overall the reliability was higher when the weight-bearing was changed from 10% to 50% WB for both testers and the dynamic system measurements.

To determine the level of association between the static and dynamic DH and FW measurements, further analysis using Pearson's correlation coefficients (r) were used. The results are listed in Tables 5.6, 5.7 and 5.8 for the 10%, 50% and 90% weight-bearing conditions respectively.

Table 5.6: Pearson's correlation between the testers' caliper measurements and the dynamic measurements at 10% WB

Correlations	**Tester 1**		**Tester2**	
	r	***p*-value**	**r**	***p*-value**
DH	0.610**	<0.01	0.655**	<0.01
FW	0.752**	<0.01	0.734**	<0.01

** Significant at the 0.01 level.

Table 5.7: Pearson's correlation between the testers' caliper measurements and the dynamic measurements at 50% WB

Correlations	**Tester 1**		**Tester2**	
	r	***p*-value**	**r**	***p*-value**
DH	0.754**	<0.01	0.819**	<0.01
FW	0.854**	<0.01	0.747**	<0.01

** Significant at the 0.01 level.

Table 5.8: Pearson's correlation between the testers' caliper measurements and the dynamic measurements at 90% WB

Correlations	**Tester 1**		**Tester2**	
	r	***p*-value**	**r**	***p*-value**
DH	0.730**	<0.01	0.775**	<0.01
FW	0.787**	<0.01	0.745**	<0.01

** Significant at the 0.01 level.

The Pearson's correlation results indicate statistically significant correlations for the DH and FW measurements for both testers across all three weight-bearing conditions ($p < 0.01$). The correlations were highest for the 50% WB condition and the weakest for both testers at 10% WB.

The Pearson's correlation results for the FMM between 10% WB and 50% WB and between 10% WB and 90% WB was not found to have any statistical level of significance between the caliper measurements and the dynamic measurements (Table 5.9). The correlations (r) were weak and ranged from 0.02 and 0.116.

Table 5.9: Pearson's correlation between testers and the dynamic system for the FMM

Correlations	**Tester 1**		**Tester2**	
WB	**r**	***p*-value**	**r**	***p*-value**
10% -50%	-0.076	0.619	0.116	0.447
10%-90%	-0.020	0.895	-0.102	0.504

5.4.2 Comparing static and dynamic AHI measurements

The mean, standard deviation and Standard Error of Measurement (SEM) values for the Foot Length (FL) and Truncated Foot Length (TFL) at 10%, 50% and 90% WB

for both testers and the dynamic measurements are summarised in Table 5.10. The mean FL and TFL values for the 10%, 50% and 90% weight-bearing conditions were consistent across both testers and dynamic data capture system measurements. From the results it is apparent that the Standard Error of Measurements (SEM) is high for the TFL and the FL indicating that the variations in the repeated foot length measurements are high. The highest SEM values were calculated for the FL measurements and were generally similar across all the weight-bearing conditions and for the static and dynamic measurements.

Table 5.10: Descriptive data for static and dynamic measurements of the FL and TFL at 10%, 50% and 90% WB

% WB	Tester 1			Tester 2			Dynamic system		
	Mean (mm)	SD (mm)	SEM (mm)	Mean (mm)	SD (mm)	SEM (mm)	Mean (mm)	SD (mm)	SEM (mm)
10% FL	268.079	17.77	2.649	268.166	17.884	2.67	267.861	18.745	2.794
TFL	197.888	14.481	2.159	198.386	14.323	2.135	199.256	13.975	2.083
50% FL	271.046	17.784	2.651	271.069	17.151	2.557	270.263	16.435	2.45
TFL	198.937	14.405	2.147	200.346	13.022	1.941	200.034	13.2	1.968
90% FL	271.387	17.303	2.579	271.017	17.515	2.611	270.937	16.598	2.474
TFL	201.019	14.077	2.172	200.548	15.081	2.327	201.183	13.294	2.051

The variations between the four sets for the measurements of the components of both versions of the AHI (AHI 1 and AHI 2) were analysed using Intra-rater reliability results (Table 5.11).

Table 5.11: Intraclass correlation coefficients (ICC) for intra-tester reliability of the FL and TFL measurements

	Tester $1_{caliper}$		Tester $2_{caliper}$		Dynamic measurements	
% WB	**ICC**	**95% C.I**	**ICC**	**95% C.I**	**ICC**	**95% C.I**
10% FL	0.999	0.998-1.00	0.999	0.999-1.00	0.999	0.998-1.00
TFL	0.995	0.990-0.998	0.996	0.991-0.998	0.998	0.995-0.998
50% FL	0.999	0.998-1.00	0.999	0.998-1.00	0.999	0.997-1.00
TFL	0.992	0.982-0.997	0.996	0.991-0.999	0.998	0.996-0.999
90% FL	0.999	0.999-1.00	0.999	0.999-1.00	0.998	0.996-0.999
TFL	0.994	0.987-0.998	0.997	0.993-0.999	0.998	0.996-0.999

The intra-rater reliability results of the Truncated Foot Length (TFL) and the Foot Length (FL) were considered *almost perfect* for all the measurements and across all weight-bearing conditions with a range of 0.992 to 0.999. The ICC values

for the TFL measurements were slightly higher for the dynamic measurements compared to the testers' measurements whereas the FL measurements were almost identical between the static and dynamic measurements. There was no significant change in the intra-rater reliability results when the weight-bearing conditions were changed. Due to the small variations between the ICC values for the dynamic image-based system measurements across weight-bearing conditions, it is evident that this measurement technique provides more robust measurement repeatability.

The inter-tester reliability (Table 5.12) showed *almost perfect* agreement between the two testers in conducting the same manual measurements. The lowest ICC value (0.984) was obtained for the TFL at 50% WB and the highest (0.999) was obtained for FL at 90% WB. The TFL showed less reliability across all the weight-bearing conditions compared to the FL measurements, indicating that the testers' measurements were closer in agreement for the FL measurements.

Table 5.12: Intraclass correlation coefficients (ICC) for inter-rater reliability

	Tester 1 and Tester 2		**Dynamic measures and Tester 2**		**Dynamic measures and Tester 1**	
% WB	**ICC**	**95% C.I**	**ICC**	**95% C.I**	**ICC**	**95% C.I**
10% FL	0.998	0.997-0.999	0.986	0.975-0.993	0.987	0.976-0.993
TFL	0.988	0.979-0.994	0.987	0.976-0.993	0.982	0.967-0.990
50% FL	0.998	0.997-0.999	0.992	0.985-0.996	0.989	0.981-0.994
TFL	0.984	0.972-0.991	0.994	0.989-0.997	0.985	0.970-0.991
90% FL	0.999	0.977-0.999	0.933	0.887-0.996	0.994	0.989-0.997
TFL	0.991	0.983-0.995	0.960	0.927-0.978	0.964	0.935-0.980

The inter-rater reliability between the dynamic measurements and the testers' measurements was also *almost perfect* with a range between 0.933 and 0.994. The lowest ICC values were found between the dynamic measurement system and Tester 2 for the FL (ICC = 0.933) and the TFL (ICC = 0.960) at 90% weight-bearing. The ICC between the dynamic system and Tester 1 was also lower for the TFL measurement at 90% weight-bearing than the 10% and 50% weight-bearing conditions (ICC = 0.964).

The ICC results were also determined for the AHI measurements and listed in Tables 5.13 and 5.14 for AHI 1 and AHI 2 respectively. The repeated measurement sets provided higher intra-rater reliabilities for the dynamic measurements when compared to the testers' measurements. For the dynamic AHI 1 and AHI 2 measurements, the highest reliability was determined for the 50% weight-bearing condition and the lowest was for the 90% WB conditions. The ICC values for the testers were similar for both variations of the AHI. For the manual testers' measurements of the AHI 1 the highest ICC values were achieved at the 10% WB and the lowest were for the 50% WB condition. In contrast, the highest ICC values for AHI 2 were found for the 90% WB measurements and the lowest were also for the 50% WB measure.

Table 5.13: Intra-rater ICC for AHI 1 (DH/TFL) at the different weight-bearing conditions

DH/TFL	Tester $1_{caliper}$		Tester $2_{caliper}$		Dynamic measurements	
% WB	**ICC**	**95% C.I**	**ICC**	**95% C.I**	**ICC**	**95% C.I**
10%	0.969	0.931-0.988	0.967	0.926-0.987	0.991	0.979-0.997
50%	0.957	0.903-0.983	0.960	0.910-0.984	0.992	0.981-0.997
90%	0.961	0.915-0.985	0.962	0.912-0.985	0.984	0.961-0.994

Table 5.14: Intra-rater ICC for AHI 2 (DH/FL) at the different weight-bearing conditions

DH/FL	Tester $1_{caliper}$		Tester $2_{caliper}$		Dynamic measurements	
% WB	**ICC**	**95% C.I**	**ICC**	**95% C.I**	**ICC**	**95% C.I**
10%	0.961	0.911-0.985	0.965	0.919-0.987	0.990	0.977-0.996
50%	0.956	0.900-0.983	0.954	0.898-0.982	0.993	0.984-0.998
90%	0.963	0.916-0.985	0.971	0.934-0.989	0.981	0.954-0.993

Inter-rater reliability was again determined to assess the correlations between the dynamic and the static weight-bearing measurements for AHI 1 and AHI 2. The results are listed in Tables 5.15 and 5.16 for AHI 1 and AHI 2 respectively. The ICC values between Tester 1 and Tester 2 were generally lower for the AHI 2 measurements than the AHI 1 measurements for the 10% and 50% WB conditions but higher for the 90% WB condition. The agreement between the static and dynamic measurements was also lower for the AHI 2 measurements with the lowest ICC value of 0.766. This was found between the dynamic measurements and the static caliper measurements conducted by Tester 1 at 10% WB. Similarly the smallest level of agreement for the AHI 1 measurements was ICC of 0.879 between the dynamic system and Tester 1 at 10% WB. The highest agreement values for both AHI 1 and AHI 2 between the dynamic and static measurements were for the 50% weight-bearing condition.

Table 5.15: Intraclass correlation coefficients (ICC) for inter-rater reliability for AHI 1 (DH/TFL) between static and dynamic measures

DH/TFL	Tester 1 and Tester 2		Tester 2 and dynamic measures		Tester 1 and dynamic measures	
% WB	**ICC**	**95% C.I**	**ICC**	**95% C.I**	**ICC**	**95% C.I**
10%	0.941	0.893-0.968	0.889	0.797-0.939	0.879	0.779-0.933
50%	0.910	0.837-0.951	0.947	0.903-0.971	0.915	0.846-0.954
90%	0.884	0.789-0.936	0.903	0.824-0.947	0.883	0.788-0.936

Table 5.16: Intraclass correlation coefficients (ICC) for inter-rater reliability for AHI 2 (DH/FL) between static and dynamic measures

DH/TFL	Tester 1 and Tester 2		Tester 2 and dynamic system		Tester 1 and dynamic system	
% WB	**ICC**	**95% C.I**	**ICC**	**95% C.I**	**ICC**	**95% C.I**
10%	0.938	0.887-0.966	0.789	0.647-0.878	0.766	0.611-0.846
50%	0.903	0.820-0.948	0.931	0.872-0.963	0.913	0.838-0.953
90%	0.887	0.795-0.938	0.829	0.709-0.902	0.785	0.641-0.876

To determine the significance of the levels of agreement between the static and dynamic system, Pearson's correlation coefficients were used for the measurements of the FL, TFL, AHI 1 and AHI 2 and the results are shown in Tables 5.17, 5.18 and 5.19 for the 10%, 50% and 90% WB conditions respectively.

Table 5.17: Pearson's correlation between testers and the dynamic measures at 10% WB

Correlations	Tester 1		Tester 2	
	r	***p*-value**	**r**	***p*-value**
FL	0.975**	<0.01	0.974**	<0.01
TFL	0.965**	<0.01	0.974**	<0.01
AHI 1	0.772**	<0.01	0.705**	<0.01
AHI 2	0.675**	<0.01	0.707**	<0.01

** Correlation significant at the 0.01 level

Table 5.18: Pearson's correlation between testers and the dynamic measures at 50% WB

Correlations	Tester 1		Tester 2	
	r	***p*-value**	**r**	***p*-value**
FL	0.989**	<0.01	0.987**	<0.01
TFL	0.973**	<0.01	0.988**	<0.01
AHI 1	0.792**	<0.01	0.826**	<0.01
AHI 2	0.791**	<0.01	0.867**	<0.01

** Correlation significant at the 0.01 level

Table 5.19: Pearson's correlation between testers and the dynamic measures at 90% WB

Correlations	Tester 1		Tester 2	
	r	***p*-value**	**r**	***p*-value**
FL	0.982**	<0.01	0.985**	<0.01
TFL	0.923**	<0.01	0.933**	<0.01
AHI 1	0.787**	<0.01	0.786**	<0.01
AHI 2	0.636**	<0.01	0.733**	<0.01

** Correlation significant at the 0.01 level

From the Pearson's correlation results, the levels of association were statistically significant ($p < 0.01$) between the dynamic measurements and each tester's measurements across the three weight-bearing conditions. The level of correlation was highest at the 50% WB condition and the correlations were similar for both testers.

5.5 Discussion

Conventional clinical assessment techniques of foot mobility are used to measure changes in bony landmarks on the foot statically between maximum and minimum weight-bearing conditions applied on the foot. The changes in the bony landmark positions are then used to infer the behaviour of the foot dynamically. The limitation with these static assessment techniques is that they assume that the foot is a single rigid body and are unable to reflect the true behaviour of the foot during dynamic mobility for activities such as gait.

The relationship between two conventional static foot assessment techniques based on the Dorsum as a point of reference and the behaviour of the same measurements dynamically were compared in this research. The FMM and AHI were selected due to their high levels of reliability and validity when compared to other clinical foot assessment techniques (McPoil et al., 2008b; McPoil et al., 2009). The developed data capture system was used to collect the dynamic measurements during gait and compare them with conventional static caliper measurements from two testers. Variations between the dynamic and static measurements were expected as a result of dynamic foot morphology.

From the inter-rater ICC reliability results, lower levels of correlations were exhibited between the dynamic measurements and each of the tester's measurements than between the two manual measurements collected between the two testers. This was expected as the weight-bearing conditions selected during gait; namely 1) the heel contact, 2) mid-stance and 3) active propulsion were based on the lowest, middle and highest foot loading stages of the gait cycle so they do not match the static 10%, 50% and 90% weight-bearing conditions exactly. The DH measurements provided lower inter-rater reliability results between Tester 1 and Tester 2 across all weight-bearing conditions compared to the other measurements. This was the result

of the difficulty in measuring the Dorsum height from the supporting ground surface every time the foot was relaxed and re-measured as opposed to measuring between foot markers.

The inter-rater ICC values between Tester 1 and Tester 2 were high for the FW measurements across all weight-bearing conditions whereas the correlations between the dynamic measurements and static measurements from both testers only provided moderate correlations. This is likely to be the direct result of the narrowing of the foot during gait as compared to the widening of the foot when weight-bearing is applied on the foot statically. Interestingly, the agreement between the dynamic and static measurements improved for the DH and FW at 50% WB which could indicate that the 50% static weight-bearing might be a better predictor of the dynamic behaviour of the foot than at 90% static weight-bearing.

In order to assess the level of association between the dynamic and static measurements, Pearson's correlation coefficients were calculated and the level of significant was determined at $p < 0.01$. The correlation results indicated a high association level for all the anthropometric markers; namely the DH, FW, FL and TFL as well as for the AHI 1 and AHI 2 calculations at all the weight-bearing conditions. The levels of correlations were also found to be higher for the FL and TFL compared to the DH and FW across all weight-bearing conditions. The agreements between the static and dynamic DH, FW and FL measurements as determined from the Pearson's correlations were the highest between the static caliper measurements from both testers at 50% WB and the dynamic foot measurements at mid-stance. The lowest levels of agreement were identified for the DH, FW and FL measurements between the static 10% WB measurements and the dynamic heel contact measurements. In contrast, the level of association between the static and dynamic TFL measurements was highest for both testers at 50% WB and the lowest was between the static 90% WB measurements and the dynamic measurements at active propulsion. Overall, the excellent reliability results from this study were in agreement to the intra-tester results found in McPoil et al. (2009).

In the current study, the authors expected the ICC values for the 90% WB condition to be lower for the manual caliper measurements as it was speculated that the subjects would find it harder to maintain 90% WB for the measurement duration. Subject fatigue was evident when the measurements were conducted as they needed to maintain 90% weight-bearing for a few minutes. The reason for the higher ICC values at 90% WB is speculated to be the result of the subject's familiarity with the measurements as it was the final weight-bearing measurements to be collected for each subject.

In contrast to the high levels of correlations between the static and dynamic individual anthropometric measurements, the FMM results were significantly different between the static and dynamic measures. As the FMM was developed as a measure of foot mobility to reflect the behaviour of the Medial Longitudinal Arch dynamically, the weak level of association between the static and dynamic foot measurements revealed that the test might not be suitable for predicting dynamic foot mobility during gait. The Intra-rater correlation ICCs were significantly higher for the repeated dynamic measurements than the static measurements. In particular, the

high intra-rater reliability between both the testers and the dynamic measurements was more evident between 10% and 50% WB than between 10% and 90% WB. It is therefore concluded that measuring the FMM between 10% WB and 50% WB results in more repeatable measures as this weight-bearing condition might provide a better prediction of foot mobility and is encouraged to be considered in future studies. The level of association between the static and dynamic measurements as evident by the Pearson's correlation results were also found to be weaker for the 10% to 90% WB confirming the above statement.

For the AHI measurements, the intra-rater ICC values showed higher repeatability results for the dynamic measurements compared to the tester's static caliper measurements. For the AHI 1 and the AHI 2, the highest reliability for the dynamic measurements was determined for the 50% WB condition and the lowest was found at the 90% WB. This indicates that the repeatability of the dynamic system measurements was better at mid-stance as at this condition, the dynamic measurements are less variable than at heel contact and active propulsion. The intra-rater results between Tester 1 and Tester 2 were similar for both testers with the 50% WB showing the lowest level of repeatability. The reason for this could be due to the lower repeatability of the manual DH measurements at the 50% WB condition than the 10% and 90% WB conditions. The was not expected as the 50% WB condition was found to be easier for the testers to conduct than the 10% WB or 90% WB conditions.

The inter-rater ICC results for the AHI 1 and AHI 2 show that the highest level of agreement between the static and dynamic measurements was for the 50% WB condition. It is hence concluded that measuring the AHI as a predictor of the dynamic foot posture at 50% WB might provide a better prediction of the dynamic foot posture. The level of agreement between the static and dynamic measurements was higher for the AHI 1 measurements than the AHI 2 measurements indicating that measuring the TFL is more correlated to the dynamic TFL than between the static and dynamic FL. Overall, the level of association was high between each of the tester's manual measurements and the dynamic measurements. The highest level of association from the Pearson's correlation analysis was between the static and dynamic measurements at 50% WB. The AHI 1 measurements showed a higher level of association than the AHI 2 measurements between the static and dynamic measurements.

5.6 Conclusion

The level of correlation between conventional static foot mobility assessments based on the changes in the dorsum and the same measurements collected dynamically during gait was investigated and reported in this chapter. The two clinical measurement techniques selected in the study were the Foot Mobility Magnitude (FMM) and the Arch height Index (AHI). These two dorsum measurement techniques were proven to have high levels of reliability and validity compared to other conventional foot mobility assessment techniques. From the results of the study, it was found that the individual anthropometric measurements used to derive the FMM had high levels of correlation between static and dynamic measurements.

However, the correlation between static and dynamic FMM measurements was weak. Two variations of the AHI were compared statically and dynamically and higher levels of inter-rater and intra-rater reliabilities were found for the individual anthropometric points used to derive the AHI measurements than for the individual measurements used to derive the FMM. High levels of correlation were also found between the static and dynamic AHI measurements for both versions of the AHI indicating that the AHI is a better predictor of foot mobility than the FMM.

The current clinical measurements of foot mobility are determined from static measurements where the subjects adjust their feet from a minimally-weighed position (usually at 10% WB) to a maximum weight-bearing position (usually 90% WB). The changes in anthropometric locations are used to infer foot mobility. In the current study, higher levels of reliability and stronger static correlations with dynamic measurements were found during the 50% WB condition (mid-stance). It is therefore suggested for the 50% WB condition to be considered in future dynamic foot mobility assessments. Overall the subjects included in this study had different arch structures and foot lengths therefore the effect these morphological changes on the foot mobility based on the Foot Posture Index (FPI) scoring system will be investigated in the next chapter.

Chapter 6: Relationship between FPI and foot mobility

6.1 Introduction

The Foot Posture Index (FPI) has in recent years become one of the most useful foot posture assessment tools due to its proven high reliability and validity (Cornwall et al., 2008; McPoil et al., 2009). The main advantage of the FPI over other foot posture assessment techniques is the ability to provide a multi-segment analysis of the foot from six different foot components. Nielsen et al. (2010) conducted a study to determine whether the multi-segment analysis from the six different foot components of the FPI provides a better indication of the dynamic foot behaviour. A 2D motion tracking system was used to determine the relationship between the Navicular Drop (ND) and the FPI scores and from their study; the authors found that the ND measurements were only 13.2% correlated to the FPI. The FPI is yet to be assessed for reliability against dynamic foot mobility and posture measures based on the dorsum as a point of reference. Therefore, this chapter utilises the developed dynamic 3D measurement system to determine the relationship between the FPI scores with the dynamic Foot Mobility Magnitude and Arch Height Index measures.

6.2 Methods

6.2.1 Subjects

For the comparison of static and dynamic foot posture measurements, 15 male participants volunteered to be included in the study after providing a written informed consent (Appendix A). The criteria for participant inclusion in the study were a minimum age of 18 years and no previous history of lower limb injury, disease or deformity. The mean age of the participants was 31.6 ± 6.2 years and the mean weight was 84.3 ± 8.5 kilograms. Only the right foot of all the participants was measured.

6.2.2 Foot Posture Index (FPI) classifications

The standing foot posture was determined through the FPI scoring system which is composed of five visual assessments of the foot and a single palpation assessment of the talus bone. Each of the component tests were graded 0 for normal foot, a minimum score of -2 if the foot is severely supinated (highly arched) and a maximum score of +2 for severe pronation (low arched). The six foot posture assessment yields collective results that range from -12 to +12. A collective FPI

score ranging between 0 and 5 indicates a normally arched foot and anything falling outside the normal range is defined as either supinated or pronated (Redmond, 2005). The six assessments are: 1) talar head palpation, 2) supra and infra lateral malleolar curvature, 3) inversion/eversion of the calcaneus, 4) bulging in the talonavicular joint, 5) height and congruence of the Medial Longitudinal Arch and 6) abduction/adduction of the forefoot on the rear foot (Redmond, 2005).

Table 6.1: Individual and collective FPI scoring for the subjects

Subject	Talar head palpation	Malleolar curves	Inv/eversion calcaneus	TNJ prominance	Congruence of MLA	Abd/adduction	Total	Classification
1	+1	+1	+1	+2	+1	0	+6	Pronated
2	+1	+1	0	+1	0	0	+3	Normal
3	0	+1	+2	0	0	+1	+4	Normal
4	-1	-1	-1	0	0	0	-3	Supinated
5	0	0	0	0	+1	+1	+2	Normal
6	+1	0	+1	0	+1	+1	+4	Normal
7	-2	-2	-1	-1	0	-1	-7	Supinated
8	+2	+1	+1	+2	+2	+1	+9	Pronated
9	-1	-1	-2	0	-1	-1	-6	Supinated
10	+2	+1	+1	+2	+1	+2	+9	Pronated
11	0	+2	+1	0	+1	+1	+5	Normal
12	+1	0	0	+1	+1	0	+3	Normal
13	0	0	0	0	+1	+1	+2	Normal
14	+1	+2	+1	0	0	+1	+5	Normal
15	-2	-1	-2	-1	-1	-1	-8	Supinated

One examiner with 12 months' FPI assessment experience conducted the tests on all the subjects' feet. Details of the assessment along with the assessment forms are provided in Appendix C. The individual and collective FPI scores for all the subjects are listed in Table 6.1.

6.2.3 Foot markings and data collection

The right foot of the subjects were marked with retro-reflective markings as discussed in Section 5.2.2. These markings allowed for the Foot Mobility Magnitude and Arch Height Index to be determined. The developed 3D dynamic data capture system was then used to collect the dynamic FMM and AHI as detailed in Section 5.2.5.

6.3 Statistical Analysis

A stepwise multiple regression analysis was applied to test which combinations of the FPI components has the highest influence on the dynamic AHI and FMM measurements. Spearman's rank correlation (r_s) was used to determine the relationship between the individual components of the FPI and the dynamic AHI and FMM measurements. Spearman's rank is calculated using:

$$r_s = 1 - \frac{6 \sum d^2}{n\,(n^2 - 1)} \qquad (6.1)$$

Where, *d* is the difference between ranks, and

n is the sample size.

An ANOVA test with a Bonferroni post hoc correction was used to determine the relationship between the individual FPI foot classification groups and the AHI and FMM during the different dynamic weight-bearing conditions during gait. The level of significance was set to $p < 0.05$ for all statistical analyses which were calculated in SPSS version 21.

6.4 Results

6.4.1 Relationship between FPI scores and dynamic FMM and AHI measurements

Figures 6.1 to 6.4 show the individual FPI group classifications for the dynamic AHI 1, AHI 2 and FMM during heel strike, mid-stance and active propulsion. An increase in the dynamic measurements was observed from the pronated to the supinated group for both the AHI 1 and the AHI 2 measurements. The FMM measurements showed similar variations for all the FPI groups. At heel strike, the range of the AHI measurements is shown to be higher for the pronated group for AHI 2 than AHI 1, whereas the normal and supinated groups depicted similar ranges and variations for both the AHI 1 and AHI 2 measurements.

The pronated group showed the least amount of data variation in the mid-stance and active propulsion loading conditions. In contrast, the normally arched group showed the least amount of measurement variation in the AHI 1 and AHI 2 measurements across all the loading conditions.

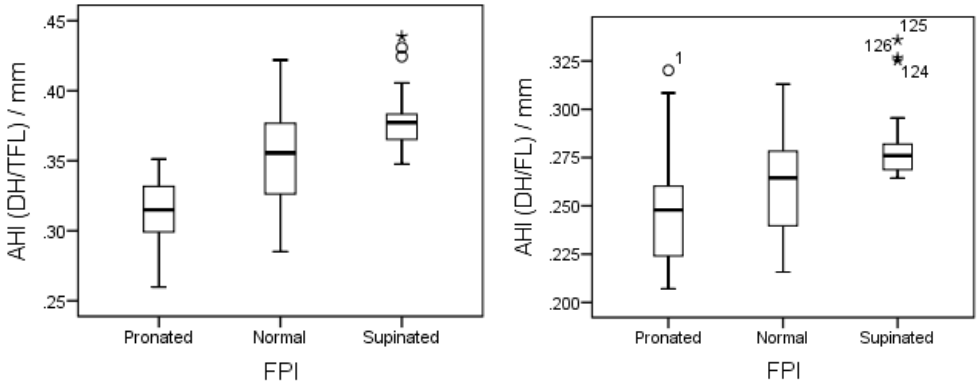

Figure 6.1: FPI group classifications and relationships with AHI 1 (left) and AHI 2 (right) during heel-strike.

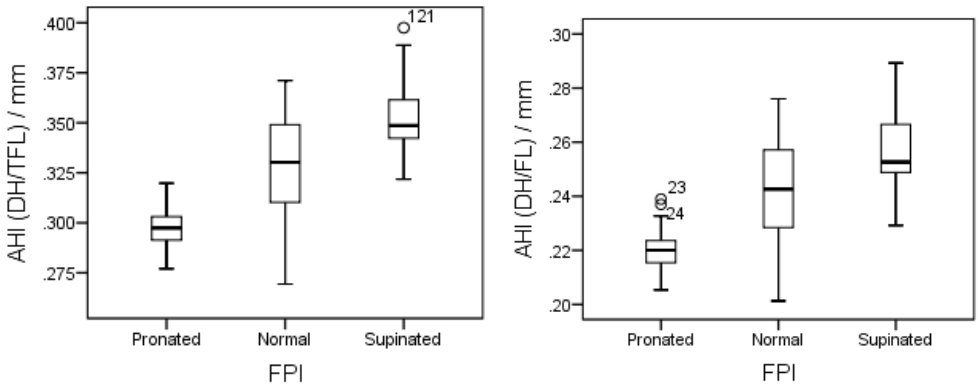

Figure 6.2: FPI group classifications and relationships with AHI 1 (left) and AHI 2 (right) during mid-stance.

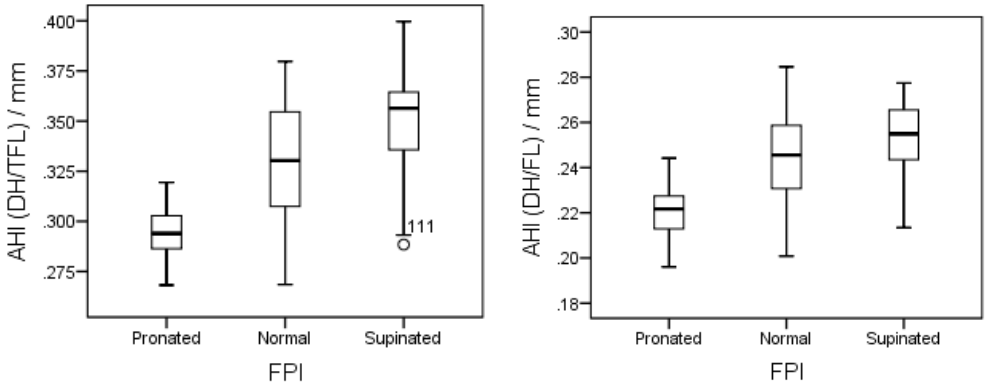

Figure 6.3: FPI group classifications and relationships with AHI 1 (left) and AHI 2 (right) during active-propulsion.

As illustrated in 6.4, no significant differences were found between the FMM and the FPI groups at heel strike to mid-stance. For the heel strike to active propulsion, both the pronated and supinated groups showed an increase in the range of data whereas the normal group measurements were relatively similar to the FMM measurements from heel strike to mid-stance.

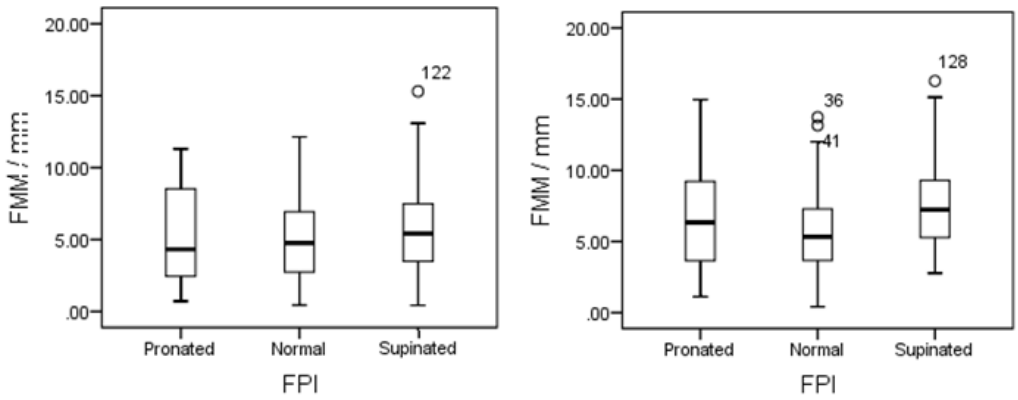

Figure 6.4:.FPI group classifications and relationships with FMM at heel-strike to mid-stance (left) and heel-strike to active-propulsion (right).

Results of the ANOVA significance tests for the relationship between the collective FPI scores and the dynamic AHI 1 and AHI 2 measurements at all three dynamic weight-bearing conditions are listed in Table 6.2 and 6.3.

Table 6.2: Relationship between FPI scores and AHI 1

	Coefficient of determination (r^2)	***f*-value**	***p*-value**
FPI vs. AHI 1 at heel-strike	0.315	5.970	0.030*
FPI vs. AHI 1 at mid-stance	0.408	8.970	0.010*
FPI vs AHI 1 at active propulsion	0.489	12.465	0.004*

* Significant at the 0.05 level.

Table 6.3: Relationship between FPI scores and AHI 2

	Coefficient of determination (r^2)	***f*-value**	***p*-value**
FPI vs. AHI 2 at heel-strike	0.285	5.180	0.040*
FPI vs. AHI 2 at mid-stance	0.337	6.610	0.023*
FPI vs AHI 2 at active propulsion	0.358	7.250	0.018*

* Significant at the 0.05 level.

As shown in Tables 6.2 and 6.3, the collective FPI scores were found to be significantly related to the dynamic AHI 1 and AHI 2 measurements at heel-strike, mid-stance and active-propulsion ($p < 0.05$). However, no significant relationships were found for any of the comparisons between the FPI and the dynamic FMM and are hence not included in the results. The coefficient of determination results reveal that the highest FPI prediction is for the AHI 1 measurements at active propulsion (48.9%) and the lowest is for the AHI 2 measurements at heel strike (28.5%). This means that the FPI predicted 48.9% of the variation of AHI 1 at active prolusion.

To determine which of the six FPI components had the highest significance level to the dynamic AHI 1 and AHI 2 measures, the Spearman's rank tests were used (Tables 6.4, 6.5 and 6.6). From the results, it was identified that the only component of the FPI to be significantly related to all the dynamic measurements of the AHI 1 and the AHI 2 was the congruence of the MLA ($p < 0.05$). The remaining components of the FPI were not found to have any significant influence on the dynamic AHI 1, AHI 2 and FMM results as shown by the Spearman's rank test results in Tables 6.4, 6.5 and 6.6 for the AHI 1, AHI 2 and FMM respectively.

Table 6.4: Relationships between the individual components of the FPI and the AHI 1

FPI component	Spearman's rank	AHI 1 at heel strike	AHI 1 at mid stance	AHI 1 at active propulsion
Talar head palpation	r_s	0.341	0.291	0.422
	p-value	0.214	0.293	0.118
Malleolar curvature	r_s	0.315	0.229	0.465
	p-value	0.252	0.412	0.081
Inversion/ Eversion	r_s	0.343	0.257	0.448
	p-value	0.210	0.354	0.094
TNJ Prominance	r_s	0.322	0.409	0.497
	p-value	0.242	0.130	0.059
Congruence of MLA	r_s	0.831*	0.713*	0.704*
	p-value	0.000	0.003	0.003
Abd/Adduction	r_s	0.563	0.365	0.435
	p-value	0.290	0.181	0.105

** Correlation significant at the 0.05 level

Table 6.5: Relationships between the individual components of the FPI and the AHI 2

FPI component	Spearman's rank	AHI 2 at heel strike	AHI 2 at mid stance	AHI 2 at active propulsion
Talar head palpation	r_s	0.293	0.311	0.355
	p-value	0.290	0.259	0.194
Malleolar curvature	r_s	0.339	0.301	0.498
	p-value	0.216	0.276	0.059
Inversion/ Eversion	r_s	0.299	0.299	0.422
	p-value	0.280	0.280	0.117
TNJ Prominance	r_s	0.302	0.390	0.439
	p-value	0.274	0.151	0.102
Congruence of MLA	r_s	0.758*	0.731*	0.669*
	p-value	0.001	0.002	0.006
Abd/Adduction	r_s	0.493	0.342	0.412
	p-value	0.062	0.213	0.127

** Correlation significant at the 0.05 level

Table 6.6: Relationships between the individual components of the FPI and the FMM

FPI component	Spearman's rank	FMM at heel strike to mid stance	FMM at mid stance to active propulsion
Talar head palpation	r_s	0.083	0.326
	p-value	0.769	0.236
Malleolar curvature	r_s	0.157	0.258
	p-value	0.577	0.353
Inversion/ Eversion	r_s	0.114	0.209
	p-value	0.686	0.455
TNJ Prominance	r_s	0.224	0.068
	p-value	0.422	0.809
Congruence of MLA	r_s	0.385	0.283
	p-value	0.157	0.307
Abd/Adduction	r_s	0.424	0.344
	p-value	0.115	0.210

The highest correlation from the Spearman's correlation test was found to be the congruence of the MLA for AHI 1 at heel strike (0.831). The congruence of the MLA correlations were higher for the AHI 1 measurements across all the dynamic loading conditions and were also the highest for the heel strike condition for both AHI 1 and AHI 2. The lowest correlations for AHI 1 and AHI 2 were for the active propulsion measurements. None of the FPI components were found to be significantly correlated to any of the FMM measurements as shown in Table 6.6.

This relationship between the congruence of the MLA and the AHI 1 and AHI 2 is shown in Tables 6.7 and 6.8 with the highest level of significance found between the congruence and the AHI 1 at heel strike (0.667). This indicates that the congruence of the MLA predicted 66.7% of the variation in the AHI 1 at heel strike, 53.7% at mid-stance and 51.1% at active propulsion. The level of prediction was lower for the congruence of the MLA for the AHI 2 measurements with the highest

prediction at heel strike (59.7%) and the lowest for the active propulsion dynamic loading (39.1%).

Table 6.7: Relationship of Congruence at MLA with AHI 1

	Coefficient of determination (r^2)	***f*-value**	***p*-value**
Congruence vs. AHI 1 at heel-strike	0.667	26.064	0.000*
Congruence vs. AHI 1 at mid-stance	0.537	15.083	0.002*
Congruence vs. AHI 1 at active propulsion	0.511	13.560	0.003*

* Significant at the 0.05 level.

Table 6.8: Relationship of Congruence at MLA with AHI 2

	Coefficient of determination (r^2)	***f*-value**	***p*-value**
Congruence vs. AHI 2 at heel-strike	0.597	19.265	0.001*
Congruence vs. AHI 2 at mid-stance	0.406	10.570	0.006*
Congruence vs. AHI 2 at active propulsion	0.391	8.356	0.010*

* Significant at the 0.05 level.

The within-group and between-group ANOVA results for the level of significance between the FPI groups for the AHI 1, AHI 2 for heel-strike, mid-stance and active propulsion are listed in Tables 6.9 to 6.14.

Table 6.9: Within group and between group ANOVA for the relationship between FPI and dynamic AHI 1 at heel strike.

	FPI	**FPI**	**Within group ANOVA *p*-value**	**Between group ANOVA**	
AHI 1	Pronated	Normal	0.118	**F value**	***p*-value**
	Normal	Supinated	1.00	3.162	0.053
	Supinated	Pronated	0.063		

Table 6.10: Within group and between group ANOVA for the relationship between FPI and dynamic AHI 1 at mid-stance.

	FPI	**FPI**	**Within group ANOVA *p*-value**	**Between group ANOVA**	
AHI 1	Pronated	Normal	1.00	**F value**	***p*-value**
	Normal	Supinated	0.104	3.651*	0.035
	Supinated	Pronated	0.048*		

* Correlation significant at the 0.05 level

Table 6.11: Within group and between group ANOVA for the relationship between FPI and dynamic AHI 1 at active propulsion.

	FPI	**FPI**	**Within group ANOVA *p*-value**	**Between group ANOVA**	
AHI 1	Pronated	Normal	0.000*	**F value**	***p*-value**
	Normal	Supinated	0.034*	21.257*	0.000
	Supinated	Pronated	0.000*		

* Correlation significant at the 0.05 level

Table 6.12: Within group and between group ANOVA for the relationship between FPI and dynamic AHI 2 at heel strike.

	FPI	**FPI**	**Within group ANOVA *p*-value**	**Between group ANOVA**	
AHI 2	Pronated	Normal	0.160	**F value**	***p*-value**
	Normal	Supinated	0.024*	8.296*	0.001
	Supinated	Pronated	0.001*		

** Correlation significant at the 0.05 level

Table 6.13: Within group and between group ANOVA for the relationship between FPI and dynamic AHI 2 at mid-stance.

	FPI	**FPI**	**Within group ANOVA *p*-value**	**Between group ANOVA**	
AHI 2	Pronated	Normal	0.000*	**F value**	***p*-value**
	Normal	Supinated	0.424	12.911*	0.000
	Supinated	Pronated	0.000*		

* Correlation significant at the 0.05 level

Table 6.14: Within group and between group ANOVA for the relationship between FPI and dynamic AHI 2 at active propulsion.

	FPI	**FPI**	**Within group ANOVA *p*-value**	**Between group ANOVA**	
AHI 2	Pronated	Normal	0.001*	F value	***p*-value**
	Normal	Supinated	0.186	13.394*	0.000
	Supinated	Pronated	0.000*		

* Correlation significant at the 0.05 level

From the between-group ANOVA results, significance differences were found between the FPI groups and the dynamic AHI 2 measurements at all three dynamic loading conditions ($p < 0.05$). For the dynamic AHI 1 measurements, significant differences were found between the FPI groups at mid-stance and active-prolusion but not at heel-strike. For the dynamic FMM measurements, significant differences were found between the FPI groups and the FMM calculated between mid-stance and active prolusion ($f = 8.778$, $p = 0.001$) but not between heel-strike and active propulsion ($f = 1.445$, $p = 0.247$).

Table 6.15: Within group and between group ANOVA for the relationship between FPI and dynamic FMM at heel strike to mid-stance.

	FPI	**FPI**	**Within group ANOVA *p*-value**	**Between group ANOVA**	
FMM	Pronated	Normal	0.001*	**F value**	***p*-value**
	Normal	Supinated	0.019*	8.778*	0.001
	Supinated	Pronated	0.263		

* Correlation significant at the 0.05 level

Table 6.16: Within group and between group ANOVA for the relationship between FPI and dynamic FMM at heel strike to active propulsion.

	FPI	**FPI**	**Within group ANOVA *p*-value**	**Between group ANOVA**	
FMM	Pronated	Normal	0.830	**F value**	***p*-value**
	Normal	Supinated	0.365	1.445	0.247
	Supinated	Pronated	1.00		

For the within-group ANOVA results of the dynamic AHI 1, none of the three FPI groups were significantly different from each other at heel strike. The only group significant difference was found between the supinated and pronated group at mid-stance ($p = 0.048$). However all the groups were significantly different at active-propulsion. In contrast, for the AHI 2 measurements, the only group found to not be significantly different for the FPI groups was between the pronated and normal groups (sig. = 0.160) for heel strike, between the normal and supinated group (sig. = 0.424) at mid-stance and between the normal and supinated group (sig. = 0.186) for active propulsion.

For the dynamic FMM measurements between heel-strike and mid-stance, the only within group significant differences were found between the pronated and the normal group ($p = 0.001$) and between the supinated and normal group ($p = 0.019$). No significant differences were found between any of the three FPI groups and the dynamic FMM measurements calculated between heel-strike and active propulsion.

6.5 Discussion

From the FPI-6 scores, the subject's feet were classified into one of three groups namely; pronated, supinated or normally arched. The level of significance between each of the FPI classification groups and the dynamic AHI and FMM measurements as determined by ANOVA tests showed that all the dynamic measurements were significantly related except for the AHI 1 at heel strike ($F= 3.162$, $P = 0.053$). Significant levels were also evident for the FMM measurements between heel strike and active propulsion ($F= 1.445$, $P = 0.247$). The box and whisker plots (Figure 6.4) show the extent of the significance of the measurements were very small variations seen across the three classification groups for the dynamic FMM measurements. This indicates that the measurements of foot posture based on the dorsum of the foot as a point of reference during dynamic loading provide good agreement with the FPI which is a useful multi-segment assessment tool. Using the dorsum for measurements of the foot posture provides higher levels of validity, reliability (Williams and McClay, 2000) and accuracy (Nielsen et al., 2010) than measuring the navicular bone which is currently the most common foot posture measurement technique. Hence, the levels of significance between the FPI score groups and the dorsum-based measurements will provide an accurate assessment tool for identifying differences based on FPI grouping.

From the significance results between the three FPI groups, it was found that the AHI 2 might provide better levels of significance between the three FPI groups than the AHI 1 measurements based on the between group ANOVA results. For the FMM measurements, significant differences between the FPI scoring groups were only identified between heel strike and mid-stance. Hence it can also be assumed that this difference in loading provides a better predictor of the differences in the dynamic foot mobility for the three different foot classification groups.

From the stepwise multiple regression analysis and the ANOVA for determination of the levels of significance between the combined FPI scores with the dynamic measurements, no significant levels were found between the FPI scores and the FMM measurements. Significant relationships were however found for both AHI 1 and AHI 2 at all dynamic loading conditions. The highest FPI predictions were for AHI 1 and AHI 2 at active propulsion where the FPI predicted 48.9% ($F = 12.465$, $P = 0.004$) of the variation for AHI 1 and 35.8% ($F = 7.250$, $P = 0.018$) of the variation for AHI 2. Previous studies only assessed the variations between dynamic measurements at mid-stance loading during dynamic gait. For instance, Redmond et al. (2006a) found the FPI predicted 41% of the dynamic variation of mid-stance based on measurements of the rear-foot angle. Nielsen et al. (2010) found the FPI predicted 45% prediction of the mid-stance navicular measurements. The results of the current study were similar to the results obtained by Nielsen et al. (2010) and Redmond et al.(2006a) where mid-stance FPI predicted 40.8% ($F = 8.970$, $P = 0.010$) of the variation for the AHI 1 measurements and 33.7% ($F = 6.610$, $P = 0.023$) of the variation for AHI 2. From these results, it is suggested that the use of active propulsion during dynamic loading instead of the mid-stance might provide a better prediction for FPI.

From the multiple regression and Spearman's rank correlation analyses it was also found that congruence of the MLA was the only component of the MLA that was significantly correlated with the dynamic AHI measurements. The highest congruence of the MLA predictions were observed at heel strike and the highest prediction of 66.7% was observed for AHI 1 ($F = 26.064$, $P < 0.001$). The reason for this high prediction level is due to the fact that the congruence of the MLA is the only FPI component which measures the sagittal plane foot posture (Redmond et al., 2006a). As there was no significant correlation between the FPI scores and the dynamic FMM measurements, a possible explanation might be that the dynamic FMM quantifies different foot characteristics to those quantified by the FPI. Hence, it is concluded that the FPI is not correlated with the dynamic FMM. This supports the statements of Cashmere et al. (1999) and Razeghi and Batt (2002) who stated that the static foot posture measurements do not measure the same qualities of foot mobility. From the results of this study, it was identified that in order to relate the FPI scoring system to foot mobility and posture, the measurements of foot posture and mobility need to be conducted dynamically.

6.6 Conclusion

Different foot classifications obtained from the Foot Posture Index (FPI) technique with the AHI and FMM at different dynamic foot loading conditions, namely heel-strike, mid-stance and active propulsion were compared and reported in this chapter.

Through the study, it was found that foot posture measurements based on the dorsum of the foot as a point of reference during dynamic loading provides a good level of agreement with the FPI scores. The AHI 2; which measures the ratio of the foot length to the truncated foot length was found to be better correlated with the FPI than the AHI 1 measurements. Conversely, FMM did not show any significant levels of association with the FPI. The highest FPI predictions were found at active propulsion compared to mid-stance and heel-strike for the dynamic AHI 1 and AHI 2 measurements. It is therefore concluded that the assessment of foot mobility at active propulsion provides a better indicator of the FPI assessment technique.

Chapter 7: Conclusions

A brief discussion of the research significance and outcomes and the original contribution achieved from this study is presented in this chapter. The research limitations are finally outlined and suggestions for future improvements and areas of applications are highlighted.

7.1 Significance of the research project

A number of techniques have been suggested for the 3D measurement of the foot dynamically. Most of these techniques have shortcomings that restrict their implementation for dynamic foot analysis. The development of a suitable measurement technique for dynamic foot assessments that allow for incorporating ground reaction force information to a high level of measurement accuracy has been developed as part of this thesis. Close-range Photogrammetry was the technique proposed for developing the 3D measurement system due its high accuracy and ability to measure dynamic objects.

7.2 General conclusions

The factors influencing the design and development of the 3D photogrammetric dynamic data capture system were investigated in Chapter 3. The design requirements such as the number and type of imaging sensors, the geometry of the sensors and the distribution of project control were optimised. Twelve HD JVC Everio GZ-500 camcorders were used to image the dynamic foot from the medial, lateral, posterior and anterior sides. To synchronise the ground reaction force information acting on the foot during gait, an elevated platform was custom-built with a force plate installed in its centre. The camcorders and the force plate were synchronised using a gen-lock system.

The accuracy capability of the camcorders was tested through individual camcorder calibrations. A range of convergent images ranging between 6 and 12 were used in the calibration to determine the effect of increasing the number of convergent images on the 3D RMS of control targets and the findings were as follows:

- A minimum of eight images are necessary to meet the 3D RMS tolerance of 0.05 mm specified for the project.
- 12 images were required to stabilise the 3D RMS across the camcorders.

- Increasing the number of images reduced the discrepancies in the 3D RMS between the camcorders.

To assess the stability of the camcorder lenses over a period of time, two calibration sessions, one month apart were conducted for all 12 camcorders. Small changes in the calibration parameters were found between the two calibration days. The effect of the small discrepancies on the measurement accuracies were however insignificant; yielding measurement discrepancies less than 0.07 mm between the two calibration sessions.

In the clinical setting, conventional caliper measurements of subjects' feet are collected and are used to infer dynamic foot mobility. The accuracy of manual caliper measurements was investigated in Chapter 4 by comparing the manual measurements to the 'gold standard' convergent mannequin measurements. The effect of changing the weight-bearing applied on the foot on the measurement accuracy was also investigated. The findings from this chapter were as follows:

- The highest discrepancy between the two testers for measuring the mannequin foot was 0.88 mm. The discrepancies between the two testers in conducting the same measurements were not statistically significant.

- Strong measurement correlations were found between the 'gold standard convergent measurements and the caliper measurements collected by the two testers for the mannequin distances. The Pearson's correlation (r) range was between 0.78 and 0.99.

- A strong measurement correlation was also found between the two testers' caliper measurements and the developed photogrammetric dynamic data capture system's measurements. The Pearson's correlation (r) range was between 0.81 and 0.99.

- When the two testers' measurements were compared at 10%, 50% and 90% WB for human subjects' foot measurements, the lowest measurement discrepancies were found for the 50% WB condition. Unlike the 10% and 90% WB conditions, none of the measurements at 50% WB had a measurement difference of more than 1 mm between the two testers.

- Strong measurement correlations were found between the human subjects' foot measurements and the dynamic measurements collected using the developed dynamic data capture system for the FL, TFL, DH and FW. The NH was the only measurement not found to be significantly correlated between the conventional static measurements and the dynamic measurements at 10% WB, 50% WB and 90% WB.

The relationship between the static and dynamic measurements of the FMM and AHI were investigated in Chapter 5 and the significant findings were:

- The intraclass correlation coefficient (ICC) for the intra-rater reliability was higher when the FMM was calculated between 10% WB and 50% WB compared to calculating the FMM between 10% WB and 90% WB.

- The correlations between the static and dynamic FMM were found to be very poor with a Pearson's correlation range between 0.020 and 0.116. Hence the findings suggest that the static FMM does not represent foot mobility dynamically.

- The dynamic AHI 1 (DH/TFL) and AHI 2 (DH/FL) resulted in higher intra-rater reliability than the static AHI 1 and AHI 2.

- Intra-rater reliabilities for the dynamic AHI 1 and AHI 2 were higher for the 50% WB condition than 10% WB and 90% WB.

- Agreements between the static and dynamic AHI 2 were lower than AHI 1. The range in inter-rater reliability for AHI 2 was between 0.766 and 0.931. In contrast, the inter-rater range for AHI 1 was between 0.879 and 0.947.

- The correlation between the static and dynamic AHI 1 and AHI 2 were statistically significant as determined by Pearson's correlations tests. The highest Pearson's correlations were for the 50% WB condition and were slightly higher for AHI 1 then AHI 2.

The effect of foot posture type based on the Foot Posture Index (FPI) classification on the dynamic FMM and AHI was investigated in Chapter 6. The significant findings from the study were:

- No relationship was found between the collective FPI score and the dynamic FMM measures.

- Both the AHI 1 and AHI 2 were correlated with the FPI scores at heel-strike, mid-stance and active propulsion. The highest prediction of the FPI was 48.9% of the variation of the AHI 1 at active prolusion.

- The congruence of the MLA was the only FPI score to have a significant influence on the AHI 1 and AHI 2 at heel-strike, mid-stance and active propulsion. The highest level of significance was between the congruence of the MLA and the AHI 1 at heel-strike where the congruence predicted 66.7% of the variation in the AHI 1 at heel-strike.

- The relationship between the three FPI foot classification groups and the dynamic AHI 1 and AHI 2 were found to be significant for all the dynamic weight-bearing conditions except for the AHI 1 at heel-strike.

- The relationship between the three FPI foot classification groups and the dynamic FMM were found to be significant between heel-strike to mid-stance but not significant between heel-strike and active-propulsion.

7.3 Limitations of the study and future directions

Overall the results achieved from this research study demonstrated the effectiveness of using photogrammetric techniques for high accuracy metric analysis of the foot during dynamic activities. However, the following points can to be addressed in future studies:

- The imaging sensors used in this study have low frame rates which limit their capability to studying slower paced dynamic objects. Imaging sensors with higher frame rates can improve the capability of analysing dynamic feet during faster activities such as running or jumping.

- Developing the technique to allow for complete high-accuracy dynamic 3D models of the foot to be created during dynamic gait. These 3D models will have the potential to lend important insight for the interaction of the foot with the ground surface during gait.

- Additional imaging sensors can be used to capture details of the interactions of the sole of the foot with the ground surface during gait. This can be useful for applications of designing and manufacturing foot orthotics and footwear. Other applications can include detailed studies on foot deformities.

References

Abboud, R. J. 2002. Relevant foot biomechanics. *Current Orthopaedics,* 16**,** 165-179.

Allen, M. K. & Glasoe, W. M. 2000. Metrecom measurement of navicular drop in subjects with anterior cruciate ligament injury. *J Athl Train,* 35**,** 403-6.

Andreasen, J.,Mølgaard, C. M.,Christensen, M.,Kaalund, S.,Lundbye-Christensen, S.,Simonsen, O. & Voigt, M. 2013. Exercise therapy and custom-made insoles are effective in patients with excessive pronation and chronic foot pain - A randomized controlled trial. *The Foot,* 23**,** 22-28.

Atkinson, K. B. 1996. *Close-range Photogrammetry and Machine Vision,* Scotland, Whittles Publishing.

Ball, K. A. & Afheldt, M. J. 2002a. Evolution of foot orthotics - part 1: Coherent theory or coherent practice? *Journal of Manipulative and Physiological Therapeutics,* 25**,** 116-124.

Ball, K. A. & Afheldt, M. J. 2002b. Evolution of foot orthotics - part 2: Research reshapes long-standing theory. *Journal of Manipulative and Physiological Therapeutics,* 25**,** 125-134.

Bandholm, T.,Boysen, L.,Haugaard, S.,Zebis, M. & Bencke, J. 2008. Foot medial longitudinal-arch deformation during quiet standing and gait in subjects with medial tibial stress syndrome. *Journal of Foot and Ankle Surgery,* 47**,** 89 - 95.

Barazzetti, L.,Scaioni, M. & Remondino, F. 2010. Orientation and 3D modelling from markerless terrestrial images: Combining accuracy with automation. *The Photogrammetric Record,* 25**,** 356-381.

Bartczak, B. & Koch, R. Dense depth maps from low resolution time-of-flight depth and high resolution color views. Proceedings of the ISVC, 2009 Las Vegas, USA. Springer Berlin Heidelberg, 228-239.

Bennett, J.,Reinking, M.,Pluemer, B.,Pentel, A.,Seaton, M. & Killian, C. 2001. Factors contributing to the development of medial tibial stress syndrome in high school runners. *Journal of Orthopaedic and Sports Physical Therapy,* 31**,** 504 - 510.

Billis, E.,Katsakiori, E.,Kapodistrias, C. & Kapreli, E. 2007. Assessment of foot posture: Correlation between different clinical techniques. *Foot,* 17**,** 65 - 72.

Blenkinsopp, R.,Harland, A.,Price, D.,Lucas, T. & Roberts, J. 2012. A method to measure dynamic dorsal foot surface shape and deformation during linear running using digital image correlation. *Procedia Engineering,* 34**,** 266-271.

Brilakis, I.,Fathi, H. & Rashidi, A. 2011. Progressive 3D reconstruction of infrastructure with videogrammetry. *Automation in Construction,* 20**,** 884-895.

Brody, D. M. 1982. Techniques in the evaluation and treatment of the injured runner. *Orthop Clin North Am,* 13**,** 541-58.

Brown, D. C. 1971. Close-range camera calibration. *Photogramm. Eng,* 37**,** 855-866.

Brown, D. C. 1976. The bundle adjustment - progress and prospects. *Int. Archives Photogrammetry,* 21**,** 1-1.

Burns, J.,Crosbie, J.,Hunt, A. & Ouvrier, R. 2005. The effect of pes cavus on foot pain and plantar pressure. *Clinical Biomechanics,* 20**,** 877-882.

Butler, R.,Hillstrom, H.,Song, J.,Richards, C. & Davis, I. 2008. Arch height index measurement system: Establishment of reliability and normative values. *Journal of the American Podiatric Medical Association,* 98**,** 102-106.

Cai, H. 2013. High dynamic range photogrammetry for synchronous luminance and geometry measurement. *Lighting Research and Technology,* 45**,** 230-257.

Cain, L. E.,Nicholson, L. L.,Adams, R. D. & Burns, J. 2007. Foot morphology and foot/ankle injury in indoor football. *Journal of Science and Medicine in Sport,* 10**,** 311-319.

Cashmere, T.,Smith, R. & Hunt, A. 1999. Medial longitudinal arch of the foot: stationary versus walking measures. *Foot & Ankle international,* 20**,** 112-118.

Castaneda, V.,Mateus, D. & Navab, N. Stereo time-of-flight. IEEE International Conference on Computer Vision (ICCV), 6-13 Nov. 2011. 1684-1691.

Catherwood, T.,Mccaughan, E.,Greer, E.,Spence, R.,Mcintosh, S. & Winder, R. 2011. Validation of a passive stereophotogrammetry system for imaging of the breast: A geometric analysis. *Medical Engineering & Physics,* 33**,** 900-905.

Chen, C.,Huang, M.,Chen, T.,Weng, M.,Lee, C. & Wang, G. 2006. The correlation between selected measurements from footprint and radiograph of flatfoot. *Archives of Physical Medicine and Rehabilitation,* 87**,** 235-240.

Chen, S.,Li, Y. & Zhang, J. 2008. Vision processing for realtime 3-D data acquisition based on coded structured light. *IEEE Transactions on Image Processing,* 17**,** 167-176.

Chong, A. K. 2007. An inexpensive stereo-image capture tool for motion study. *The Photogrammetric Record,* 22**,** 226-237.

Chong, A. K. 2011. Low-cost compact cameras: A medical application in CMT disease monitoring. *The Photogrammetric Record,* 26**,** 263-273.

Chong, A. K. 2012. Exploiting HD camcorders for close-up human movement applications. *The Photogrammetric Record,* 27**,** 227-237.

Chong, A. K.,Milburn, P.,Newsham-West, R. & Voert, M. 2009. High-accuracy photogrammetric technique for human spine measurement. *The Photogrammetric Record,* 24**,** 264-279.

Cooper, M. & Cross, P. 1988. Statistical concepts and their application in photogrammetry and surveying. *The Photogrammetric Record,* 12**,** 637-663.

Cooper, M. & Robson, S. 2001. Theory of close range photogrammetry *Close Range Photogrammetry and Machine Vision.* Caithness: Whittles.

Cornwall, M. & Mcpoil, T. 1999. Relative movement of the navicular bone during normal walking. *Foot and Ankle International,* 20**,** 507-512.

Cornwall, M. W. & Mcpoil, T. G. 2011. Relationship between static foot posture and foot mobility. *J Foot Ankle Res,* 4**,** 1-9.

Cornwall, M. W.,Mcpoil, T. G.,Lebec, M.,Vicenzino, B. & Wilson, J. 2008. Reliability of the modified foot posture index. *Journal of the American Podiatric Medical Association,* 98**,** 7-13.

Cote, K.,Brunet, M.,Gansneder, B. & Shultz, S. 2005. Effects of pronated and supinated foot postures on static and dynamic postural stability. *Journal of Athletic Training,* 40**,** 41-46.

Coudert, T.,Vacher, P.,Smits, C. & Van Der Zande, M. A method to obtain 3D foot shape deformation during the gait cycle. 9th International Symposium on the 3D analysis of Human Movement: 28-30th June 2006 Valenciennes, France, 2006.

Creath, K. 1988. Phase-measurement interferometry techniques. *Progress in Optics,* 26**,** 349-393.

Cui, Y.,Schuon, S.,Chan, D.,Thrun, S. & Theobalt, C. 3D shape scanning with a time-of-flight camera. Proceedings of the IEEE Conference on Computer Vision and Pattern Recognition (CVPR), 2010. 1173-1180.

De Menezes, M.,Rosati, R.,Ferrario, V. & Sforza, C. 2010. Accuracy and reproducibility of a 3-dimensional stereophotogrammetric imaging system. *Journal of Oral and Maxillofacial Surgery,* 68**,** 2129-2135.

De Mits, S.,Coorevits, P.,De Clercq, D.,Elewaut, D.,Woodburn, J. & Roosen, P. 2009. Validity and reliability of the infoot 3D foot digitizer for rheumatoid arthritis patients. *Footwear Science,* 1**,** 101-103.

De Mits, S.,Coorevits, P.,De Clercq, D.,Elewaut, D.,Woodburn, J. & Roosen, P. 2010. Reliability and validity of the Infoot 3D foot digitizer for normal healthy adults. *Footwear Science,* 2**,** 65-75.

Deng, J.,Joseph, R. & Wong, C. 2010. Reliability and validity of the sit-to-stand navicular drop test: Do static measures of navicular height relate to the dynamic navicular motion during gait? *Journal of Student Physical Therapy Research,* 2**,** 21-8.

Diraco, G.,Leone, A. & Siciliano, P. Geodesic-based human posture analysis by using a single 3D TOF camera. Proceedings of the IEEE International Symposium on Industrial Electronics (ISIE '11), 2011. 1329-1334.

Fan, Y.,Fan, Y.,Li, Z.,Lv, C. & Luo, D. 2011. Natural gaits of the non-pathological flat foot and high-arched foot *PLos ONE,* 6**,** 3.

Fraser, C. & Al-Ajlouni, S. 2006. Zoom-dependent camera calibration in digital close-range photogrammetry. *Photogrammetric Engineering and Remote Sensing,* 72**,** 1017.

Fraser, C. S. 1996. Network design. *Close Range Photogrammetry and Machine Vision***,** 256-281.

Fraštia, M. 2005. Possibilities of using inexpensive digital cameras in applications of close-range photogrammetry. *Slovak Journal of Civil Engineering,* 8**,** 20-28.

Geng, J. 2011. Structured-light 3D surface imaging: a tutorial. *Advances in Optics and Photonics,* 3**,** 128-160.

Gilmour, J. C. & Burns, Y. 2001. The measurement of the medial longitudinal arch in children. *Foot & Ankle International,* 22**,** 493-498.

Gomes, P.,Sesselmann, M.,Faria, C.,Araújo, P. & Teixeira-Salmela, L. 2010. Measurement of scapular kinematics with the moiré fringe projection technique. *Journal of Biomechanics,* 43**,** 1215-1219.

Granshaw, S. I. 1980. Bundle adjustment methods in engineering photogrammetry. *The Photogrammetric Record,* 10**,** 181-207.

Gruen, A. & Beyer, H. A. 2001. System calibration through self-calibration. *Calibration and Orientation of Cameras in Computer Vision.* Springer.

Guan, C.,Hassebrook, L. & Lau, D. 2003. Composite structured light pattern for three-dimensional video. *Optics Express,* 11**,** 406-417.

Hartley, R. & Kang, S. 2007. Parameter-free radial distortion correction with center of distortion estimation. *IEEE Transactions on Pattern Analysis and Machine Intelligence* 29**,** 1309-1321.

Hobbs, S.,Seynat, C. & Matakidis, P. 2007. Videogrammetry: A practical method for measuring vegetation motion in wind demonstrated on wheat. *Agricultural and Forest Meteorology,* 143**,** 242-251.

Hunt, A. E.,M Smith, R.,Torode, M. & Keenan, A.-M. 2001. Inter-segment foot motion and ground reaction forces over the stance phase of walking. *Clinical Biomechanics,* 16**,** 592-600.

Igbigbi, P. S. & Msamati, B. C. 2002. The footprint ratio as a predictor of pes planus: A study of indigenous Malawians. *The Journal of Foot and Ankle Surgery,* 41**,** 394-397.

Ishii, I.,Yamamoto, K. & Tsuji, T. High-speed 3D image acquisition using coded structured light projection. IEEE/RSJ International Conference on Intelligent Robots and Systems, 2007. 925-930.

Jensen, K. & Juhl, J. 2009. Gait analysis by multi video sequence analysis. *Photogrammetric Journal of Finland,* 21**,** 25-34.

Jezeršek, M. & Možina, J. 2009. High-speed measurement of foot shape based on multiple-laser-plane triangulation. *Optical Engineering,* 48**,** 113604-113608.

Jezeršek, M.,Novak, B. & Možina, J. 2011. Three-dimensional laser based measurement of human foot during walking. *Footwear Science,* 3**,** S81-S83.

Johnson, J.,Hughes, S. & Van Dam, J. 2009. A stereo-videogrammetry system for monitoring wind turbine blade surfaces during structural testing. *ASME Early Career Tech. J,* 8**,** 1-10.

Jonely, H.,Brismée, J.,Sizer Jr, P. & James, C. 2011. Relationships between clinical measures of static foot posture and plantar pressure during static standing and walking. *Clinical Biomechanics,* 26**,** 873-879.

Jones, T. & Lunsford, C. A photogrammetric system for model attitude measurement in hypersonic wind tunnels. 45th AIAA Aerospace Sciences meeting and Exhibit, 8-11 January 2007 Reno, Nevada.

Kanatli, U.,Yetkin, H. & Cila, E. 2001. Footprint and radiographic analysis of the feet. *Journal of Pediatric Orthopaedics,* 21**,** 225-228.

Kappel, S. L.,Rathleff, M. S.,Hermann, D.,Simonsen, O.,Karstoft, H. & Ahrendt, P. 2012. A novel method for measuring in-shoe navicular drop during gait. *Sensors,* 12**,** 11697-11711.

Kau, C.,Olim, S. & Nguyen, J. 2011. The future of orthodontic diagnostic records. *Seminars in Orthodontics,* 17**,** 39-45.

Kau, C. H.,Richmond, S.,Incrapera, A.,English, J. & Xia, J. J. 2007. Three-dimensional surface acquisition systems for the study of facial morphology and their application to maxillofacial surgery. *The International Journal of Medical Robotics and Computer Assisted Surgery,* 3**,** 97-110.

Kau, C. H.,Richmond, S.,Zhurov, A.,Ovsenik, M.,Tawfik, W.,Borbely, P. & English, J. D. 2010. Use of 3-dimensional surface acquisition to study facial morphology in 5 populations. *American Journal of Orthodontics and Dentofacial Orthopedics,* 137**,** S56-e1.

Ke, Y.,Li, L. & Jiang, K. 2009. Foot shape reconstruction based on a monocular system using structured light projection. *Applied Mechanics and Materials,* 16**,** 340-346.

Keenan, A.,Redmond, A.,Horton, M.,Conaghan, P. & Tennant, A. 2007. The foot posture index: Rasch analysis of a novel, foot-specific outcome measure. *Archives of Physical Medicine and Rehabilitation,* 88**,** 88-93.

Khamis, S. & Yizhar, Z. 2007. Effect of feet hyperpronation on pelvic alignment in a standing position. *Gait & Posture,* 25**,** 127-134.

Kimura, M.,Mochimaru, M. & Kanade, T. 2011. 3D measurement of feature cross-sections of foot while walking. *Machine Vision and Applications,* 22**,** 377-388.

Kimura, M.,Mochimaru, M.,Kouchi, M. & Kanade, T. 3D cross-sectional shape measurement of the foot while walking. Proceedings of the 7th Symposium on Footwear Biomechanics, International Society of Biomechanics, 2005. 34-35.

King, B. 2012. A webcam-based photogrammetric system for the measurement of facial landmarks on newborns. *Photogrammetric Engineering & Remote Sensing,* 78**,** 1285-1294.

Kondo, S.,Akagi, Y. & Kitajima, K. Study on a method of generating a 3D virtual foot model with use of a measuring technique based on multiple camera image data. SICE Annual Conference 17-20 Sept 2007 Takamatsu.

Korpelainen, R.,Orava, S.,Karpakka, J.,Siira, P. & Hulkko, A. 2001. Risk Factors for Recurrent Stress Fractures in Athletes *The American Journal of Sports Medicine,* 29**,** 304-310.

Kouchi, M.,Kimura, M. & Mochimaru, M. 2009. Deformation of foot cross-section shapes during walking. *Gait & Posture,* 30**,** 482-486.

Kouchi, M. & Mochimaru, M. 2001. Development of a low cost foot-scanner for a custom shoe making system. *5th ISB Footwear Biomechanics***,** 58-59.

Ladeira, P. R.,Bastos, E. O.,Vanini, J. V. & Alonso, N. 2013. Use of stereophotogrammetry for evaluating craniofacial deformities: a systematic review. *Revista Brasileira de Cirurgia Plástica,* 28**,** 147-155.

Landis, J. R. & Koch, G. G. 1977. The measurement of observer agreement for categorical data. *Biometrics,* 33**,** 159 - 174.

Leardini, A.,Benedetti, M.,Berti, L.,Bettinelli, D.,Nativo, R. & Giannini, S. 2007. Rear-foot, mid-foot and fore-foot motion during the stance phase of gait. *Gait & Posture,* 25**,** 453-462.

Leifer, J.,Weems, B.,Kienle, S. & Sims, A. 2011. Three-dimensional acceleration measurement using videogrammetry tracking data. *Experimental Mechanics,* 51**,** 199-217.

Lindner, M.,Schiller, I.,Kolb, A. & Koch, R. 2010. Time-of-flight sensor calibration for accurate range sensing. *Computer Vision and Image Understanding,* 114**,** 1318-1328.

Liu, S.,Cui, Y.,Sanchez, S. & Stricker, D. 2011. Foot scanning and deformation estimation using time-of-flight cameras. *Footwear Science,* 3**,** S98-S99.

Luhmann, T. 2010. Close range photogrammetry for industrial applications. *ISPRS Journal of Photogrammetry and Remote Sensing,* 65**,** 558-569.

Luhmann, T.,Robson, S.,Kyle, S. & Hartley, I. 2006. *Close Range Photogrammetry, Principles, Methods and Applications.*, Whittles Publishing.

Luo, S. & Gong, Z. 2014. Customize last from multiple foot images by a little interaction. *Computers & Electrical Engineering,* 40**,** 956-963.

Luo, S.,Pana, X. & Gong, Z. 2012. Customization of foot lasts from multi-view images. *Journal of Information and Computational Science* 9**,** 5603-5619.

Luximon, A. & Goonetilleke, R. S. 2004. Foot shape modeling. *The Journal of the Human Factors and Ergonomics Society,* 46**,** 304-315.

Madden, M. & Karlan, M. 1979. Moiré photography as a means of topographical mapping of the human face. *Annals of Biomedical Engineering,* 7**,** 95-102.

Mall, N.,Hardaker, W.,Nunley, J. & Queen, R. 2007. The reliability and reproducibility of foot type measurements using a mirrored foot photo box

and digital photography compared to caliper measurements. *Journal of Biomechanics,* 40**,** 1171-1176.
Martedi, S.,Saito, H. & Servieres, M. Shape measurement system of foot sole surface from flatbed scanner image. MVA, 2009. 338-341.
Mason, S. 1995. Expert system-based design of close-range photogrammetric networks. *ISPRS Journal of Photogrammetry and Remote Sensing,* 50**,** 13-24.
Mavroidis, C.,Ranky, R.,Sivak, M.,Patritti, B.,Dipisa, J.,Caddle, A.,Gilhooly, K.,Govoni, L.,Sivak, S. & Lancia, M. 2011. Patient specific ankle-foot orthoses using rapid prototyping. *Journal of Neuroengineering and Rehabilitation,* 8.
Mccrory, J. L.,Young, M. J.,Boulton, A. J. M. & Cavanagh, P. R. 1997. Arch index as a predictor of arch height. *The Foot,* 7**,** 79-81.
Mcpoil, T.,Cornwall, M.,Abeler, M.,Devereaux, K. & Flood, L. 2013. The optimal method to assess the vertical mobility of the midfoot: Navicular drop versus dorsal arch height difference. *Clin Res Foot Ankle,* 1**,** 104.
Mcpoil, T.,Cornwall, M.,Medoff, L.,Vicenzino, B.,Forsberg, K. & Hilz, D. 2008a. Arch height change during sit-to-stand: an alternative for the navicular drop test. *Journal of Foot and Ankle Research,* 1**,** 3.
Mcpoil, T.,Vicenzino, B.,Cornwall, M.,Collins, N. & Warren, M. 2009. Reliability and normative values for the foot mobility magnitude: A composite measure of vertical and medial-lateral mobility of the midfoot. *Journal of Foot and Ankle Research,* 2**,** 6.
Mcpoil, T. G. & Cornwall, M. W. 1996. Relationship between three static angles of the rearfoot and the pattern of rearfoot motion during walking. *Journal of Orthopaedic & Sports Physical Therapy,* 23**,** 370-375.
Mcpoil, T. G.,Cornwall, M. W.,Vicenzino, B.,Teyhan, D. S.,Molloy, J. M.,Christie, D. S. & Collins, N. 2008b. Effect of using truncated versus total foot length to calculate the arch height index. *Foot,* 18**,** 220 - 227.
Menz, H. B. 1998. Alternative techniques for the clinical assessment of foot pronation. *Journal of the American Podiatric Medical Association,* 88**,** 119-29.
Menz, H. B. & Munteanu, S. E. 2005. Validity of 3 clinical techniques for the measurement of static foot posture in older people. *Journal of Orthopaedic & Sports Physical Therapy,* 35**,** 479-486.
Mikhail, E. M.,Bethel, J. S. & Mcglone, J. C. 2001. *Introduction to Modern Photogrammetry,* John Wiley & Sons Inc.
Mochimaru, M. & Kouchi, M. 2011. 4D measurement and analysis of plantar deformation during walking and running. *Footwear Science,* 3**,** S109-S112.
Moul, J. L. 1998. Differences in selected predictors of anterior cruciate ligament tears between male and female NCAA Division I collegiate basketball players. *Journal of Athletic Training,* 33**,** 118.
Mueller, M.,Host, J. V. & Norton, B. 1993. Navicular drop as a composite measure of excessive pronation. *Journal of the American Podiatric Medical Association,* 83**,** 198 - 202.
Murley, G.,Menz, H. & Landorf, K. 2009. Foot posture influences the electromyographic activity of selected lower limb muscles during gait. *Journal of Foot and Ankle Research,* 2**,** 35.
Murphy, D. F.,Connolly, D. a. J. & Beynnon, B. D. 2003. Risk factors for lower extremity injury: a review of the literature. *British Journal of Sports Medicine,* 37**,** 13-29.

Myronenko, A. & Song, X. 2010. Point set registration: Coherent point drift. *IEEE Transactions on Pattern Analysis and Machine Intelligence,* 32**,** 2262-2275.

Nack, J. D. & Phillips, R. D. 1990. Shock absorption. *Clinics in podiatric medicine and surgery,* 7**,** 391-397.

Nielsen, R.,Rathleff, M.,Moelgaard, C.,Simonsen, O.,Kaalund, S.,Olesen, C.,Christensen, F. & Kersting, U. 2010. Video based analysis of dynamic midfoot function and its relationship with foot posture index scores. *Gait and Posture,* 31**,** 126-130.

Nielsen, R.,Rathleff, M.,Simonsen, O. & Langberg, H. 2009. Determination of normal values for navicular drop during walking: A new model correcting for foot length and gender. *Journal of Foot and Ankle Research,* 2.

Nigg, B.,Cole, G. & Nachbauer, W. 1993. Effects of arch height of the foot on angular motion of the lower extremities in running. *Journal of Biomechanics,* 26**,** 909-916.

Novak, B.,Možina, J. & Jezeršek, M. 2014. 3D laser measurements of bare and shod feet during walking. *Gait & posture,* 40**,** 87-93.

Ogon, M.,Aleksiev, A.,Pope, M.,Wimmer, C. & Saltzman, C. 1999. Does arch height affect impact loading at the lower back level in running? *Foot & Ankle International,* 20**,** 263-266.

Onodera, A.,Sacco, I.,Morioka, E.,Souza, P.,Sá, M. & Amadio, A. 2008. What is the best method for child longitudinal plantar arch assessment and when does arch maturation occur? *The Foot,* 18**,** 142-149.

Ordóñez, C.,Arias, P.,Herráez, J.,Rodríguez, J. & Martín, M. T. 2008. Two photogrammetric methods for measuring flat elements in buildings under construction. *Automation in Construction,* 17**,** 517-525.

Ozbek, M.,Rixen, D. J.,Erne, O. & Sanow, G. 2010. Feasibility of monitoring large wind turbines using photogrammetry. *Energy,* 35**,** 4802-4811.

Paulsen, U. S.,Schmidt, T. & Erne, O. 2011. Developments in large wind turbine modal analysis using point tracking videogrammetry. *Structural Dynamics and Renewable Energy, Volume 1*. Springer.

Peter Heng, B.,Chandler, J. & Armstrong, A. 2010. Applying close range digital photogrammetry in soil erosion studies. *The Photogrammetric Record,* 25**,** 240-265.

Pezzan, P.,Sacco, I. & João, S. 2009. Foot posture and classification of the plantar arch among adolescent wearers and non-wearers of high-heeled shoes. *Brazilian Journal of Physical Therapy,* 13**,** 398-404.

Pohl, M. B. & Farr, L. 2010. A comparison of foot arch measurement reliability using both digital photography and calliper methods. *Foot and Ankle Research,* 3**,** 14-19.

Powers, C. M. 2003. The influence of altered lower-extremity kinematics on patellofemoral joint dysfunction: A theoretical perspective. *Journal of Orthopaedic & Sports Physical Therapy,* 33**,** 639-646.

Razeghi, M. & Batt, M. 2002. Foot type classification: A critical review of current methods. *Gait and Posture,* 15**,** 282-291.

Redmond, A.,Burns, J.,Crosbie, J.,Ouvrier, R. & Peat, J. 2001. An initial appraisal of the validity of a criterion based, observational clinical rating system for foot posture. *J Orthop Sports Phys Ther,* 31**,** 160.

Redmond, A.,Crosbie, J. & Ouvrier, R. 2006a. Development and validation of a novel rating system for scoring standing foot posture: The Foot Posture Index. *Clinical Biomechanics,* 21**,** 89-98.

Redmond, A. C. 2005. The Foot Posture Index: user guide and manual.
Redmond, A. C.,Crane, Y. Z. & Menz, H. B. 2008. Normative values for the foot posture index. *J Foot Ankle Res,* 1**,** 6.
Redmond, A. C.,Crosbie, J. & Ouvrier, R. A. 2006b. Development and validation of a novel rating system for scoring standing foot posture: The Foot Posture Index. *Clinical Biomechanics,* 21**,** 89-98.
Reel, S.,Rouse, S.,Vernon, W. & Doherty, P. 2010. Reliability of a two-dimensional footprint measurement approach. *Science & Justice,* 50**,** 113-118.
Remondino, F. & Fraser, C. S. 2006. Digital camera calibration methods: considerations and comparisons. *International Archives of Photogrammetry, Remote Sensing and Spatial Information Sciences,* 36**,** 266-272.
Richie Jr, D. H. 2007. Biomechanics and clinical analysis of the adult acquired flatfoot. *Clinics in Podiatric Medicine and Surgery,* 24**,** 617-644.
Rieke-Zapp, D. H. & Nearing, M. A. 2005. Digital close range photogrammetry for measurement of soil erosion. *The Photogrammetric Record,* 20**,** 69-87.
Riveiro, B.,Caamaño, J. C.,Arias, P. & Sanz, E. 2011. Photogrammetric 3D modelling and mechanical analysis of masonry arches: An approach based on a discontinuous model of voussoirs. *Automation in Construction,* 20**,** 380-388.
Saadatseresht, M.,Samadzadegan, F. & Azizi, A. 2005. Automatic camera placement in vision metrology based on a fuzzy inference system. *Photogrammetric Engineering & Remote Sensing,* 71**,** 1375-1385.
Salvi, J.,Fernandez, S.,Pribanic, T. & Llado, X. 2010. A state of the art in structured light patterns for surface profilometry. *Pattern Recognition,* 43**,** 2666-2680.
Samson, W.,Van Hamme, A.,Sanchez, S.,Chèze, L.,Jan, S. & Feipel, V. 2014. Foot roll-over evaluation based on 3D dynamic foot scan. *Gait & Posture,* 39**,** 577-582.
Samson, W.,Van Hamme, A.,Sanchez, S.,Chèze, L.,Van Sint Jan, S. & Feipel, V. 2012. Dynamic footprint analysis by time-of-flight camera. *Computer Methods in Biomechanics and Biomedical Engineering,* 15**,** 180-182.
Schmeltzpfenning, T.,Plank, C.,Fritz, B.,Aswendt, P. & Grau, S. 2011. 3D dynamic behaviour of foot structure may provide additional information for last design. *Footwear Science,* 3**,** S147-S148.
Schmeltzpfenning, T.,Plank, C.,Krauss, I.,Aswendt, P. & Grau, S. 2009. Dynamic foot scanning: A new approach for measurement of the human foot shape while walking. *Footwear Science,* 1**,** 28-30.
Schuon, S.,Theobalt, C.,Davis, J. & Thrun, S. High-quality scanning using time-of-flight depth superresolution. IEEE Computer Society Conference on Computer Vision and Pattern Recognition Workshops, 23-28 June 2008 Anchorage, AK.
Schwarz, L. A.,Mkhitaryan, A.,Mateus, D. & Navab, N. Estimating human 3d pose from time-of-flight images based on geodesic distances and optical flow. IEEE Conference on Automatic Face and Gesture Recognition (FG), 21-25 March 2011 Santa Barbara, CA.
Scott, G.,Menz, H. & Newcombe, L. 2007. Age-related differences in foot structure and function. *Gait & Posture,* 26**,** 68-75.
Sell, K.,Verity, T.,Worrell, T.,Pease, B. & Wigglesworth, J. 1994. Two measurement techniques for assessing subtalar joint position: A reliability study. *Journal of Orthopaedic and Sports Physical Therapy,* 19**,** 162 - 167.

Sheykhi-Dolagh, R.,Saeedi, H.,Farahmand, B.,Kamyab, M.,Kamali, M.,Gholizadeh, H.,Derayatifar, A. A. & Curran, S. 2014. The influence of foot orthoses on foot mobility magnitude and arch height index in adults with flexible flat feet. *Prosthetics and orthotics international***,** 0309364614521652.

Shiang, T. Y.,Lee, S. H.,Lee, S. J. & Chu, W. C. 1998. Evaluating different footprints parameters as a predictor of arch height. *Engineering in Medicine and Biology Magazine, IEEE,* 17**,** 62-66.

Shrader, J.,Popovich, J.,Gracey, G. & Danoff, J. 2005. Navicular drop measurement in people with rheumatoid arthritis: Interrater and intrarater reliability. *Physical Therapy,* 85**,** 656-664.

Shrout, P. & Fleiss, J. 1979. Intraclass correlations - uses in assessing rater reliability. *Psychological Bulletin,* 86**,** 420-428.

Statler, T. & Tullis, B. 2005. Pes cavus. *Journal of the American Podiatric Medical Association,* 95**,** 42-52.

Takasaki, H. 1970. Moiré topography. *Applied Optics,* 9**,** 1467-1472.

Taylor, N.,Campbell, J. & Metcalfe, S. 2012. Radiographic measurement of the first metatarsal: A new technique to improve the accuracy of intermetatarsal angle measurement. *Journal of the American Podiatric Medical Association,* 102**,** 105-113.

Telem, G. & Filin, S. 2010. Photogrammetric modeling of underwater environments. *ISPRS Journal of Photogrammetry and Remote Sensing,* 65**,** 433-444.

Telfer, S.,Gibson, K.,Hennessy, K.,Steultjens, M. & Woodburn, J. 2012. Computer-aided design of customized foot orthoses: Reproducibility and effect of method used to obtain foot shape. *Archives of Physical Medicine and Rehabilitation,* 93**,** 863-870.

Telfer, S. & Woodburn, J. 2010. The use of 3D surface scanning for the measurement and assessment of the human foot. *J Foot Ankle Res,* 5**,** 19.

Teyhen, D.,Stoltenberg, B.,Collinsworth, K.,Giesel, C.,Williams, D.,Kardouni, C.,Molloy, J.,Goffar, S.,Christie, D. & Mcpoil, T. 2009. Dynamic plantar pressure parameters associated with static arch height index during gait. *Clinical Biomechanics,* 24**,** 391-396.

Thabet, A.,Trucco, E.,Salvi, J.,Wang, W. & Abboud, R. 2014. Dynamic 3D shape of the plantar surface of the foot using coded structured light: A technical report. *Journal of Foot and Ankle Research,* 7**,** 1-12.

Tong, J. & Kong, P. 2013. Association between foot type and lower extremity injuries: Systematic literature review with meta-analysis. *Journal of Orthopaedic & Sports Physical Therapy,* 43**,** 700-714.

Triggs, B.,Mclauchlan, P.,Hartley, R. & Fitzgibbon, A. 2000. Bundle Adjustment - A Modern Synthesis. *Vision Algorithms: Theory and Practice.* Springer Berlin Heidelberg.

Van Loon, B.,Maal, T.,Plooij, J.,Ingels, K.,Borstlap, W.,Kuijpers-Jagtman, A.,Spauwen, P. & Bergé, S. 2010. 3D stereophotogrammetric assessment of pre-and postoperative volumetric changes in the cleft lip and palate nose. *International Journal of Oral and Maxillofacial Surgery,* 39**,** 534-540.

Vass, G. & Perlaki, T. Applying and removing lens distortion in post production the 2nd Hungarian Conference on Computer Graphics abd Geometry 2003 Budapest, Hungary. 9-12.

Vecchio, S.,Araújo, P.,Rubio, J.,Pinotti, M. & Sesselmann, M. 2012. 3D measurement of human plantar foot by projection moiré technique. *International Journal of Mechatronics and Manufacturing Systems,* 5**,** 3-16.

Villarroya, M.,Esquivel, J.,Tomás, C.,Moreno, L.,Buenafé, A. & Bueno, G. 2009. Assessment of the edial longitudinal arch in children and adolescents with obesity: Footprints and radiographic study. *European Journal of Pediatrics,* 168**,** 559-567.

Vinicombe, A.,Raspovic, A. & Menz, H. 2001. Reliability of navicular displacement measurement as a clinical indicator of foot posture. *Journal of the American Podiatric Medical Association,* 91**,** 262-268.

Viswanathan, N. K. 2013. Calibration and 3D Model Generation for a Low-Cost Structured Light Foot Scanner.

Wackrow, R. & Chandler, J. H. 2008. A convergent image configuration for DEM extraction that minimises the systematic effects caused by an inaccurate lens model. *The Photogrammetric Record,* 23**,** 6-18.

Wackrow, R. & Chandler, J. H. 2011. Minimising systematic error surfaces in digital elevation models using oblique convergent imagery. *The Photogrammetric Record,* 26**,** 16-31.

Wearing, S.,Hills, A.,Byrne, N.,Hennig, E. & Mcdonald 2004. The srch index: A measure of flat or fat feet? *Foot & Ankle International,* 25**,** 575-581.

Weinberg, S.,Scott, N.,Neiswanger, K.,Brandon, C. & Marazita, M. 2004. Digital three-dimensional photogrammetry: Evaluation of anthropometric precision and accuracy using a Genex 3D camera system. *The Cleft Palate-Craniofacial Journal,* 41**,** 507-518.

Williams, D. & Mcclay, I. 2000. Measurements used to characterize the foot and the medial longitudinal arch: Reliability and validity. *Physical Therapy,* 80**,** 864 - 871.

Williams, D.,Mcclay, I. & Hamill, J. 2001. Arch structure and injury patterns in runners. *Clinical Biomechanics,* 16**,** 341-347.

Witana, C.,Xiong, S.,Zhao, J. & Goonetilleke, R. 2006. Foot measurements from three-dimensional scans: A comparison and evaluation of different methods. *International Journal of Industrial Ergonomics,* 36**,** 789-807.

Wong, J.,Oh, A.,Ohta, E.,Hunt, A.,Rogers, G.,Mulliken, J. & Deutsch, C. 2008. Validity and reliability of craniofacial anthropometric measurement of 3D digital photogrammetric images. *The Cleft Palate-Craniofacial Journal,* 45**,** 232-239.

Woodford-Rogers, B.,Cyphert, L. & Denegar, C. 1994. Risk factors for anterior cruciate ligament injury in high school and college athletes. *J Athl Train,* 29**,** 343-346.

Wrobel, J. & Najafi, B. 2010. Diabetic foot biomechanics and gait dysfunction. *Journal of Diabetes Science and Technology,* 4**,** 833-845.

Xenofos, S. & Jones, C. 1979. Theoretical aspects and practical applications of Moire topography. *Physics in Medicine and Biology,* 24**,** 250.

Yoshida, Y.,Saito, S.,Aoki, Y.,Kouchi, M. & Mochimaru, M. Shape completion and modeling of 3D foot shape while walking. International Symposium on Optomechatronic Technologies (ISOT) 29-31 Oct 2012 2012 Paris, France.

Yu, C. & Tu, H. 2009. Foot surface area database and estimation formula. *Applied Ergonomics,* 40**,** 767-774.

Yu, J.,Cheung, J.,Fan, Y.,Zhang, Y.,Leung, A. & Zhang, M. 2008. Development of a finite element model of female foot for high-heeled shoe design. *Clinical Biomechanics,* 23**,** S31-S38.

Zhao, J. & Goonetilleke, R. Locating anatomical points on foot from 3D point cloud data. 16th International Conference on Artificial Reality and Telexistence, 2006 Hangzhou.

Appendix A

The University of Southern Queensland

Participant Information Sheet

Ethics approval number: H12REA041

To: Participants

Full Project Title: A 3D Image-based Measurement Approach for Analysing Dynamic Foot Posture and Mobility

Principal Researcher: Dr. Albert Chong

Student Researcher: Ms. Duaa Alshadli

I am a PhD student at the Faculty of Engineering and Surveying at the University of Southern Queensland and my research interests are in the field of 3D modelling which can be used to obtain high level accuracy measurements (less than 0.5 mm). Through my PhD, I aim to apply my knowledge in the field of Spatial Science to help identify problems associated with inconsistencies between researchers when they determine the changes in foot posture during gait based on the structure of the Medial Longitudinal Arch of the foot. I identified a gap in the research in this area and I believe that through my research I will be able to accurately predict the behaviour of the Medial Longitudinal Arch. This has the potential for the identification of any inconsistencies in the current clinical techniques used by medical practitioners and can bring researchers closer to identifying foot injuries and designing appropriate foot orthoses. I would therefore like to invite you to take part in this research project.

You are invited to participate in this research project because I believe that this research will be beneficial for the medical community in a way that can help them improve current foot posture assessment techniques. The participants in this

study are fellow postgraduate students from the Faculty of Engineering and Surveying at USQ.

Please read this Plain Language Statement carefully. Its purpose is to explain to you as openly and clearly as possible all the procedures involved so that you can make a fully informed decision as to whether you are going to participate. Feel free to ask questions about any information in the document. You may also wish to discuss the project with a relative or friend or your local health worker. Feel free to do this.

Once you understand what the project is about and if you agree to take part in it, it is asked that you sign the Consent Form. By signing the Consent Form, you indicate that you understand the information and that you give your consent to participate in the research project.

- **Purpose of Research**

The purpose of this project is to develop a non-invasive technique which will allow for the shape of the Medial Longitudinal Arch of the foot to be mapped during gait. The Medial Longitudinal Arch of the foot is the largest arch that can be viewed from the lateral side of the foot and it is the best predictor of the behaviour of the foot. The research will be conducted as part of a PhD degree.

There are currently many clinical techniques that aim to predict the dynamic behaviour of the Medial Longitudinal Arch during gait based on static measurements which do not provide an accurate assessment of the Medial Longitudinal Arch during gait. The most common techniques are the Navicular drop and drift (Williams and McClay, 2000; McPoil et al., 2008a) and the Foot Posture Index (Redmond et al., 2006b). However, many studies were conducted to identify the reliability of such static techniques for the prediction of the dynamic behaviour of the foot and the results were found to be varied and sometimes with poor reliability (McPoil et al., 2009). Therefore the technique proposed for this research is to be able to identify the direct behaviour of the foot arch during gait and determine the reliability of this developed technique and compare the results with the previous studies of the Navicular drop, the Navicular Drift and the Foot Posture Index.

- **Procedures**

The research will be conducted at the Photogrammetry lab which is located on the ground floor in the S block at USQ. Each participant will be asked to walk barefoot on an elevated platform while six video cameras will be setup around the platform to image the only one foot for each participant while he/she walks 2 metres across the platform at his/her own pace. The video cameras will only record the movement of the foot during the 2 metre walk.

The Platform has been designed and constructed at the USQ workshop. To climb the platform, each participant will climb 4 steps while holding on to the hand railings on either side of the steps. The top of the platform has safety railings running through the entire length which each participant needs to grip while walking on the platform.

Each video session is estimated to take 10 seconds and the video session will be repeated three times for each participant. The researchers will not be recording any information about each patient other than the foot size and gender as these two parameters will influence the measurement accuracy.

All the researchers involved in this study will be available during the study to provide assistance and answer any participant questions if they arise.

The participants will be a part of a novel study and if they wish to have any follows ups on the final results of the study, they can contact the researchers. To the best of our knowledge the risks are minimal as the technique is non-invasive. As the participants will be walking barefoot during the study, the platform will be cleaned properly to ensure that the surface is clean for the participants on not cause any risks of injury from small debris. There is minimal risk of injury from falling from the platform due to the design of the safety railings.

- **Confidentiality**

The raw videos recorded for each participant will be immediately downloaded and stored on a folder labelled with the foot size and gender of each participant. These

folders will be stored in a password protected research computer at the Faculty of Engineering and Surveying and access will not be granted to anyone other than the researchers involved in this study. The data will be stored until the PhD researchers finalises their PhD and this is estimated to be in December 2013.

Any information obtained in connection with this project and that can identify you will remain confidential. It will only be disclosed with your permission, subject to legal requirements. If you give us your permission by signing the Consent Form, we plan to publish the results at journals with interest in foot research.

In any publication, information will be provided in such a way that you cannot be identified. Personal information such as names or images that can lead to the identification of the participant will not be included. If sample images are used, it will only be for the part of the foot focussing on the Medial Longitudinal Arch. Any images with scars or tattoos will not be used. Information regarding gender and foot size of participants may be published but again this will not be in a way which allows for individuals to be identified. We cannot guarantee group discussions between participants but we can ask for each participant to maintain the confidentiality of others.

- **Voluntary Participation**

Participation is entirely voluntary. If you do not wish to take part you are not obliged to. If you decide to take part and later change your mind, you are free to withdraw from the project at any stage. Any information already obtained from you will be destroyed.

Your decision whether to take part or not to take part, or to take part and then withdraw, will not affect your relationship with the University of Southern Queensland.

Before you make your decision, a member of the research team will be available to answer any questions you have about the research project. You can ask for any information you want. Sign the Consent Form only after you have had a chance to ask your questions and have received satisfactory answers.

- **Queries or Concerns**

Should you have any queries regarding the progress or conduct of this research, you can contact the principal researcher:

Dr. Albert Chong
Faculty of Engineering and Surveying
Room Z412
University of Southern Queensland
Tel (+61) 7 4631 2546
Mobile: 0420534762

If you have any ethical concerns with how the research is being conducted or any queries about your rights as a participant please feel free to contact the University of Southern Queensland Ethics Officer on the following details:

Ethics and Research Integrity Officer
Office of Research and Higher Degrees
University of Southern Queensland
West Street, Toowoomba 4350
Ph: +61 7 4631 2690
Email: ethics@usq.edu.au

The University of Southern Queensland

Consent Form

To: Participants

Full Project Title: A 3D Image-based Measurement Approach for Analysing Dynamic Foot Posture and Mobility

Principal Researcher: Dr. Albert Chong

Student Researcher: Ms. Duaa Alshadli

- I have read the Participant Information Sheet and the nature and purpose of the research project has been explained to me. I understand and agree to take part.
- I understand the purpose of the research project and my involvement in it.
- I understand that I may withdraw from the research project at any stage and that this will not affect my status now or in the future.
- I confirm that I am over 18 years of age.
- I understand that while information gained during the study may be published, I will not be identified and my personal results will remain confidential.
- I understand that the video footage recorded of my foot during the research will be stored in a password protected computer at the University of Southern Queensland and access will only be granted to the researchers involved in the study.
- I understand that only my foot will be videotaped during the study.

Name of participant…….....

Signed……**Date**……
.

If you have any ethical concerns with how the research is being conducted or any queries about your rights as a participant please feel free to contact the University of Southern Queensland Ethics Officer on the following details:

Ethics and Research Integrity Officer

Office of Research and Higher Degrees

University of Southern Queensland

West Street, Toowoomba 4350

Ph: +61 7 4631 2690

Email: ethics@usq.edu.au

Appendix B

Mean differences in the seven mannequin distances between the conventional caliper measurements and the developed dynamic data capture system measurements.

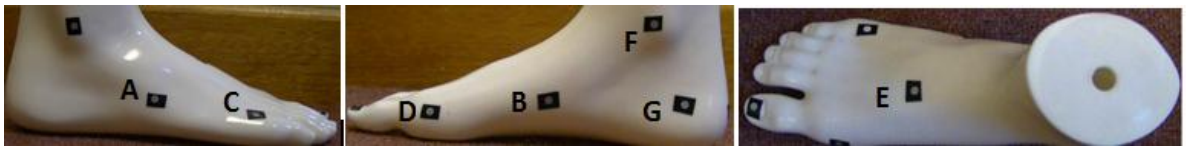

The seven distances are shown in the figure above and are summarised in Table B.1 for the measurements collected by Tester 1, Tester 2 and the developed dynamic data capture system measurements.

Table B.1: Mean mannequin distance measurements from the conventional caliper and developed dynamic system

Distances	Tester 1 (mm)	Tester 2 (mm)	Dynamic system measurements (mm)
A-B	56.68	56.31	55.43
C-D	51.31	51.52	50.10
A-E	62.31	62.66	62.97
B-E	54.87	55.52	55.10
C-E	48.76	48.91	48.58
D-E	44.55	44.24	43.46
F-G	52.69	52.26	52.03

The mean mannequin measurement differences between the conventional caliper measurements and the developed dynamic data capture measurements are provided in Table B.2.

Table B.2: Mean mannequin measurement differences between the conventional caliper measurements form each tester and the developed dynamic data capture system

Distances	Dynamic – Tester 1 (mm)	Dynamic – Tester 2 (mm)
A-B	0.37	1.25
C-D	0.21	1.21
A-E	0.35	0.66
B-E	0.65	0.23
C-E	0.15	0.18
D-E	0.31	1.09
F-G	0.43	0.66

Appendix C

Summary of the FPI assessment test from Redmond (2005)

The Foot Posture Index (FPI) consisted of the six tests demonstrated as follows:

1. Talar head palpation

This is the only test out of the six other scoring criteria which relies on palpation. The head of the Talus bone is palpated on the medial and the lateral side of the anterior aspect of the ankle as shown in the figure below:

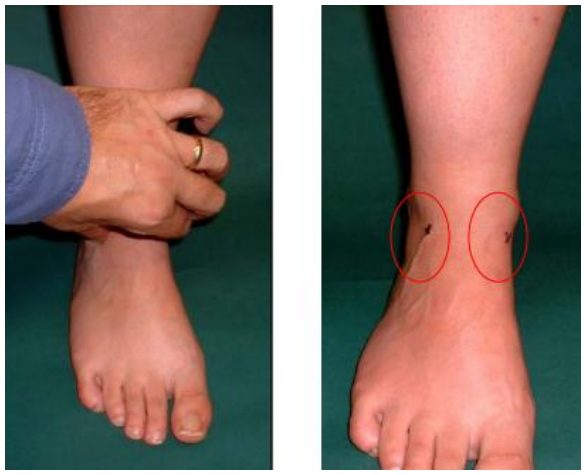

The scoring criterion for the different foot classifications is provided as follows:

Score	-2	-1	0	1	2
	Talar head palpable on lateral side but not on medial side	Talar head palpable on lateral side and slightly on the medial side	Talar head equally palpable on lateral and medial side	Talar head slightly palpable on lateral side and medial side	Talar head not palpable on lateral side but palpable on medial side

2. . Supra and infra lateral Malleolar curvature

For this visual assessment, the Malleolar curvature is inspected from the posterior side of the foot. If the curve below the Malleolus is concave, the foot is classified as pronated and if it is either straight or convex, it is a supinated foot. If the curves are approximately equal the foot is classified as normal.

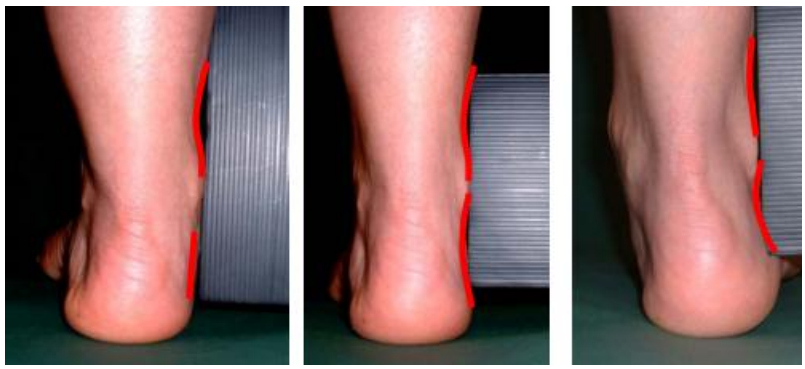

The scoring criterion for the different foot classifications is provides as follows:

Score	-2	-1	0	1	2
	Curve below the malleolus either straight or convex	Curve below the malleolus is concave but flatter than the curve above the malleolus	Both infra and supra Malleolar curves are roughly equal	Curve below the malleolus is concave	Curve below the malleolus is severely concave

3. Inversion/ eversion of the calcaneus

This is a visual assessment of the angular position of the posterior part of the calcaneus. Only a visual estimate is required with a supinated foot having more than five degrees inversion while the pronated foot while have an eversion of more than five degrees. A normal foot will have an approximately vertical calcaneus.

The scoring criterion for the different foot classifications is provides as follows:

Score	-2	-1	0	1	2
	More than five degree inversion	Between vertical and five degree eversion	Vertical	Between vertical and five degree eversion	More than five degree eversion

4. Bulking of the Talonavicular

If the area of skin around the Talonavicular is bulging, the foot is pronated and if it is concave it is supinated. A normal foot will have a flat area around the Talonavicular.

The scoring criterion for the different foot classifications is provides as follows:

Score	-2	-1	0	1	2
	Severely concave area around the Talonavicular	Slightly concave area around the Talonavicular	Flat area around the Talonavicular	Slight bulge around the Talonavicular	Severe bulging on the area around the Talonavicular

5. Height of the congruence of the MLA

This visual assessment is for the shape of the Medial Longitudinal Arch (MLA) shape. The MLA shape is acute for a supinated foot and flattened for a pronated foot. A normal foot will have a uniform arch shape.

The scoring criterion for the different foot classifications is provides as follows:

Score	-2	-1	0	1	2
	High arch shape	Moderately high arch shape	Normal arch height	Flattened arch	Severely flattened arch

6. Abduction/adduction of the forefoot on the rear foot

If the foot is viewed from behind and the forefoot is more prominent on the medial side, the foot is supinated. If the forefoot is angled towards the lateral side then the foot is pronated. A neutral foot will show the forefoot to be equal on the medial and the lateral sides.

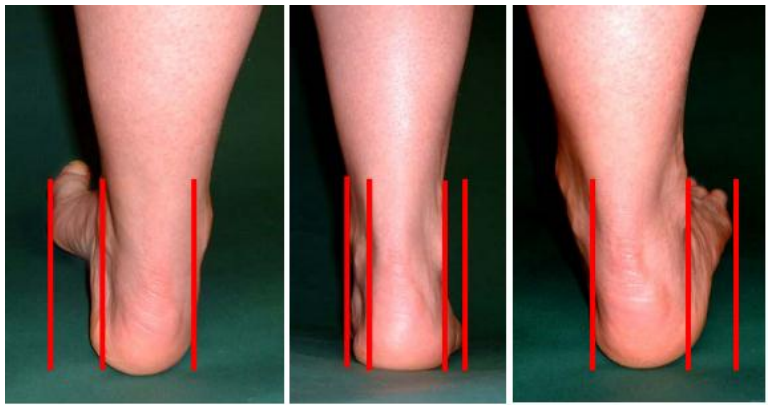

The scoring criterion for the different foot classifications is provides as follows:

Score	-2	-1	0	1	2
	Forefoot visible on the medial side only	Forefoot more visible on the medial side than the lateral side	Forefoot equally visible on the medial and lateral sides	Forefoot more visible on the lateral side than the medial side	Forefoot visible on the lateral side only

Foot Posture Index Datasheet

Patient name ***ID number***

	FACTOR	PLANE	SCORE 1 Date_____ Comment_____		SCORE 2 Date_____ Comment_____		SCORE 3 Date_____ Comment_____	
			Left -2 to +2	**Right** -2 to +2	**Left** -2 to +2	**Right** -2 to +2	**Left** -2 to +2	**Right** -2 to +2
Rearfoot	Talar head palpation	*Transverse*						
	Curves above and below the lateral malleolus	*Frontal/ transverse*						
	Inversion/eversion of the calcaneus	*Frontal*						
Forefoot	Prominence in the region of the TNJ	*Transverse*						
	Congruence of the medial longitudinal arch	*Sagittal*						
	Abd/adduction forefoot on rearfoot	*Transverse*						
	TOTAL							

Reference values
Normal = 0 to +5
Pronated = +6 to +9, Highly pronated 10+
Supinated = -1 to –4, Highly supinated –5 to -12